Modeling, Simulation, and Hardware-in-the-Loop Implementation of Distributed Voltage Control in Power Systems with Renewable Energy Sources

Ali Dehghan Banadaki

Dissertation submitted to the
Benjamin M. Statler College of Engineering and Mineral Resources
at West Virginia University
in partial fulfillment of the requirements for the degree of

Doctor of Philosophy
in
Electrical Engineering

Ali Feliachi[1], Ph.D., Chair
Muhammad A. Choudhry[1], Ph.D.
Yaser P. Fallah[2], Ph.D.
Vinod K. Kulathumani[3], Ph.D.
Hong-Jian Lai[4], Ph.D.

[1]Lane Department of Computer Science and Electrical Engineering, WVU
[2]Department of Electrical and Computer Engineering, University of Central Florida
[3]Senior Applied Scientist, Amazon
[4]Statitistics Department, WVU

Lane Department of Computer Science and Electrical Engineering

Morgantown, West Virginia
April 2022

Keywords: VSI inverter, Small Signal Modeling, Voltage Zoning Analysis, Distributed, Control, Microgrids Control, Real-Time Simulator; Hardware-in-the-Loop

Abstract

Modeling, Simulation, and Hardware-in-the-Loop Implementation of Distributed Voltage Control in Power Systems with Renewable Energy Sources

Ali Dehghan Banadaki

This dissertation develops and analyzes distributed controllers for power systems with renewable energy sources. A comprehensive state space modeling of voltage source inverters (VSIs) is developed specifically to address the secondary voltage control. This model can be used for simulation and control design. Unlike frequency, voltage is a local phenomenon, meaning that it cannot be controlled from a far distance. Therefore, a voltage zoning matrix that relates the sensitivity of the loads to the sources is proposed. The secondary voltage control is designed by applying the eigenvalue decomposition of the voltage zoning matrix to obtain the reference generators voltages. The developed algorithm in this study has been tested on multiple IEEE case studies, and the results show its effectiveness, yet it is a centralized control algorithm. To reduce the risk of a single point of failure in the centralized controllers, distributed secondary voltage controllers have been proposed in the recent literature. However, the communication messages are still exchanged among all controllers in the system. Therefore, a fully distributed algorithm is proposed in this dissertation study through the design of a communication layer by clustering the sources based on a developed sensitivity methodology. A modified IEEE 13 bus feeder with integrating renewable energy sources shows a significant improvement in time of convergence. A real communication protocol is then applied to the system to analyze the communication effect of packet loss and latency on the given distributed control system. Furthermore, to demonstrate the voltage control problem on the hardware-in-the-loop system, the detailed steps to implement the simulation model in the OPAL-RT real-time simulator (RTS) are discussed. The results of RTS coordinate with the software modeling outcomes.

CONTENTS

List of Figure

List of Abbreviations and Acronyms

LFC	**Load Frequency Control**
MGCC	Micro Grid Central Controller
VSI	Voltage Source Inverter
DG	Distributed Generation
DER	Distributed Energy Resources
CSI	Current Source Inverter
MA	Multi Agent
RA	Regional Agent
LA	Local Agent
SA	Service Agent
PV	Photo Voltaic
BESS	Battery Energy Storage System
PVECS	Photovoltaic Energy Conversion System
SOC	State of Charge
SPWM	Sinusoidal Pulse Width Modulation
ESS	Energy Storage System

1 Introduction

1.1 Problem Statement

The electric power system is one of the largest interconnected systems in the world. It is dramatically changing due to the penetration of renewable energies. There is an ever-increasing trend in utilizing local renewable energies, such as solar energy or wind energy, in the power system [1]. The goal is to reduce the stress on the transmission lines and reduce carbon dioxide emissions. Increasing reliability and flexibility are two other reasons to encourage higher penetration of renewable energies in power systems. However, this will add some complexities to the control of the power system, especially in the islanded mode, where the voltage and frequency should be adjusted to supply the required active and reactive power. Since these low to non-inertia inverter-based generators are different from the conventional power sources with high inertia, controlling methods should be revised. In addition, the power rating of local distributed generators (DGs) is lower than large conventional generators; therefore, so many DGs are needed to serve the total load compared to the conventional power sources. Hence, the conventional centralized control algorithm may not be feasible due to the extensive

communications within the DGs and the control center. Considering these issues, the following questions are raised:

1- Is there any comprehensive modeling of microgrids (MGs), including DGs, networks and loads, that can be used for controlling purposes especially for the secondary voltage control?
2- How is it possible to control DGs to meet the load demands in a distributed way with less communication among the controllers rather than using a centralized algorithm?

Before designing any controller for a system, an important preliminary step is to have a detailed modular model that can be easily integrated into other systems.

The next significant step is to design a distributed controller for the system. Droop controllers are one of the most popular distributed algorithms that share the active and reactive power based on the rating of each DG. However, this controller might not be able to keep the voltage and frequency of the DGs at their nominal values. Therefore, a secondary controller is needed to readjust the voltage and frequency set-points of DGs to their nominal values. The centralized secondary controller has a high risk of single point of failure due to the high number of communication messages throughout the system. Thus, a distributed control algorithm considering the local nature of the voltage is proposed in this work.

1.2 Significance of Statement

The electric power grid, as the largest physical interconnected system in the world, has a significant impact on human life. For instance, high technology industries, residential loads, and electric vehicles all depend on a reliable electric power. This indicates the importance of having a reliable power system in the economy and the social welfare of any country in the world. A reliable power system needs a properly controlled structure that keeps the power grid

working even during a change of operating points or any other disturbances that might arise. Because of the recent advances in the power electronic devices, a higher penetration of renewable energies in the power system is used. Therefore, in any places where the solar irradiation or wind speed is sufficient, residential or industrial loads can be equipped to act as a generator. In these cases, any groups of these loads and generators can make a microgrid that can operate either in the islanded or grid-connected mode. Controlling structure for these microgrids are crucial because of the difference in power electronic sources and the synchronous power sources. Hence, in a stand-alone mode where there is very low or almost no inertia in the system, controllers of power electronic sources must act precisely and fast. This controller can compensate any imbalances between the sources and the loads in order to maintain the voltage and frequency within the normal limit. Moreover, the structure of the controller plays a significant role. In the systems with so many distributed generators (DGs), centralized controllers will be overwhelmed by the number of communication exchanges between the DGs and the centralized controller. Furthermore, there is always a chance of single point of failure in the centralized controller which can make it less reliable. Therefore, a distributed control algorithm that can act on local areas is designed here to improve the system reliability and efficiency.

1.3 Approach

The approach of this research study is as follows. First, a detailed model of a microgrid is studied. This model includes the modeling of sources, networks, and loads. An inverter based voltage source is modeled, which is a common distributed generator (DG) used as an interface between renewable energies and the grid. The models discussed in the literature are only considering the primary controller but not a secondary controller. Therefore, for the sake of regulating the voltage of the buses after any disturbances, the secondary voltage control is modeled as well.

After completing the model, in order to apply the secondary controller, the state space model is linearized around the operating point. The given approach is easily expandable since individual blocks for each part of the circuit have been used. In other words, a separated block is designed for the inverter, network, and load so that they can be connected to each other to make a system.

By having the state space model, different structures of controllers from a central one to a distributed one could be applied to the system. However, due to the risk of a single point of failure for the system in the centralized controller, a distributed controller is designed in this study. This controller is a distributed tracker controller in which each DG merely communicates with the DGs connected to it via the communication graph. Information that needs to flow in the circuit is only the bus voltages. Each PI controller finds the difference among its own bus voltage and the neighboring ones with the reference value. The calculated value changes the voltage set point to push all the voltages to go back to the reference value.

In the next step, the fact that the voltage has a local nature rather than a global one is considered in designing the secondary voltage controller. In other words, the voltage of a load bus that is far from a DG cannot be easily controlled with the DG itself; otherwise, many efforts have to be made to control the load bus voltage with that DG. Instead, it would be much more efficient to use the closer DGs to control the voltage of that bus. Therefore, in this part, a sensitivity analysis has been performed to find out the different voltage zones in power systems. A sensitivity matrix is derived from the Fast Decoupled Load Flow Jacobian matrix which relates the sensitivity of the voltage of load bus to the generating bus. After finding this matrix, a central controller is designed to find out the changes in each DG voltage set point in order to control the voltage of any load bus in the system. This controller finds out the set points by the

developed model which is based on the eigenvalue decomposition of the quadratic form of the given sensitivity matrix.

Although this is a fast controller, it is a centralized controller with a chance of single point of failure. Therefore, as the last step in this work, a real distributed algorithm is proposed that only needs the information from limited buses to control its own voltage area. This idea has been simulated in MATLAB and the results show the effectiveness of this methodology in controlling the voltages by the neighboring buses.

1.4 Overview

The rest of this dissertation consists of the following chapters:

- Chapter II: Literature Review:

In this section, an overview of previous work in modeling and control of renewable energies sources in MGs is given.

- Chapter III: State Space Modeling of Inverter Based Microgrids Considering Distributed Secondary Voltage Control:

In this chapter, a detailed state space modeling of the system is developed with the capability of controlling the secondary voltage level.

- Chapter IV: Optimal Voltage Control and Voltage Zoning Analysis

In this chapter, a sensitivity matrix has been designed which has been used for an optimal voltage controller in Chapter V.

- Chapter V: Proposed Distributed Microgrid Control on a Dynamic System

In this chapter, a comprehensive Microgrid model is developed to study the effect of distributed controls. The algorithm is applied to different microgrids and the findings show promising result.

- Chapter VI: Microgrid Simulation and Hardware-in-the-loop Testing:

In this chapter, the HIL testing of the microgrid model is developed. This model is ultimately used to analyze and verify a distributed voltage control in the system after losing a DG due to a fault in the system. The proposed system has proven to effectively control the voltage. The result of the real-time simulator matches closely with the result of software simulation with Matlab.

2 Literature Review

A typical hierarchical control structure for controlling the MGs is divided into three categories, namely primary, secondary, and tertiary control levels [2]. In a primary control level, droop controllers utilize local negative feedback to control the load disturbances in the system. The basic idea comes from synchronous generators that share any increase in the loads based on their ratings. The instantaneous increase in the power of demand will be compensated from the mechanical power of the rotor. The similar idea is used in the exciter control of synchronous machines (i.e. the voltage drops when the reactive power is increasing). These two characteristics are implemented in power electronic MGs via two droop Equations [3]. However, primary control may not be able to bring back the voltage and the frequency of the system to its normal point hence a secondary controller is applied to the system. The secondary controller can set the operating point based on the centralized controller. The global minimum can be found with the centralized method but some disadvantages such as a single point of failure and communication limitations restrict its efficiency. Hence, a distributed controller is taking much more attraction as an alternative method to the centralized controller [4].

Previous dynamic analysis of standalone MGs has been carried out with some simplifying assumptions in the modeling of the system [5]; therefore, the analysis of the voltage control is not accurate for these models. In [6], a simple inductance L is modeled as the output filter while an RLC is needed to filter the high-frequency modes. In [7], a single MG connected to an AC stiff bus is modeled; therefore, the interaction among the inverters has not been considered. In [8], multiple ideal inverter based MGs have been modeled without modeling the fast response of the voltage control and the current control loops. In a high switching frequency, dynamics

of these two loops cannot be neglected. In [9], a secondary voltage controller has been proposed on a MG with multiple DGs while the frequency effect on the inductance load and transmission lines is not considered. In [5], a comprehensive small signal model for inverter based MGs has been considered with considering the primary control loop only. In [10], a secondary controller is proposed but only for the frequency control. In this dissertation, the present model is expanded by modeling the secondary voltage controller.

In a Secondary Voltage Control (SVC), due to the local nature of voltage control and reactive power, the regional analysis should be done [11]; otherwise, controlling a voltage bus from a long distance needs many efforts and might not be reasonable. Different papers proposed on SVC used the pilot buses in the system in which total voltage profile can be controlled by a class of disturbance [12, 13, 14]. The procedure of finding pilot buses is nontrivial since it can be a nonlinear and combinatorial problem [15]. Considering different assumptions such as minimizing active power losses, reactive power injection or voltage deviation, different pilot buses can be found for the system [16]. In [17], the zoning evaluation has been done for AVR in the primary controller. Reference [18] uses a sensitivity matrix to identify voltage control areas rather than proposing an algorithm to control the system. In [19], the voltage control has been proposed by considering the zonal effect but it has a high chance of trial and error [20]. An optimal control that is controlling the voltages of a power system with considering the zonal effect at the same time is exploited in my study in [21]. Since in transmission level, the reactance of the lines is much more than the resistance of the lines, reactive power control can be assumed to be decoupled from the active power. Therefore, Fast Decoupled Load Flow Jacobian (FDLFJ) has been used to find system zonal areas. In other words, from FDLFJ, the sensitivity matrix is made that shows the sensitivity of load buses to generator buses. The Eigen Value Decomposition (EVD) has been applied to this sensitivity matrix to find the best set of inputs (voltage of generators) that can control the optimal output (voltage of violated buses).

This set of inputs will indicate the participation of each generator to compensate a voltage violation. However, a conflict can happen in case of controlling the multiple voltage violations. In this part of the dissertation, the conflict is resolved by modifying the given set of inputs coming from the EVD based on the conflicted zone. In the next part, the sensitivity matrix found from FDLFJ can be used to utilize the real distributed secondary voltage controller in each zone instead of the centralized method used in Chapter IV.

In the secondary controller, some researchers have used a centralized algorithm to achieve the global minimum. However, due to high dependability of this algorithm to the communication network, the probability of single point of failure is very high. Hence, the distributed algorithm has been proposed in [22] to alleviate a single point of failure. In these algorithms, researchers have been working on DGs to communicate together to reach their voltages to a synchronous value or to an average value. In other words, neighboring DGs will communicate together to reach an agreement that can be a reference value or an average value. This method is called distributed voltage consensus. While in this method, each DG communicates only with its neighboring DGs, eventually the messages broadcast throughout the whole system. In this dissertation, it is emphasized that the voltage control is a local phenomenon rather than a global one. Therefore, the real distributed algorithm only works on individual zones of power systems that can have maximum effect on the area of error around them. Therefore, in this dissertation the DGs that are in close vicinity and not just neighboring nodes in terms of the communication network are used to control the system.

The remainder of this dissertation is given as follows: In Chapter III, a comprehensive modeling of Microgrids considering VCVSIs, Networks, and Loads is given with the aim of developing a secondary voltage control. In Chapter IV, zonal analysis and optimal voltage control based on the EigenValue Decomposition is given. In Chapter V, simulation from

applying a real distributed voltage control with the consensus method on each zone is given. Furthermore, in Chapter VI, a hardware in the loop testing of the proposed microgrid model is given.

3 State Space Modeling of an Inverter Based Microgrid Considering Distributed Secondary Voltage Control

3.1 Introduction

Microgrids (MGs) are a smaller scale of power systems that integrate high penetration of renewable energies and energy storage systems (ESSs) into the grid. Power electronic converters are used as the interface between the grid and renewable energies such as solar power, wind power, and fuel cells. Utilizing renewable energies in MGs as well as the flexibility of MGs in connecting and disconnecting to/from the grid is counted as two main advantages of MGs over the conventional power systems.

Appropriate control of high penetration renewable energies in power systems requires a complete modeling of the system. In this work, a comprehensive state space modeling of voltage source inverters, networks, and loads is studied specifically for a distributed voltage controller. A fully distributed control algorithm in this work only requires the local communication network among the each cluster of distributed generators rather than the whole system. The proposed secondary voltage control model is applied on a microgrid with three DGs and two loads to verify the results.

The rest of the chapter is structured as follows: In Section 3.2, the state space model of a voltage control voltage source inverters (VCVSI) with considering the secondary voltage control is developed. A modeling of the network and load is also discussed in this section. In Section 3.2.4, a distributed voltage controller is explained. In Section 3.4, the simulation for a MG with 3 DGs has been shown and finally, the conclusion is given in Section 3.5.

3.2 Microgrid Model

3.2.1 VCVSI Model

The dynamical system of a VCVSI can be described with a nonlinear differential Equation in (3-1)

$$\dot{x} = f(x(t), u(t), t) \tag{3-1}$$

A linearized model of the form (3-1) around the nominal operating point can be found by considering the first order of Taylor Series expansion as in (3-2) and (3-3):

$$\dot{x}(t) = \mathrm{x}_0 + \Delta \mathrm{x}(t) \tag{3-2}$$

$$\dot{x}(t) = \mathrm{f}(x_0(t), u_0(t), \mathrm{t}) + \mathrm{A}\Delta x(t) + B\Delta u(t) \tag{3-3}$$

where $A = \frac{\partial f}{\partial x}(x_0(t), u_0(t), B = \frac{\partial f}{\partial u}(x_0(t), u_0(t), t)$

By using Equations (3-2) and (3-3), the state space model of a VCVSI can be found. VCVSI are commonly used as an interface between renewable energies and the grid in the stand-alone mode. In this mode, the voltage and frequency of the system should be controlled via DGs of the system, hence VCVSIs are appropriate interfaces used in MGs.

A VCVSI consists of a DC link, three leg inverters, an RLC filter, and an RL coupling inductor. The controller part of the VCVSI consists of three parts including a power controller, a voltage controller, and a current controller which has been shown in Figure 3-1. A secondary voltage controller will be applied to the voltage set-point v_n as it shown in Figure 3-1. In the next

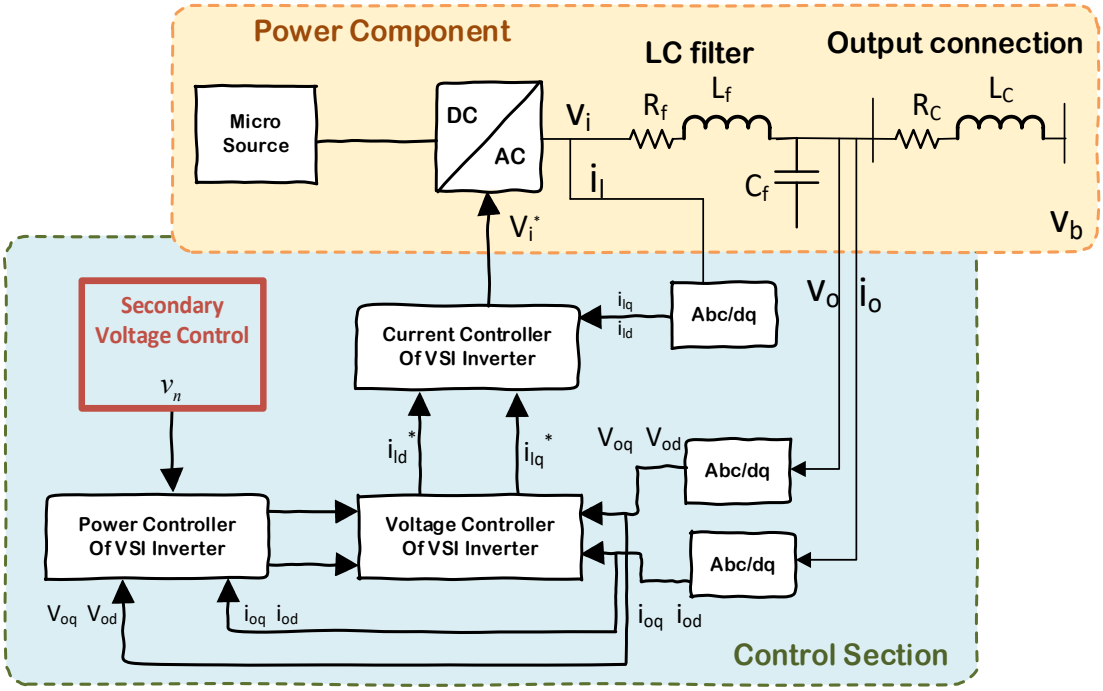

Figure 3-1: Block diagram of VCVSI [45]

section, each part of the controller is explained according to the method of ref. [5].

3.2.1.1 Power controller

In a transmission system with a high transmission line ratio (X>>R), active power and reactive power are decoupled and can be controlled by the angle and magnitude of the bus voltage respectively. Therefore, the power flow can be managed via the voltage of each bus (i.e. phase and magnitude). In conventional power systems, adjusting of active power is automatically done in the synchronous machines. In the case of changing of electrical load in the system, the

required new power is automatically compensated from the kinetic energy of the rotor of each generator which is dependent on the respective rotor size. The transfer of kinetic energy to electric energy changes the frequency of the rotor leading to the change of the electric frequency. Therefore, the active power is shared among the synchronous machines based on their ratings. The similar approach is implemented in the exciter of synchronous machines to control the reactive power of loads by changing the voltage magnitude. However, inverter based MGs cannot automatically share the active or reactive power since they have either low or null interia. As a result, the following controlling method explained in the next section is applied to the inverter based MGs to make them capable of automatically sharing the active and reactive power among themselves similar to the synchronous machines.

The three blocks of inverter based microgrids consist of:

3.2.1.1.1 Power calculation block

Calculates the output power in the system via (3-4,3-5):

$$p = v_{od} i_{od} + v_{oq} i_{oq} \tag{3-4}$$

$$p = v_{od} i_{oq} - v_{oq} i_{od} \tag{3-5}$$

3.2.1.1.2 Low pass filter

Due to the high switching impact of the inverter-based MGs on voltage and currents, a low pass filter is used in (3-6, 3-7) to filter the high-frequency distortion of MGs:

$$\mathrm{P} = \left(\frac{\omega_{c0}}{s + \omega_{c0}}\right) P \tag{3-6}$$

$$\mathrm{Q} = \left(\frac{\omega_{c0}}{s + \omega_{c0}}\right) \mathrm{q} \tag{3-7}$$

3.2.1.1.3 Power Controller

The primary controller consists of two droop controllers that represent two negative feedback controllers to share the active and reactive power based on the rating of the sources in MGs:

$$\omega = \omega_n - m\,P \tag{3-8}$$

$$v_{od}^{*} = V_n - nQ \tag{3-9}$$

$$v_{oq}^{*} = 0 \tag{3-10}$$

Where m and n are the droop gains that are calculated based on the rating of DGs as in (3-11, 3-12):

$$m = \frac{\Delta\omega_{max}}{P_{max}} \tag{3-11}$$

$$n = \frac{\Delta V_{od\,max}}{Q_{max}} \tag{3-12}$$

In order to construct the complete model of a whole MG system, everything should be transformed to a common reference frame. Here the angle of inverter 1 is assumed to be the reference, hence all other DGs' angles are calculated from (3-13). It is worth mentioning that this is a similar assumption on the transmission level where the angle of the slack bus is picked to be the reference angle (i.e. zero) and all other angles are calulcated based on it.

$$\delta = \int(\omega - \omega_{com}) \tag{3-13}$$

$$\dot{\delta} = \omega - \omega_{com} \tag{3-14}$$

By using Taylor Series, Equations (3-6 to 3-10) can be written in a small signal form as in (3-15 and 3-16):

$$\begin{bmatrix}\Delta\dot{\delta}\\ \Delta\dot{P}\\ \Delta\dot{Q}\end{bmatrix} = A_p\begin{bmatrix}\Delta\delta\\ \Delta P\\ \Delta Q\end{bmatrix} + B_p\begin{bmatrix}\Delta i_{ldq}\\ \Delta v_{odq}\\ \Delta i_{odq}\end{bmatrix} \tag{3-15}$$

$$A_p = \begin{bmatrix}0 & -m_p & 0\\ 0 & -\omega_c & 0\\ 0 & 0 & -\omega_c\end{bmatrix}, B_p = \begin{bmatrix}0 & 0 & 0 & 0 & 0 & 0\\ 0 & 0 & \omega_c I_{od} & \omega_c I_{oq} & \omega_c V_{od} & \omega_c V_{oq}\\ 0 & 0 & \omega_c I_{oq} & -\omega_c I_{od} & -\omega_c I_{oq} & \omega_c V_{od}\end{bmatrix}$$

$$\begin{bmatrix}\Delta\omega\\ \Delta v^*_{odq}\end{bmatrix} = \begin{bmatrix}C_{pw}\\ C_{pv}\end{bmatrix}\begin{bmatrix}\Delta\delta\\ \Delta P\\ \Delta Q\end{bmatrix} + \begin{bmatrix}0\\ B\_pvn\end{bmatrix}[\Delta v_n] \tag{3-16}$$

$$\mathrm{C_{pw}} = [0 \quad -\mathrm{m_p} \quad 0], \mathrm{C_p} = \begin{bmatrix}0 & 0 & -\mathrm{n_q}\\ 0 & 0 & 0\end{bmatrix}, \mathrm{B_{pvn}} = \begin{bmatrix}1\\ 0\end{bmatrix}$$

3.2.2 Voltage controller

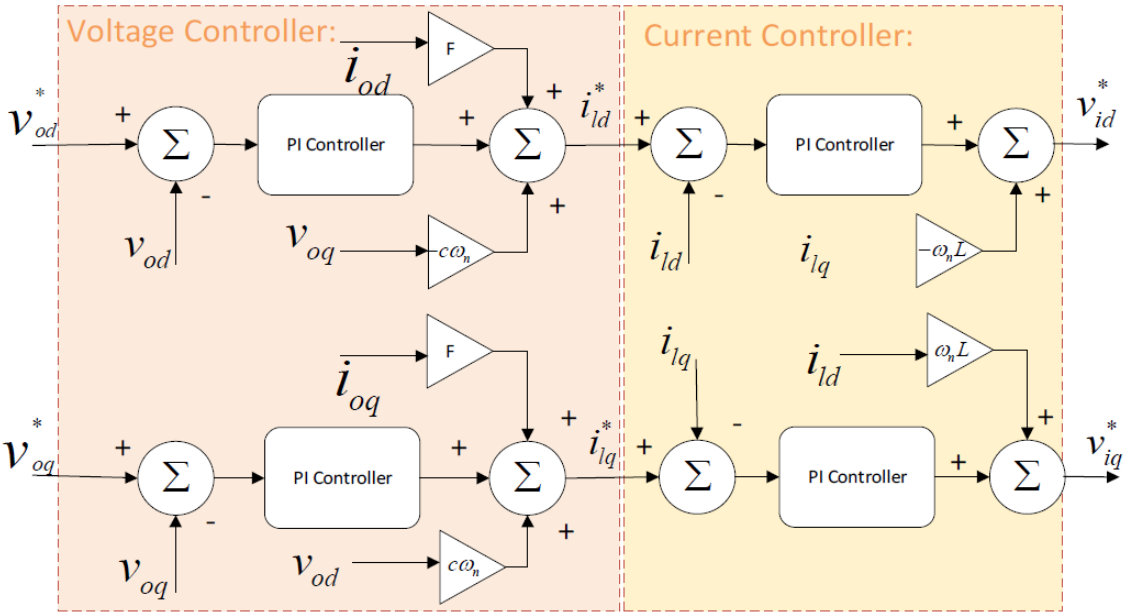

Figure 3-2 Circuit diagram for voltage controller and current controller [23]

A voltage controller with standard PI controller considering the feedbacks and feedforwards is shown in Figure 3-2 and formulated in (3-17 to 3-19).

$$\dot{\phi}_{dq} = v^*{}_{odq} - v_{odq} \tag{3-17}$$

$$i^*_{ld} = Fi_{od} - \omega_n C_f v_{oq} + K_{pv(vStar_{od}-v_{od})} + k_{iv}\phi_d \tag{3-18}$$

$$i^*_{lq} = Fi_{oq} + \omega_n C_f v_{od} + K_{pv(vStar_{oq}-v_{oq})} + k_{iv}\phi_q \tag{3-19}$$

Equation (3-17) can be rewritten by using Equation (3-14) as in (3-20):

$$[\Delta\dot{\phi}_{dq}\,] = B_{v1}C_{pv}\begin{bmatrix}\Delta\delta\\ \Delta P\\ \Delta Q\end{bmatrix} + B_{v2}\begin{bmatrix}\Delta i_{ldq}\\ \Delta v_{odq}\\ \Delta i_{odq}\end{bmatrix} + B_{v1}B_{pvn}[\Delta V_n] \tag{3-20}$$

$$B_{v1} = \begin{bmatrix}1 & 0\\ 0 & 1\end{bmatrix}, B_{v2} = \begin{bmatrix}0 & 0 & -1 & 0 & 0 & 0\\ 0 & 0 & 0 & -1 & 0 & 0\end{bmatrix}$$

3.2.3 Current Controller

A Current controller which is shown in Figure 3-2 can be used to find out the set points for the input voltage references as shown in (3-21 to 3-23):

$$\dot{\gamma}_{dq} = i^*_{ldq} - i_{ldq} \tag{3-21}$$

$$V^*_{id} = -\omega_n L_f i_{lq} + K_{pc}(i^*_{ld} - i_{ld}) + K_{ic}\gamma_d \tag{3-22}$$

$$V^*_{iq} = -\omega_n L_f i_{ld} + K_{pc}\left(i^*_{lq} - i_{lq}\right) + K_{ic}\gamma_q \tag{3-23}$$

A small signal model of Equation (3-21) can be rewritten by using Equations (3-9, 3-10, 3-18, 3-19) as in (3-24):

$$[\Delta\dot{\gamma}_{dq}] = [0][\Delta\gamma_{dq}] + B_{c1}D_{v1}C_{pv}\begin{bmatrix}\Delta\delta\\ \Delta P\\ \Delta Q\end{bmatrix} + (B_{c1}D_{v2} + B_{c2})\begin{bmatrix}\Delta i_{ldq}\\ \Delta v_{odq}\\ \Delta i_{odq}\end{bmatrix} + B_{c1}C_v[\Delta\phi_{dq}] + B_{c1}D_{v1}B_{pvn}[\Delta v_n] \tag{3-24}$$

3.2.4 Output RLC Filter and Coupling Filter

Nonlinear Equations for the output filter regulating the high frequency distortions as well as the coupling filter are given in (3-2 to 3-30):

$$\frac{di_{ld}}{dt} = -\frac{r_f}{L_f}\,i_{ld} + \omega i_{lq} + \frac{1}{L_f}v_{id} - \frac{1}{L_f}v_{od} \tag{3-25}$$

$$\frac{di_{lq}}{dt} = -\frac{r_f}{L_f}\,i_{lq} + \omega i_{ld} + \frac{1}{L_f}v_{iq} - \frac{1}{L_f}v_{oq} \tag{3-26}$$

$$\frac{dv_{od}}{dt} = \omega v_{oq} + \frac{1}{C_f}i_{ld} - \frac{1}{C_f}i_{od} \tag{3-27}$$

$$\frac{dv_{oq}}{dt} = -\omega v_{od} + \frac{1}{C_f} i_{lq} - \frac{1}{C_f} i_{oq} \tag{3-28}$$

$$\frac{di_{od}}{dt} = -\frac{r_c}{L_c}\, i_{od} + \omega i_{oq} + \frac{1}{L_c} v_{od} - \frac{1}{L_c} v_{bd} \tag{3-29}$$

$$\frac{di_{oq}}{dt} = -\frac{r_c}{L_c}\, i_{oq} - \omega i_{od} + \frac{1}{L_c} v_{oq} - \frac{1}{L_c} v_{bq} \tag{3-30}$$

By using Equation (3-18, 3-19) and Equations (3-22, 3-23) with the assumption that $v_{idq} = v^*_{idq}$, the state space modeling of this part can be derived as in (3-31):

$$\begin{bmatrix} \Delta i_{ldq} \\ \Delta \dot{v}_{odq} \\ \Delta i_{odq} \end{bmatrix} = (A_{LCL} + B_{LCL1}[D_{c1}D_{v2} + D_{c2}]) \begin{bmatrix} \Delta i_{ldq} \\ \Delta v_{odq} \\ \Delta i_{odq} \end{bmatrix} + B_{LCL1}D_{c1}D_{c1}C_{pv} \begin{bmatrix} \Delta\delta \\ \Delta P \\ \Delta Q \end{bmatrix}$$
$$+B_{LCL1}C_c[\Delta\gamma_{dq}] + B_{LCL1}D_{c1}C_v[\Delta\phi_{dq}] + BLCL2[\Delta v_{bdq}] + B_{LCL3}[\Delta\omega]$$
$$+B_{LCL1}D_{c1}D_{v1}B_{pvn}[\Delta v_n] \tag{3-31}$$

$$C_v = \begin{bmatrix} k_{iv} & 0 \\ 0 & k_{iv} \end{bmatrix}, D_{v1} = \begin{bmatrix} K_{pv} & 0 \\ 0 & K_{pv} \end{bmatrix}, CD_v = \begin{bmatrix} 0 & 0 & -K_{pv} & -\omega C_f & F & 0 \\ 0 & 0 & \omega c_f & -K_{pv} & 0 & F \end{bmatrix}$$

Equations of (3-15, 3-16, 3-20, 3-24, 3-31) can be used to find out the complete state space model for each inverter as in (3-32).

$$[\Delta \dot{x}_{invi}] = A_{INVi}[\Delta x_{INV}] + B_{INVi[\Delta v_{bdq}]} + B_{i\omega com[\Delta\omega_{com}]} + B_{vn}[\Delta v_n] \tag{3-32}$$

However, in order to combine all of the inverters model together, the transformation Equation (3-33) is needed to transform each reference frame to a common reference frame:

$$[\mathrm{f_{oDQ}}] = [\mathrm{T_s}][\mathrm{f_{odq}}] \tag{3-33}$$

Where $T_s = \begin{bmatrix} \cos(\delta_i) & -\sin(\delta_i) \\ \sin(\delta_i) & \cos(\delta_i) \end{bmatrix}$.

The small signal of (3-33) is given in (3-34):

$$[\Delta f_{oDQ}] = T_s(0)[\Delta f_{odq}] + T_c(0)[\Delta\delta] \tag{3-34}$$

Where $T_c = \begin{bmatrix} -F_{od}\sin(\delta_i) & -F_{oq}\cos(\delta_i) \\ F_{od}\cos(\delta_i) & -F_{oq}\sin(\delta_i) \end{bmatrix}$

By assuming i_o (or v_b) as the output of each inverter, then Equation (3-34) can be used to transform the output of each inverter to the common reference frame:

$$[\Delta i_{ODQ}] = [T_S(0)][\Delta i_{odq}] + [T_C(0)][\Delta\delta] \tag{3-35}$$

On the other hand,v_b (or i_o) is assumed to be the input signal to each inverter; therefore, reverse transformation is used as in (3-36):

$$[\Delta v_{bdq}] = [T_S(0)]^{-1}[\Delta v_{bDQ}] + [T_{V(0)}]^{-1}[\Delta\delta] \tag{3-36}$$

Where $T_V^{-1} = \begin{bmatrix} -V_{bD}sin(\delta_i) + V_{bD}cos(\delta_i) \\ -V_{bD}cos(\delta_i) - V_{bD}sin(\delta_i) \end{bmatrix}$

$$A_{INi} = \begin{bmatrix} A_{Pi} & 0 & 0 & B_{Pi} \\ B_{V1i}C_{Pvi} & 0 & 0 & B_{V2i} \\ B_{C1i}D_{V1i}C_{Pvi} & B_{C1i}C_{Vi} & 0 & B_{c1i}D_{v2i} + B_{C2i} \\ B_{LCL1i}D_{C1i}D_{V1i}C_{Pvi} + B_{LCL3i}C_{P\omega i} + B_{LCL2i}[T_{Vi}^{-1} \quad 0 \quad 0] & B_{LCLi}D_{C1i}C_{Vi} & B_{LCL1i}C_{Ci} & A_{LCLi} + B_{LCL1i}(D_{Ci}D_{V2i} + D(\end{bmatrix}$$

3.2.5 Aggregated State Space Model of All Inverters

Equations (3-35) and (3-36) can be used to find the state space model of each inverter in the common reference frame as in the Equation (3-37):

$$[\Delta\dot{x}_{INVi}] = A_{INVi}[\Delta x_{INVi}] + B_{INVi}[\Delta v_{bDQi}] + B_{p\omega com}C_{INVcom}[\Delta x_{INVcom}] + B_{iVn}[\Delta v_n] \tag{3-37}$$

$$B_{INVi} = \begin{bmatrix} 0 \\ 0 \\ 0 \\ B_{LCL2}T_S^{-1} \end{bmatrix}, B_{i\omega com} = \begin{bmatrix} B_{P\omega com} \\ 0 \\ 0 \\ 0 \end{bmatrix}, C_{INVcom} = \begin{bmatrix} C_{p\omega} \\ 0 \\ 0 \\ 0 \end{bmatrix}^T, B_{iVn} = \begin{bmatrix} 0 \\ B_{V1}B_{pvn} \\ B_{C1}D_{v1}B_{pvn} \\ B_{LCL1}D_{c1}D_{v1}B_{pvn} \end{bmatrix}$$

In a MG with several DGs, a combined inverter model that includes the whole state space model is shown in (3-38):

$$[\Delta \dot{x}_{INV}] = A_{INV}[\Delta x_{INV}] + B_{INV}[\Delta v_{bDQ}] + B_{Vn}[\Delta v_n] \tag{3-38}$$

$$A_{INV} = \begin{bmatrix} A_{INVcom} + B_{1\omega com}C_{INVcom} & 0 & \dots & 0 \\ B_{2\omega com}C_{INVcom} & A_{INV2} & \dots & 0 \\ \dots & \dots & \dots & 0 \\ B_{s\omega com}C_{INVcom} & 0 & 0 & A_{INVs} \end{bmatrix}_{13s*13s}$$

$$B_{INV} = \begin{bmatrix} B_{INVcom} \\ B_{INV2} \\ \dots \\ B_{INVs} \end{bmatrix}, B_{Vn} = \begin{bmatrix} B_{iVN} \\ B_{iVN} \\ \dots \\ B_{iVN} \end{bmatrix}, C_{INVc} = \begin{bmatrix} C_{INVc1} & 0 & 0 & . \\ 0 & C_{INVc2} & 0 & . \\ . & . & . & . \\ . & . & . & C_{INVcs} \end{bmatrix}$$

3.2.6 Network model

A network consists of ‘s’ inverters, ‘n’ lines ad m’ nodes. In a network with RL lines, the inductor current is the state variable and the Equations for the whole network can be written as follows in (3-39):

$$[\Delta i_{lineDQ}] = A_{NET}[\Delta i_{lineDQ}] + B_{1NET}[\Delta v_{bDQ}] + B_{2NET}\Delta\omega_{com} \tag{3-39}$$

$$A_{NET} = \begin{bmatrix} A_{NET1} & 0 & \dots & 0 \\ 0 & A_{NET2} & \dots & 0 \\ \dots & \dots & \dots & \dots \\ 0 & 0 & \dots & A_{NET1} \end{bmatrix}_{2n*2n}, B_{1NET} = \begin{bmatrix} B_{1NET1} \\ B_{1NET2} \\ \cdots \\ B_{1NETn} \end{bmatrix}_{2n*1}, B_{2NET} = \begin{bmatrix} B_{2NET1} \\ B_{2NET2} \\ \cdots \\ B_{2NETn} \end{bmatrix}_{2n*1}$$

$$B_{1NETi} = \begin{bmatrix} \dots & \frac{1}{L_i} & 0 & \dots & \frac{-1}{L_i} & 0 & \dots \\ \dots & 0 & \frac{1}{L_i} & \dots & 0 & \frac{-1}{L_i} & \dots \end{bmatrix}, A_{NETi} = \begin{bmatrix} \frac{-r_i}{L_i} & \omega_0 \\ \omega_0 & \frac{-r_i}{L_i} \end{bmatrix}, B_{2NETi} = \begin{bmatrix} I_{Qi} \\ -I_{Di} \end{bmatrix}$$

3.2.7 Load Model

RL load model that is considered in this work is similar to the network model in Equation (3-40):

$$[\Delta i_{loadDQi}] = A_{load}[\Delta i_{loadDQ}] + B_{1LOAD}[\Delta v_{bDQ}] + B_{2LOAD}\Delta\omega_{com} \quad (3\text{-}40)$$

Where A_{load}, B_{1LOAD} and B_{2lOAD} are similar to the matrices A_{NET}, B_{1NET}, B_{2NET} respectively as it is explained in [5].

3.2.8 Complete Microgrid State Space Model

State space modeling for inverters, lines, and loads have been defined in (3-38 to 3-40). In order to make sure that the node voltage is well-defined and numerical solution exists, a virtual resistor r_N is added between each node and the ground [5] and [24]. The value of r_N is chosen to be high (1000 Ohms) so that it does not affect the results. The Equations of each node can be written as in (3-41, 3-42):

$$v_{bDi} = r_N(i_{oDi} - i_{loadDi} + i_{lineDi,j}) \quad (3\text{-}41)$$

$$v_{bQi} = r_N(i_{oQi} - i_{loadQi} + i_{lineQi,j}) \quad (3\text{-}42)$$

Now for connecting the DGs to the network and loads, the following Equation can be used:

$$[\Delta v_{bDQ}] = R_N M_{INV}[\Delta i_{loadDQ}] + R_N M_{load}[\Delta i_{loadDQ}] + R_N M_{NET}[\Delta i_{lineDQ}] \quad (3\text{-}43)$$

Where matrix $M_{INV(2m*2s)}$ connects the inverters to the nodes. The entries of this matrix is one if DG-i is connected to the node j and zero otherwise. Matrix $M_{load(2m*2p)}$ connects the nodes to the loads with -1 as its entry and zero otherwise. Matrix $M_{NET(2m*2n)}$ maps the connecting lines onto the network nodes where it is 1 or -1 depending on entering the line current or leaving the node. Finally, $R_{N(2m*2m)}$ is a diagonal matrix which has r_N as its diagonal entries. Now the whole state space modeling can be written by using Equations (3-38, 3-39,3-40, 3-43) as in (3-44):

$$\begin{bmatrix} \Delta\dot{x}_{INV} \\ \Delta i_{lineDQ} \\ \Delta i_{loadDQ} \end{bmatrix} = A_{mg} \begin{bmatrix} \Delta x_{INV} \\ \Delta i_{lineDQ} \\ \Delta i_{loadDQ} \end{bmatrix} + B_{vn}\Delta V_n \quad (3\text{-}44)$$

$$A_{mg} = \begin{bmatrix} A_{INV} + B_{INV}R_N M_{INV} C_{INVc} & B_{INV}R_N M_{NET} & B_{INV}R_N M_{load} \\ B_{1NT}R_N M_{INV} C_{INVc} + B_{2NET} C_{INV\omega} & A_{NET} + B_{1NET}R_N M_{NET} & B_{1NET}R_N M_{load} \\ B_{1load}R_N M_{INV} C_{INVc} + B_{2LOAD} C_{INV\omega} & B_{1LOAD}R_N M_{NET} & A_{load} + B_{1LOAD}R_N M_{LOAD} \end{bmatrix}, B_{vn} = \begin{bmatrix} B_{Vn} \\ 0 \\ 0 \end{bmatrix}$$

3.3 Distributed Secondary Voltage Control

An autonomous controller in primary level stabilizes the system and shares the load based on the ratings of each inverter. The primary control level is automatic and it does not rely on communication. However, it might not be able to bring back the voltages to their nominal values. Hence, the secondary control level is applied to the system.

In the secondary control level, the voltage set point (i.e. v_n in Equation (3-9)) will be adjusted to regulate the output voltage. A distributed cooperative tracker algorithm is proposed in [22]. In this algorithm, only the immediate neighbors share the voltage output among each other. The reference voltage is just needed to be known by one of the DGs that is connected to any other DGs in the system directly or indirectly (i.e. communication system has a spanning tree). The differences between the neighboring voltages are calculated as it is shown in Equation (3-45) and Figure 3-1 to change the v_n . In addition, only the root node considers the difference between its voltage and the v_{ref} (i.e. g_i=1 for the root node and zero for the other nodes).

$$\Delta v_{ni} = c_{vi} \int \left(\Sigma_j \, a_{ij}(v_{odi} - v_{odj}) + g_i(v_{odi} - v_{ref}) \right) dt \qquad (3\text{-}45)$$

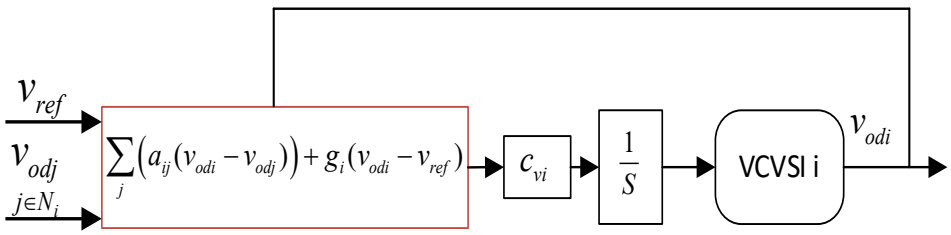

Figure 3-3 : Distributed secondary voltage control [22]

3.4 Simulation

A system with 3 DGs and 2 loads is studied here. The state space modeling of the system has been calculated based on the Equation (3-43) and is implemented in Matlab Simulink. System parameters including controller parameters are shown in Table 3-1. Initial condition of the system is shown in Table 3-2 and can be found from the load flow solution. However, the nonlinear model of the system can also be used to find the initial condition [5]. At the time equal to 0.2 seconds, a load disturbance is added to the system. Then, the secondary controller is activated at t=1 second to show how it improves the voltage deviation after the disturbance.

Table 3-1: UNDERSTUDIED SYSTEM PARAMETERS

Inverters Parameters

rf	**0.1 Ω**	**Lc**	**0.35 mH**	**Kpc**	**10.5**	**mp**	**9.4e-5**
Lf	1.35 mH	ωc	31.41	Kic	16e3	nq	1.3e-3
Cf	50 µF	rc	0.03 Ω	Kpv	0.05	Kiv	390
Cv [-5 10 -10]		g1	1	a12	1	a13	1

Table 3-2: Initial Conditions [5]

Par.	Value	Par.	Value
V_{odq}	$\begin{bmatrix} 380.8 & 381.8 & 380.4 \\ 0 & 0 & 0 \end{bmatrix}$	V_{bd}	$\begin{bmatrix} 379.5 & 380.5 & 379 \\ -6 & -6 & -5 \end{bmatrix}$
I_{odq}	$\begin{bmatrix} 11.4 & 11.4 & 11.4 \\ 0.4 & -7.3 & -4.3 \end{bmatrix}$	I_{ldq}	$\begin{bmatrix} 11.4 & 11.4 & 11.4 \\ -5.5 & -7.3 & -4.6 \end{bmatrix}$
$I_{line1dq}$	$\begin{bmatrix} -3.8 \\ 0.4 \end{bmatrix}$	$I_{line2dq}$	$\begin{bmatrix} 7.6 \\ -1.3 \end{bmatrix}$
ω_0	314	δ_0	$[0 \quad 1.9e-3 \quad -0.0113]$

3.4.1 Scenario one

In the first scenario, the voltage profile is regulated via an ideal distributed algorithm which has been explained in the previous section. It can be seen from Figure 3-4 that the voltages are going back to their normal operating points by changing the voltage set points of each inverter.

3.4.2 Scenario Two

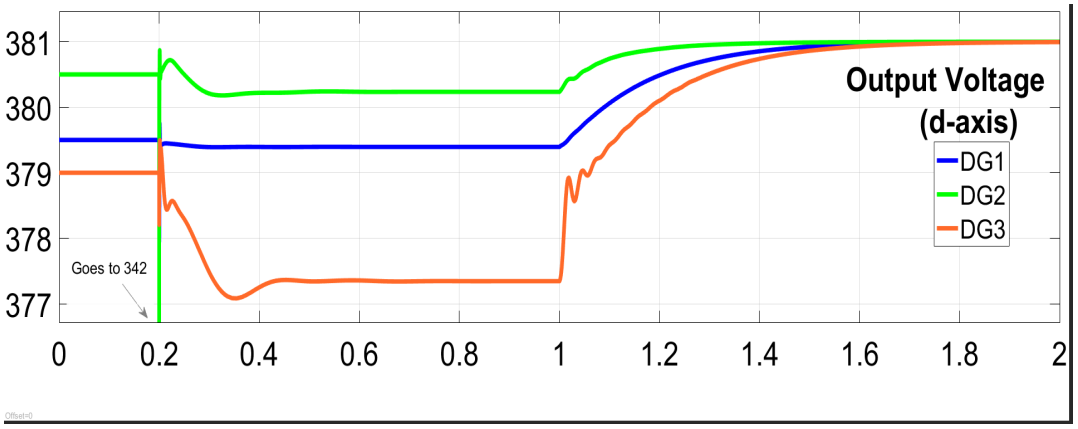

Figure 3-4: Output voltage profile

In the second scenario, a time delay of 0.1 seconds is added to the system. Although the system has more oscillations and needs more time to reach its steady state value, it becomes stable eventually. The result is shown in Figure 3-5.

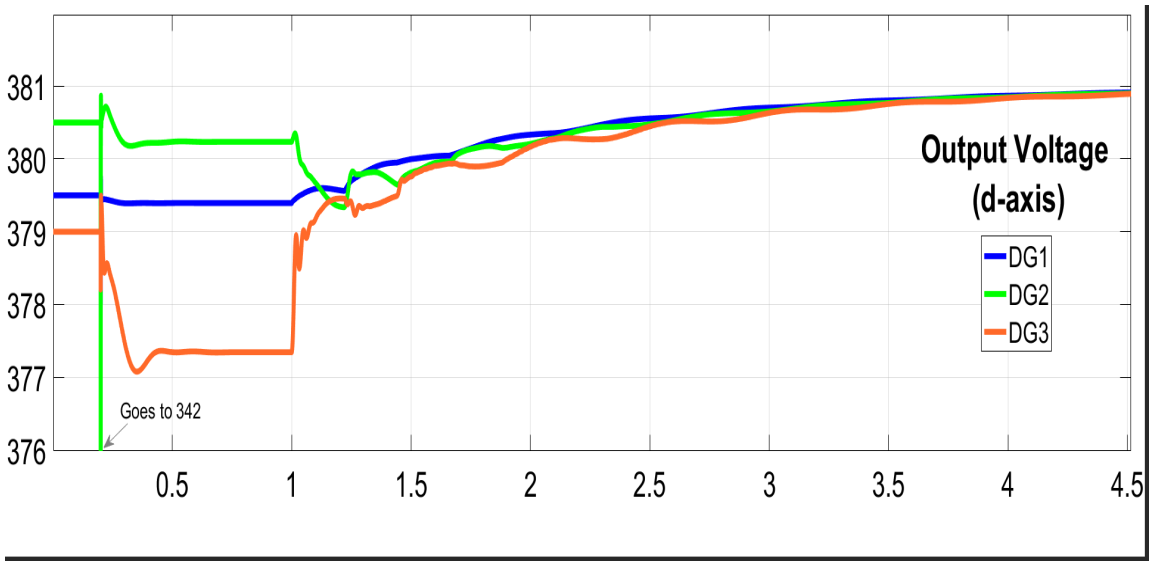

Figure 3-5: Output voltage profile with considering delay

3.5 Conclusion

In this chapter, a secondary voltage control has been developed for a comprehensive state space modeling of an inverter-based MG which was introduced in [4]. A distributed control algorithm has been applied to the proposed state space model to verify the model. The results show that the secondary voltage control achieves its goal via the proposed state space model.

4 Optimal Steady State Voltage Control and Zoning Analysis

4.1 Introduction

Voltage control has been known as one of the important issues in the power system for decades [14]. As an example, the blackout in Western Europe was caused by the phenomenon of voltage collapse [25]. Different voltage control devices for injecting reactive power have been used such as synchronous condensers [26], tap changer transformers [27], capacitor banks [28], and Flexible AC transmission systems (FACTS) [29, 30]. Voltage controllers are typically categorized in a hierarchical structure including three levels: primary, secondary, and tertiary levels [31, 32, 17]. In the primary control, the voltage is controlled locally and instantly through the Automatic Voltage Control (AVR). It might be seen that the voltage profile is not still optimal after applying the primary controllers. Therefore, the secondary voltage controllers have been used to bring back the voltage to its nominal value. The time constant of the secondary controllers is more than the primary controllers to prevent interaction between these two types of controllers. In the tertiary level, other controlling objectives such as an economic dispatch and optima power flow are met [33, 34]. In this section of the dissertation, the following two methods are designed. First, a voltage sensitivity matrix is developed which divides the system into different voltage zones. Second, a steady state secondary voltage control derived from the voltage sensitivity matrix is designed to control the voltage of the load buses. This control is a steady state feedforward control. The assumption here is that the system is stable while the controller setpoints is adjusted based on the proposed model.

The remainder of this section has been organized as follows: In Section 4.2, the preliminary math on eigenvector and eigendecomposition has been explained. In Section 4.3, problem formulation and objectives are explained. In Section 4.4, the proposed method has been implemented in four different IEEE case studies. Finally, in Section 4.5, the conclusion is given.

4.2 Preliminary Math on Eigenvalue Decomposition

An eigenvector is a special vector (V) of matrix A which results in another vector with the same direction when multiplied by matrix A. The magnitude of this multiplication is scaled by its corresponding eigenvalue as it is shown in Equation (4-1) and illustrated in Figure 4-1:

$$\mathrm{AV} = \Lambda \mathrm{V} \tag{4-1}$$

Where $V = [v_1 v_2 \dots v_n]$ is a set of eigenvectors of matrix A and $\Lambda = diag[\lambda_1 \lambda_2 \dots \lambda_n]$ is the diagonal form of corresponding eigenvalues. This characteristic has been shown in Figure 4-1 for one eigenvector.

Given a real symmetric matrix A, all of the eigenvectors are mutually orthogonal for distinct eigenvalues. In other words, this means that each of the eigenvectors points to a direction that

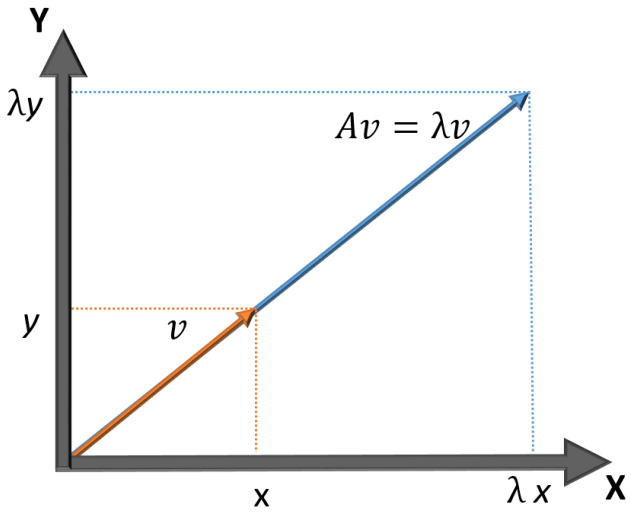

Figure 4-1 Eigenvector and Eigenvalue

is perpendicular to the other one. For instance, eigenvectors of an arbitrary identity matrix N of size 2 are $v1 = [1 \quad 0]^T$ and $v2 = [0 \quad 1]^T$ that are orthogonal vectors.

Now consider the set of linear Equations in (4-2):

$$Y = AX \tag{4-2}$$

where A is a real matrix. A performance index is defined as the weighted L_2-norm of the output vector Y as in Equation (4-3):

$$J = Y^T MY = X^T NX \tag{4-3}$$

where $N = A^T A$. Now we can represent matrix N with its eigenvectors and eigenvalues (i.e. eigendecomposition of matrix N) as in (4-4):

$$N = V.\Lambda.V^{-1} \tag{4-4}$$

It can be shown that when input X is chosen to be equal to one of the eigenvectors of matrix N in Equation (4-4), the performance index J would be equal to its corresponding eigenvalue. (Proof is given in the section 4.3.4):

$$X = v_i \rightarrow J = X^T NX = {v_i}^T N v_i = \lambda_i \tag{4-5}$$

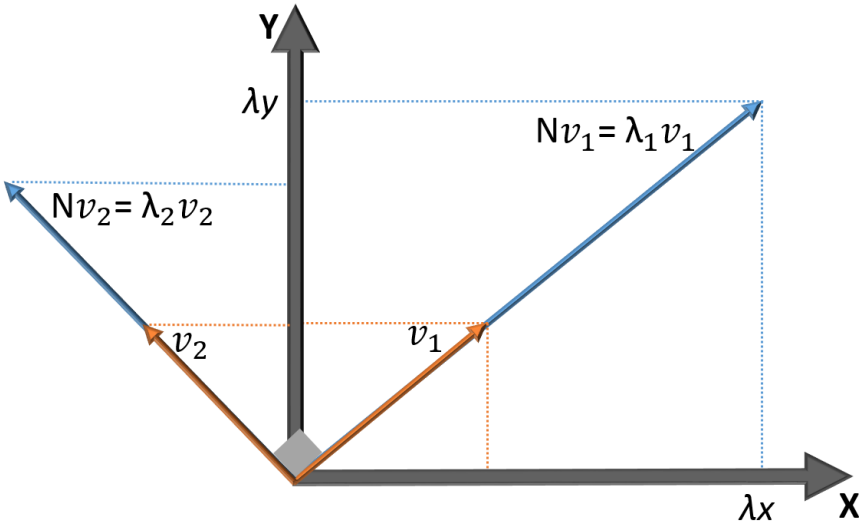

Figure 4-2: Orthogonal Eigenvectors of Matrix N

It is shown in Figure 4-2 that by choosing each eigenvector as an input, different vectors could be obtained in the direction of its own eigenvector (which is perpendicular to the other one) but with the magnitude that are related to its own eigenvalue. Therefore, if the objective is to find the maximum of J, the eigenvector corresponding to the largest eigenvalue of matrix N can be chosen. This eigenvector is called $v_{\lambda_{max}}$ in Equation (4-6):

$$X = v_{\lambda_{max}} \rightarrow J_{max} = {v_{\lambda_{max}}}^T N v_{\lambda_{max}} = \lambda_{max} \tag{4-6}$$

It is worth mentioning that if N is not a square matrix, in a more general way, the same approach can be kept by choosing $X = U_1$, where U_1 is the left singular vector of the matrix N. In this case the maximum of J is equal to:

$$J_{max} = X^T NX = \sigma_1^2 \tag{4-7}$$

Where σ_1 is the singular value of matrix N.

4.3 Problem Formulation:

4.3.1 Voltage Sensitivity Matrix:

Using the FDLFJ algorithm, the relationships between voltages of load buses and generator buses can be written by:

$$\begin{bmatrix} \Delta V_G \\ \Delta V_D \end{bmatrix} = \begin{bmatrix} S_{11} & S_{12} \\ S_{21} & S_{22} \end{bmatrix} \begin{bmatrix} \Delta Q_G \\ \Delta Q_D \end{bmatrix} \quad (4\text{-}8)$$

Where ΔV_G and ΔQ_G are voltages and reactive power changes at generating buses, respectively and $\Delta V_D$and ΔQ_D are voltages and reactive power at load buses, respectively. Solving Equation (4-8) for ΔV_D is led to Equation (4-9):

$$\Delta V_D = S_{21} S_{11}^{-1} \Delta V_G + W \quad (4\text{-}9)$$

Where $W = (S_{22} - S_{21} S_{11}^{-1} S_{12}) \Delta Q_D$

In this method, W is considered as a disturbance since reactive power changes in the load is not assumed to be available. On the other hand, the first term in Equation (4-9) shows the effect of a change in the source voltages on the load voltages. This matrix is called voltage sensitivity matrix and can be calculated from Equation (4-10):

$$\boldsymbol{S_{GL} = S_{21} S_{11}^{-1}} \quad (4\text{-}10)$$

For example, from S_{GL} matrix of the IEEEE 9 bus system (shown in Figure (4-4)), it can be concluded that bus 8 is more sensitive to generators two, three, and one, respectively. It means that in order to control this bus voltage optimally, generator 2 should be used more than generator 3 and 1 until it reaches its maximum limit. Therefore, this matrix plays an important role in formulating the objective function discussed in the next section.

4.3.2 The objective of the controller:

The objective of the controller is to find the best set of inputs $X = \Delta V_G$ that has the maximum effect on the outputs $Y = \Delta V_D$. The L2-norm has been used here as the performance index of change in the output:

$$\begin{matrix} Objective & \underset{\Delta V_G}{max} J = \Delta V_D^T M \Delta V_D \\ s.t. & |\Delta V_G| \leq \Delta V_{Gmax} \end{matrix} \quad (4\text{-}11)$$

Where M is a square matrix with the size of load buses. Now by using Equation (4-9)(while neglecting the disturbance W), Equation (4-11) can be rewritten as follows:

$$\underset{\Delta V_G}{max} J = \Delta V_D^T M \Delta V_D \approx \Delta V_G^T N \Delta V_G \text{ [21]} \quad (4\text{-}12)$$

Where $N = S_{11}^{-T} S_{21}^T M S_{21} S_{11}^{-1}$

Based on Equation (4-6), this control objective can be solved by choosing the input as $\Delta V_G = \alpha . v_{\lambda_{max}}$, where α is a scaler that has been added as a design parameter and $v_{\lambda_{max}}$ is the eigenvector corresponding to the highest eigenvalue of the matrix N. To control a single bus *i,* matrix M is defined as a zero matrix for all entries except the entry of *(i,i)* that is set to one. In this case, we can find α from Equation (4-13) if no constraint is included:

$$J_{max} = \Delta V_{ctr}^T M \Delta V_{ctr} = \Delta V_{ctr}^2 = \alpha^2 . \lambda_{max} \quad (4\text{-}13)$$

Therefore, by selecting desired ΔV_{ctr} which is the difference of controlled bus from 1 pu, α can be calculated. By using the calculated α from Equation (4-13), the voltage of the control bus moves towards 1 pu; however, it may impose an extra effort on generators to meet this goal leading to the violation of the generator voltage constraint given in Equation (4-11). Therefore, the control input is normalized in (4-14) so that the new generator voltages does not exceed their maximum limits:

$$\Delta V_G = \alpha . v_{\lambda_{max}} \xrightarrow{|\Delta V_G| \preccurlyeq \Delta V_{G_{max}}} |\Delta V_G|_{norm} = \bar{\alpha} . v_{\lambda_{max}} \quad (4\text{-}14)$$

Where $\bar{\alpha} = \alpha . \frac{\Delta V_{G_{max}}}{\Delta V_G}$

By applying the generators control input found in Equation (4-14), the voltage of the controlled bus is going to be controlled. However, this can cause another load voltage to go beyond its limit which is considered to be a new control bus for the next iteration. This process is repeated until all load voltages are within their limits.

The method used in the above approach is concerned with controlling a single violated bus in the system. A similar approach can be applied to the cases with multiple violated buses in the system which can be defined in the following two cases:

Case 1) Voltages of the violated buses are either less than the lower limit (0.9 pu) or higher than the upper limit (1.1 p.u.). This is a single-sided control procedure in which the less violated bus is chosen to be the control bus (i.e. the one that is out of the limit but is closer to 1 p.u. among all violated buses). The rest of the approach is the same as the single violated bus voltage discussed above meaning that the new generator voltages are calculated and applied to the system. Then the load voltages are checked again to make sure they are not out of the limit. Otherwise, a new control bus is chosen and the process of finding a new set of generator voltages is going to be repeated until all voltages are within their limits.

Case 2) Here, the voltages of the violated buses are both less and higher than the lower and upper limits, respectively. In this case, one control bus is chosen for each side using the same approach explained before. This is called the double-sided procedure and it requires to be checked if any conflict of interest in the system exists. A conflict of interest happens when controlling a lower limit violated bus (i.e. a bus with the voltage lower than 0.9 pu) deteriorates the voltage of an upper limit voltage bus (i.e. a bus with the voltage higher than 1.1 pu). In this case, control input should be updated by Equation (4-15) to check if a conflict of interest exists in controlling bus voltages i and j at the same time,

$$\Delta V_{ctr} = \Delta V_{Gi} \cap \Delta V_{Gj} \tag{4-15}$$

Where symbol ∩ is used here as an operator that removes the confliction among the conflicted buses as in Equation (4-16):

$$X \cap Y = \begin{cases} 0 & sign(x_i . y_i) < 0 \\ x_i + y_i & otherwise \end{cases} \quad (4\text{-}16)$$

In Figure 4-3 (a), a basic conflict of voltage control is illustrated where the voltage of G1

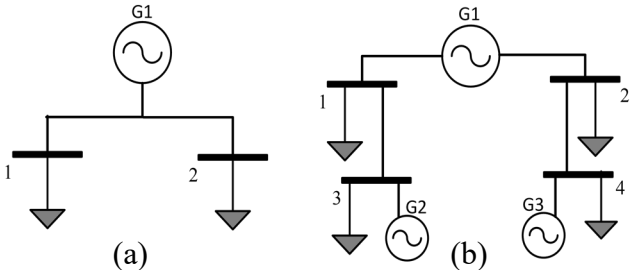

Figure 4-3: (a) A Two Bus System With A Single Generator (b) A Four Bus System With Three Generators [46]

changes the voltage of buses 1 and 2 in the same direction. This means that if the voltage of bus 1 is higher than 1.1 pu and the voltage of bus 2 is lower than .9 pu, there is no way to control the voltages of both buses at the same time with the help of G1. However, there are more than one sources in the power system which provide more flexibility to control the violated buses by ignoring the conflicting generator. For example, in Figure 4-3 (b), with the assumption of having the voltage of bus 1 to be higher than the upper limit and the voltage of bus 2 to be less than the lower limit, G1 cannot bring back the two voltages to their limits at the same time; however, it is possible to control the voltages of buses 1 and 2 by using generators 2 and 3 and ignoring generator 1 even if it is more sensitive to the affected buses in terms of the sensitivity matrix. This procedure is considered in Equation 4-16. In the following section, the proposed algorithm is explained in detail:

4.3.3 Proposed Algorithm for optimal voltage control:

1- Solve the load flow and determine the violated bus(es).

2- End if there is no violated bus(es).

3- Determine the control bus in a single-sided procedure or two control buses in a double-sided procedure.

4- Determine $v_{\lambda_{max}}$ which is the eigenvector of the matrix *N* in (4-12), corresponding to its highest eigenvalue.

5- Calculate the deviation: $\Delta V_{ctr} = 1 - V_{ctr}$.

6- Determine α from $\alpha^2 = \Delta V_{ctr}^2 / \lambda_{max}$.

7- Determine the control input $\Delta V_G = \alpha . v_{\lambda_{max}}$.

8- Update α by Equation (4-14) if the generator voltages are not within their limits in step 4.

9- Control input should be checked and updated by Equation (4-15) for the double-sided conflict.

10- Update voltage of generators: $V_{Gnew} = V_{Gold} + |\Delta V_G|_{norm}$.

11- Go to Step 1 if there is any voltages beyond its limit.

12- Finish.

4.3.4 Appendix for Proof

Proof: let N be a symmetric matrix, then it has three characteristics: 1- It has only real eigenvalues. 2- It has independent eigenvectors for distinct eigenvalues (i.e. $V^{-1}\ exists$ for the subset of independent eigenvalues and it is equal to V^T). 3- It has orthogonal eigenvectors for distinct eigenvalues (i.e. ${v_i}^T v_j = 0$ for $i \neq j$). By using characteristics number 2 and 3, eigendecomposition of matrix N can be defined as in (Ap.1):

$$N = V . \Lambda . V^{-1} = V . \Lambda . V^T \quad \text{(Ap. 1)}$$

where Λ is the diagonal of eigenvalues of matrix N. Therefore, by substituting $X = v_{\lambda max}$ in Equation (4-5), the output will move towards a direction that gives the maximum value which is equal to λ_{max}:

$$J_{max} = {v_{\lambda_{max}}}^T V.\Lambda.V^T v_{\lambda_{max}} = \lambda_{max}$$

4.4 Case studies:

In this part of the chapter, four IEEE cases have been chosen to illustrate the proposed method. Each case is initially in its normal mode (i.e. all voltages are within their normal limits). In order to show that the algorithm can control the voltages of the system, loads of type inductive or capacitive have been added to the original system to make some voltages go out of their limits. These simulations have been done in Matlab and load flow solution has been verified by Matpower package [35].

4.4.1 Case Study One: IEEE 9-Bus System

The IEEE 9-bus system is shown in Figure 4-4. It has 3 generating units which are producing 319.95 MW and 34.88 Mvar altogether. The total loads of the system are 315.00 MW and 115.00 Mvar. All the voltages are within their normal limits (i.e. 0.9 pu to 1.1 pu). 115 Mvar has been added to bus 7 to make one of the voltages go out of its limit. In this case, the voltage of bus 7 goes out of its limit; thus, it is chosen as the control bus in the system. The control command for the generators to bring the voltage of bus 7 back to its limit is calculated by the proposed algorithm and is given here: $[\Delta V_{G1} \quad \Delta V_{G2} \quad \Delta V_{G3}] = [0.0307 \quad 0.1 \quad 0.0851]$

From this control input, it is obvious to see that the more sensitive generators to the controlled bus (here G2 and G3) are participating more than G1 in controlling the voltage of bus 7. In

Table 4-1, voltages of the normal case (before applying the disturbance), disturbance case (before applying the control), and control case (after applying the control) are shown.

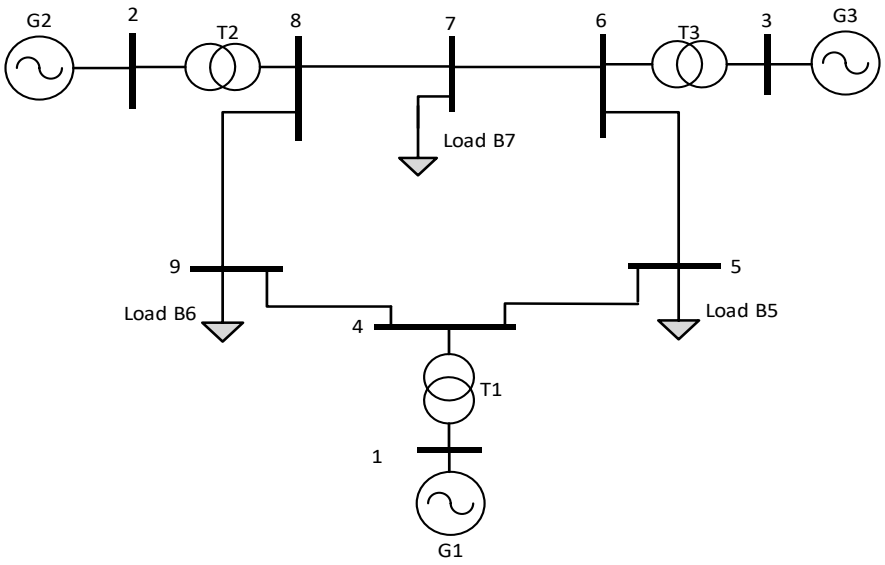

Figure 4-4: IEEE 9 bus system

Table 4-1 : Bus Voltages before and after Control (IEEE 9-bus System)

Bus	Voltage (pu)		
	Normal	Disturbance	Control
1	1	1	1.031
2	1	1	1.1
3	1	1	1.085
4	0.987	0.974	1.029
5	0.975	0.955	1.025
6	1.003	0.971	1.06
7	0.986	0.891	0.994
8	0.996	0.955	1.053
9	0.958	0.933	1.008

In this part, a case with having multiple violated voltage buses is considered. To illustrate this case, a load of 150 Mvar has been added to bus number 4 and another load of 70 Mvar has been added to bus number 5. The voltages of buses 4, 5 and 9 become less than their lower limits (i.e. the single-sided conflict). The proposed algorithm chooses bus number 4 as the

Table 4-2 : Bus Voltages before and after Control

Bus	Voltage (pu)		
	Normal	Disturbance	Normal
1	1	1	1.1
2	1	1	1.018
3	1	1	1.018
4	0.987	0.883	0.977
5	0.975	0.84	0.922
6	1.003	0.97	1.006
7	0.986	0.956	0.993
8	0.996	0.971	1.007
9	0.958	0.876	0.955

control bus since it has less deviation among the other violated buses. Results are shown in Table 4-2.

Modified IEEE case studies: Since the ratio of R/X in the distribution system lines is higher than the transmission system lines, some modified IEEE case studies with an increase in the ratio of R/X are considered in the followings to evaluate the effectiveness of the method in the distribution system.

4.4.2 Case study Two: Modified IEEE 9-Bus system

In this system, values of resistance of lines before and after the modification are shown in Table 4-3.

Table 4-3: Line parameter of modified IEEE 9-Bus system

Lines From	Lines To	R	X	R Modified
1	4	0	0.0576	0.023
4	5	0.017	0.092	0.0368
5	6	0.039	0.17	0.068
3	6	0	0.0586	0.0234
6	7	0.0119	0.1008	0.0403
7	8	0.0085	0.072	0.0288
8	2	0	0.0625	0.025
8	9	0.032	0.161	0.0644
9	4	0.01	0.085	0.034

Values for the modified R have been considered to be at least 40% of the reactance of the lines, i.e. $R_{modified}$=0.4 * X. The same algorithm is used for modified IEEE case study to show how it

works in a system that is closer to a distribution system (with higher R/X ratio). It can be seen from Table 4-5 that by adding 150 Mvar to bus 7, the voltages of buses 7 and 9 go out of their limits. In this case, bus 9 is chosen as the control bus and the results are shown in Table 4-4.

Table 4-4 : Bus voltages before and after control
(Modified IEEE 9-Bus system)

Bus	Voltage (pu)		
	Normal	Disturbance	Control
1	1	1	1.1
2	1	1	1.0611
3	1	1	1.029
4	0.987	0.944	1.0395
5	0.9755	0.9122	0.9976
6	1.0034	0.9429	0.9952
7	0.9856	0.84	0.9122
8	0.9962	0.9195	0.9918
9	0.9576	0.8799	0.9753

4.4.3 Case Study Three: IEEE 14-Bus system

IEEE 14-bus system is shown in Figure 4-5. It has 11 loads that consume 259 MW and 73.5 Mvar totally. A disturbance of 30 kvar has been added to bus 14. The result of the algorithm after applying the control input to the disturbance case is shown in Figure 4-6.

In another scenario, 300 Mvar is added to bus 5. Since the amount of disturbance is too high, three generators reach their maximum limits to control the violated bus; Therefore, the algorithm brings back the voltage of bus 5 to 0.92 pu instead of 1 pu. The result is shown in Table 4-5.

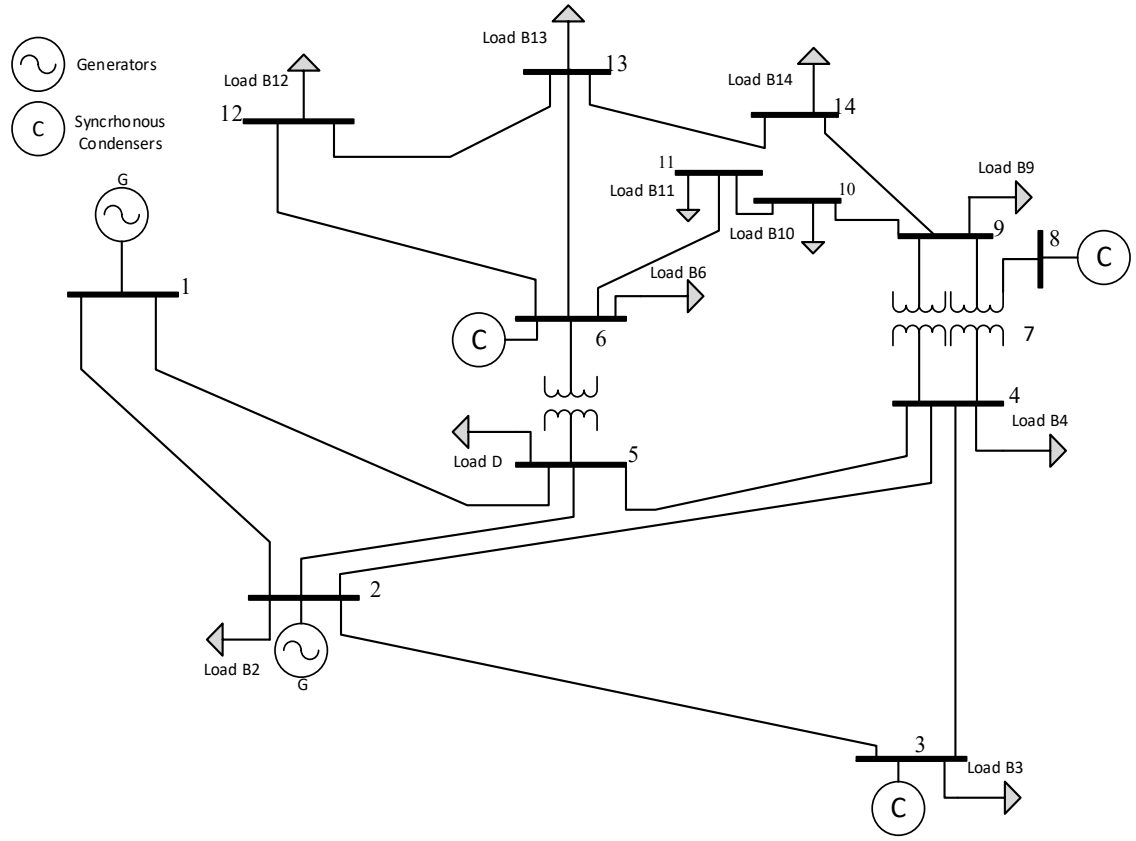

Figure 4-5 : IEEE 14-bus system

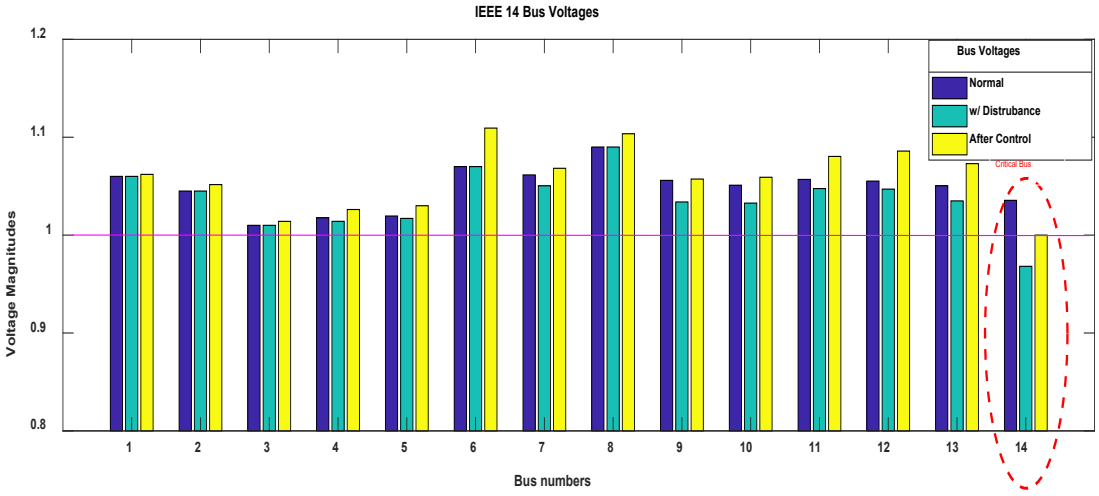

Figure 4-6 : Voltage profile of IEEE 14-bus system [21]

Table 4-5: Bus voltages before and after Control (IEEE 14-bus)

Bus	Voltage (pu)		
	Normal	Disturbance	Control
1	1.06	1.06	1.09
2	1.045	1.045	1.1
3	1.01	1.01	1.03
4	1.018	0.929	0.97
5	1.02	0.874	0.92
6	1.07	1.07	1.1
7	1.062	1.021	1.049
8	1.09	1.09	1.1
9	1.056	1.016	1.05
10	1.051	1.018	1.05
11	1.057	1.04	1.07
12	1.055	1.052	1.09

4.4.4 Case Study Four: Modified IEEE 14-Bus system:

In this part, line parameters of IEEE 14-bus system have been modified to increase the resistance of lines to 45% of the reactance lines which is shown in Table 4-6.

Table 4-6: Line properties for Modified IEEE 14-bus system

From	**To**	**R**	**X**	**R Modified**
1	2	0.0194	0.0592	0.0266
1	5	0.054	0.223	0.1004
2	3	0.047	0.198	0.0891
2	4	0.0581	0.1763	0.0793
2	5	0.057	0.1739	0.0782
3	4	0.067	0.171	0.077
4	5	0.0134	0.0421	0.0189
4	7	0	0.2091	0.0941
4	9	0	0.5562	0.2503
5	6	0	0.252	0.1134

6	11	0.095	0.1989	0.0895
6	12	0.1229	0.2558	0.1151
6	13	0.0662	0.1303	0.0586
7	8	0	0.1762	0.0793
7	9	0	0.11	0.0495
9	10	0.0318	0.0845	0.038
9	14	0.1271	0.2704	0.1217
10	11	0.082	0.1921	0.0864
12	13	0.2209	0.1999	0.0899
13	14	0.1709	0.348	0.1566

The same disturbance as the previous case is applied to show the comparison (i.e. 300 Mvar has been added to bus 5). Results in Table 4-7 show almost the same behavior as the previous case.

Table 4-7: Bus voltages before and after control (IEEE 14-bus)

Bus	Voltage (pu)		
	Normal	Disturbance	Control
1	1.06	1.06	1.0868
2	1.045	1.045	1.1
3	1.01	1.01	1.0312
4	1.0177	0.9254	0.9674
5	1.0195	0.8726	0.9187
6	1.07	1.07	1.1008
7	1.0615	1.0085	1.0374
8	1.09	1.09	1.0991
9	1.0559	0.9943	1.0272
10	1.051	0.9997	1.0325
11	1.0569	1.031	1.0629
12	1.0552	1.05	1.0814
13	1.0504	1.0428	1.0743
14	1.0355	0.9973	1.0303

4.4.5 Case Study Five: IEEE 30-bus system

IEEE 30-bus system has 6 generators located at buses 1, 2, 13, 22, 23 and 27. The total generating power is 191.64 MW and 100.41 Mvar. In this case study, multiple bus violations and a two-sided conflict in the system are considered. For this example, 130 Mvar, 40 Mvar, 40 Mvar, -35 Mvar and -35 Mvar are added to buses 28, 24, 19, 29 and 30, respectively. The voltages of buses 29 and 30 exceed 1 pu while some other voltages are less than 0.9 pu (i.e. two-sided conflict). In this case, two controlled buses are defined for each side. Bus 29 is chosen as the controlled bus from section one and bus 20 is chosen as the controlled bus from section two. After the conflicted bus is removed by Equation (4-15), it is seen that the voltage of bus 28 goes out of its limit after applying the new generator voltages to the system. Therefore, the process is repeated for the second iteration by choosing bus 28 as the control bus. Now, it can be seen that the voltage of bus 22 goes out of its limit after applying the new generator voltages to the system. Finally, by controlling bus 22 for the third iteration, all of the voltages go back to their normal limits and the process is done. The result is shown in Table 4-8.

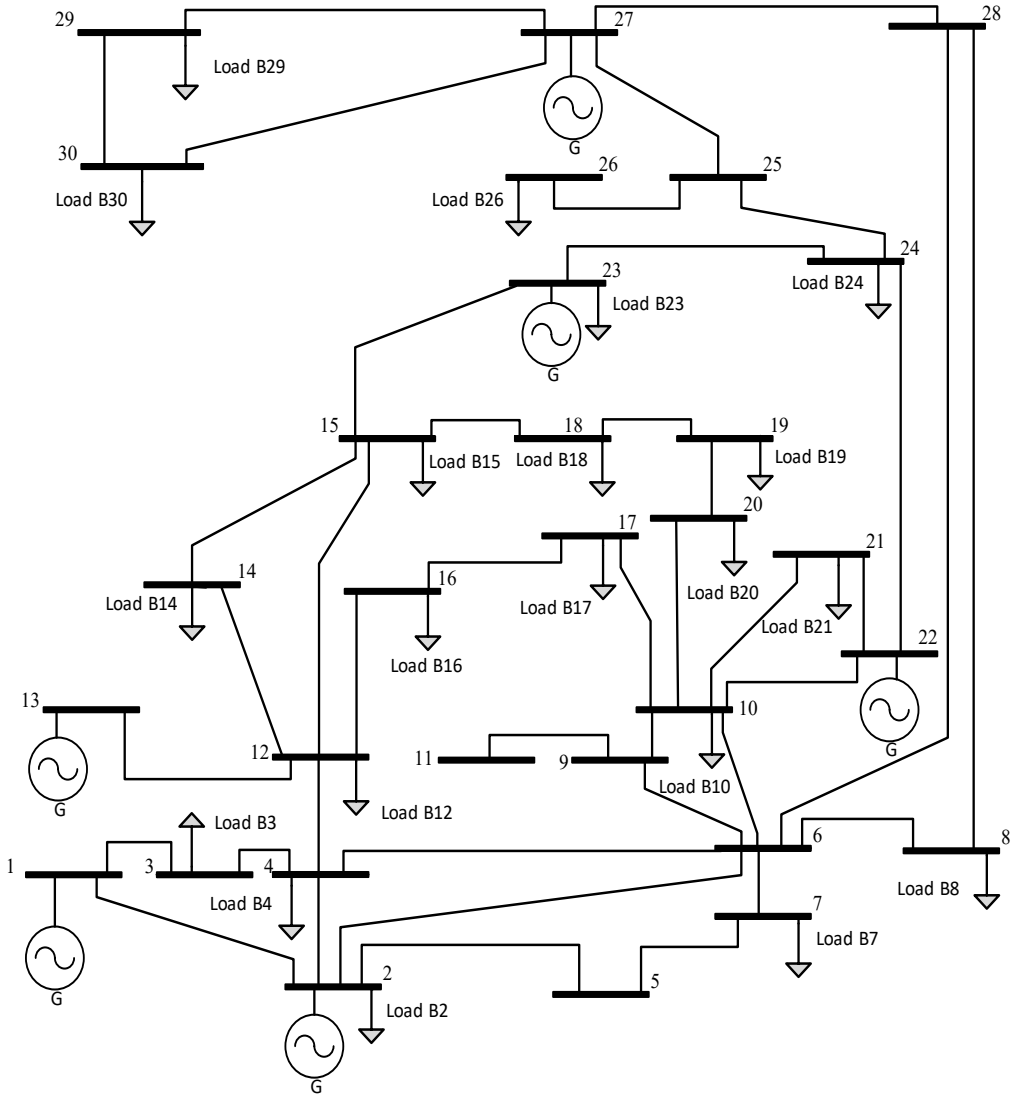

Figure 4-7: IEEE 30-bus system

Table 4-8: Bus voltages in each iteration (IEEE 30-bus)

Bus	Voltage (pu)								
	Dist.	Iter. 1	Iter. 2	Iter.3	Bus	Dist.	Iter. 1	Iter. 2	Iter.3
1	1.00	1.01	1.03	1.03	16	0.95	1.03	1.05	1.00
2	1.00	1.03	1.10	1.10	17	0.95	1.03	1.06	0.98
3	0.95	0.98	1.02	1.00	18	0.894	0.98	1.00	0.95
4	0.93	0.97	1.02	1.00	19	0.86	0.95	0.98	0.91
5	0.95	0.98	1.04	1.03	20	0.897	0.97	1.00	0.93
6	0.91	0.94	0.99	0.97	21	0.99	1.09	1.11	1.00
7	0.91	0.95	1.00	0.98	22	1.00	1.10	1.12	1.01
8	0.88	0.92	0.97	0.95	23	1.00	1.08	1.08	1.08
9	0.94	1.01	1.05	0.98	24	0.95	1.02	1.04	0.97
10	0.96	1.04	1.07	0.98	25	0.98	0.95	0.98	0.95
11	0.94	1.01	1.05	0.98	26	0.96	0.93	0.96	0.93
12	0.96	1.03	1.05	1.03	27	1.00	0.92	0.95	0.95
13	1.00	1.06	1.07	1.07	28	0.85	0.87	0.93	0.90
14	0.95	1.02	1.04	1.02	29	1.12	1.05	1.08	1.08
15	0.95	1.02	1.04	1.02	30	1.13	1.06	1.09	1.08

4.4.6 Case study Six: Modified IEEE 30-bus system

In this system, the same disturbances as in the previous section are applied to the system to compare the results (130 Mvar, 40 Mvar, 40 Mvar, -35 Mvar and -35 Mvar are added to buses 28, 24, 19, 29 and 30, respectively). The proposed algorithm converges in two iterations and the results are shown in Table 4-9.

Table 4-9: Bus voltages in each iteration for modified IEEE 30-bus system

Bus	Disturbance	Iteration 1	Iteration 2
1	1.0087	1.0268	1.0292
2	1.0275	1.1	1.097
3	0.9705	1.0147	1.0018
4	0.9631	1.0128	0.9966
5	0.9743	1.0382	1.0255
6	0.9344	0.9882	0.9663
7	0.9405	0.999	0.9806
8	0.9077	0.9627	0.9405
9	1.0024	1.0396	0.9768
10	1.039	1.0672	0.9826
11	1.0024	1.0396	0.9768
12	1.0142	1.0366	1.0164

13	1.0557	1.0678	1.0683
14	1.0113	1.0311	1.0092
15	1.0172	1.0348	1.0119
16	1.0177	1.0428	0.995
17	1.0275	1.0549	0.9808
18	0.9716	0.9943	0.9464
19	0.9476	0.9732	0.9107
20	0.9696	0.9958	0.9278
21	1.0838	1.1071	0.9994
22	1.1	1.1218	1.0079
23	1.0809	1.0839	1.0788
24	1.0168	1.0347	0.9738
25	0.9505	0.9769	0.9536
26	0.9354	0.9622	0.9386
27	0.9178	0.949	0.9495
28	0.8652	0.9207	0.9001
29	1.0539	1.0819	1.0823
30	1.0627	1.0905	1.0909

4.4.7 Case Study Seven: IEEE 57-bus System

This system has 7 generators that are producing 1278.66 MW and 321.08 Mvar altogether. There are 42 load buses which are consuming 1250.8 MW and 336.4 Mvar totally. In this case study, 320 Mvar and 180 Mvar are added to buses 13 and 55, respectively. As a result, multiple buses including 13, 31-34, 52-55 go out of their voltage limits. The algorithm controls bus 34 in the first iteration and the result is shown in Table 4-10. For the second iteration, a two-sided conflict between bus 51 and bus 55 is occurred, so these two buses are chosen as the controlled buses. The controlled buses are chosen as bus 51 and bus 55 which bring the voltage of bus 51 back to its normal limit and resolves the conflicting issue. For the last iteration, bus 55 is chosen as the controlled bus leading to bring its voltage back to the normal limit. The results of this IEEE case study are shown in Table 4-10.

Table 4-40: Bus voltages in each iteration (IEEE 57-bus)

Bus	Voltage (pu)

	Norm.	Dist.	Iter.1	Iter.2	Iter.3	Bus	Norm.	Dist.	Iter.1	Iter.2	Iter.3
1	1.040	1.040	1.084	1.072	1.070	30	0.963	0.903	0.995	0.945	0.954
2	1.010	1.010	1.010	1.010	1.010	31	0.936	0.874	0.971	0.917	0.927
3	0.985	0.985	1.063	1.045	1.050	32	0.950	0.888	0.987	0.930	0.940
4	0.981	0.980	1.041	1.029	1.033	33	0.948	0.886	0.985	0.928	0.938
5	0.977	0.976	1.007	1.007	1.008	34	0.959	0.899	0.996	0.939	0.949
6	0.980	0.980	0.996	1.002	1.001	35	0.966	0.908	1.003	0.946	0.956
7	0.984	0.971	0.997	0.996	0.997	36	0.976	0.918	1.013	0.955	0.966
8	1.005	1.005	1.024	1.023	1.022	37	0.985	0.927	1.022	0.964	0.974
9	0.980	0.980	1.066	1.070	1.100	38	1.013	0.956	1.048	0.990	0.999
10	0.986	0.977	1.064	0.984	0.995	39	0.983	0.925	1.020	0.962	0.973
11	0.974	0.930	1.018	0.982	1.000	40	0.973	0.915	1.010	0.953	0.963
12	1.015	1.015	1.100	0.954	0.950	41	0.996	0.945	1.042	0.998	1.015
13	0.979	0.898	0.987	0.918	0.927	42	0.967	0.912	1.012	0.964	0.981
14	0.970	0.910	0.994	0.938	0.946	43	1.010	0.962	1.056	1.016	1.035
15	0.988	0.953	1.030	0.990	0.996	44	1.017	0.964	1.054	0.999	1.008
16	1.013	1.013	1.087	0.979	0.975	45	1.036	0.993	1.076	1.030	1.037
17	1.018	1.017	1.077	1.015	1.012	46	1.060	0.996	1.089	1.028	1.036
18	1.001	0.994	1.062	1.046	1.050	47	1.033	0.972	1.066	1.004	1.013
19	0.970	0.947	1.023	0.992	0.998	48	1.027	0.968	1.061	1.000	1.009
20	0.964	0.929	1.010	0.971	0.978	49	1.036	0.975	1.071	1.003	1.012
21	1.009	0.956	1.045	0.991	1.000	50	1.023	0.977	1.074	0.999	1.009
22	1.010	0.954	1.044	0.989	0.997	51	1.052	1.034	1.129	1.045	1.056
23	1.008	0.953	1.043	0.988	0.996	52	0.980	0.885	0.948	0.946	0.959
24	0.999	0.948	1.026	0.985	0.993	53	0.971	0.842	0.918	0.917	0.935
25	0.983	0.925	1.014	0.965	0.974	54	0.996	0.799	0.900	0.902	0.930
26	0.959	0.912	0.984	0.947	0.954	55	1.031	0.772	0.894	0.898	0.936
27	0.982	0.944	0.995	0.978	0.983	56	0.968	0.912	1.013	0.962	0.978
28	0.997	0.963	1.006	0.997	1.001	57	0.965	0.908	1.009	0.956	0.971
29	1.010	0.979	1.016	1.012	1.015						

4.4.8 Case study eight: Modified IEEE 57-bus system

In the modified version of the IEEE 57-bus system, the lines resistances have been increased to 40% of the values of their corresponding lines reactances as it shown in Table 4-11.

Table 4-5: Line parameters for modified IEEE 57-Bus system

From	To	R	X	R_Modified	From	To	R	X	R_Modified
1	2	0.0083	0.028	0.0112	7	29	0	0.0648	0.0259
2	3	0.0298	0.085	0.034	25	30	0.135	0.202	0.0808

3	4	0.0112	0.0366	0.0146	30	31	0.326	0.497	0.1988
4	5	0.0625	0.132	0.0528	31	32	0.507	0.755	0.302
4	6	0.043	0.148	0.0592	32	33	0.0392	0.036	0.0144
6	7	0.02	0.102	0.0408	34	32	0	0.953	0.3812
6	8	0.0339	0.173	0.0692	34	35	0.052	0.078	0.0312
8	9	0.0099	0.0505	0.0202	35	36	0.043	0.0537	0.0215
9	10	0.0369	0.1679	0.0672	36	37	0.029	0.0366	0.0146
9	11	0.0258	0.0848	0.0339	37	38	0.0651	0.1009	0.0404
9	12	0.0648	0.295	0.118	37	39	0.0239	0.0379	0.0152
9	13	0.0481	0.158	0.0632	36	40	0.03	0.0466	0.0186
13	14	0.0132	0.0434	0.0174	22	38	0.0192	0.0295	0.0118
13	15	0.0269	0.0869	0.0348	11	41	0	0.749	0.2996
1	15	0.0178	0.091	0.0364	41	42	0.207	0.352	0.1408
1	16	0.0454	0.206	0.0824	41	43	0	0.412	0.1648
1	17	0.0238	0.108	0.0432	38	44	0.0289	0.0585	0.0234
3	15	0.0162	0.053	0.0212	15	45	0	0.1042	0.0417
4	18	0	0.555	0.222	14	46	0	0.0735	0.0294
4	18	0	0.43	0.172	46	47	0.023	0.068	0.0272
5	6	0.0302	0.0641	0.0256	47	48	0.0182	0.0233	0.0093
7	8	0.0139	0.0712	0.0285	48	49	0.0834	0.129	0.0516
10	12	0.0277	0.1262	0.0505	49	50	0.0801	0.128	0.0512
11	13	0.0223	0.0732	0.0293	50	51	0.1386	0.22	0.088
12	13	0.0178	0.058	0.0232	10	51	0	0.0712	0.0285
12	16	0.018	0.0813	0.0325	13	49	0	0.191	0.0764
12	17	0.0397	0.179	0.0716	29	52	0.1442	0.187	0.0748
14	15	0.0171	0.0547	0.0219	52	53	0.0762	0.0984	0.0394

18	19	0.461	0.685	0.274	53	54	0.1878	0.232	0.0928
19	20	0.283	0.434	0.1736	54	55	0.1732	0.2265	0.0906
21	20	0	0.7767	0.3107	11	43	0	0.153	0.0612
21	22	0.0736	0.117	0.0468	44	45	0.0624	0.1242	0.0497
22	23	0.0099	0.0152	0.0061	40	56	0	1.195	0.478
23	24	0.166	0.256	0.1024	56	41	0.553	0.549	0.2196
24	25	0	1.182	0.4728	56	42	0.2125	0.354	0.1416
24	25	0	1.23	0.492	39	57	0	1.355	0.542
24	26	0	0.0473	0.0189	57	56	0.174	0.26	0.104
26	27	0.165	0.254	0.1016	38	49	0.115	0.177	0.0708
27	28	0.0618	0.0954	0.0382	38	48	0.0312	0.0482	0.0193
28	29	0.0418	0.0587	0.0235	9	55	0	0.1205	0.0482

The same disturbances as the previous case are applied to this modified case to compare the results (i.e. 320 Mvar and 180 Mvar have been added to buses 13 and 55, respectively). It can be seen that the system is controlled almost the same way as it was in the previous case. Results are shown in Table 4-12.

Table 4-62: Bus voltages in each iteration (Modified IEEE 57-bus)

Bus	Normal	Disturbance	Iter. 1	Iter. 2	Iter. 3
1	1.04	1.04	1.0802	1.0721	1.0841
2	1.01	1.01	1.01	1.01	1.01
3	0.985	0.985	1.0608	1.0456	1.0769
4	0.9808	0.9783	1.037	1.0315	1.0557
5	0.9765	0.976	1.0053	1.0164	1.0286
6	0.98	0.98	0.9946	1.0138	1.02
7	0.9842	0.9634	0.9886	1.012	1.0222

8	1.005	1.005	1.0216	1.0546	1.0627
9	0.98	0.98	1.0672	1.07	1.1
10	0.9862	0.9694	1.0574	0.9884	1.0167
11	0.974	0.9244	1.0136	0.9822	1.0123
12	1.015	1.015	1.1	0.9741	0.9995
13	0.9789	0.8916	0.9802	0.9215	0.9511
14	0.9702	0.9012	0.9847	0.9375	0.9661
15	0.988	0.9441	1.0195	0.9866	1.0135
16	1.0134	1.0064	1.0801	0.9878	1.0098
17	1.0175	1.0095	1.0679	1.0166	1.034
18	1.0007	0.9581	1.0267	1.0163	1.0438
19	0.9702	0.9196	0.9961	0.9742	1.003
20	0.9638	0.9045	0.9853	0.9562	0.9857
21	1.0085	0.9326	1.0233	0.9802	1.0116
22	1.0097	0.9311	1.0227	0.9778	1.0093
23	1.0083	0.9303	1.0212	0.9774	1.0087
24	0.9992	0.9283	1.0075	0.9826	1.0101
25	0.9825	0.8631	0.9588	0.925	0.9578
26	0.9588	0.8951	0.9674	0.9479	0.9731
27	0.9815	0.9228	0.9753	0.9792	0.998
28	0.9967	0.9377	0.9826	0.9952	1.0116
29	1.0102	0.9497	0.9898	1.0077	1.0225
30	0.9627	0.8457	0.9442	0.9083	0.942
31	0.9359	0.8224	0.9255	0.8854	0.9205
32	0.9499	0.8354	0.9401	0.8953	0.931
33	0.9476	0.8339	0.9388	0.894	0.9297

34	0.9592	0.8879	0.9849	0.9385	0.9716
35	0.9662	0.8943	0.9909	0.9442	0.9772
36	0.9758	0.9019	0.9978	0.9511	0.9839
37	0.9849	0.9089	1.0042	0.9574	0.99
38	1.0128	0.9323	1.0253	0.9779	1.0098
39	0.9828	0.9075	1.003	0.9563	0.9889
40	0.9728	0.8996	0.9956	0.9491	0.9819
41	0.9962	0.905	1.0056	0.9669	1.0009
42	0.9665	0.8788	0.9826	0.9411	0.9761
43	1.0096	0.9462	1.0416	1.0071	1.0394
44	1.0168	0.9397	1.0304	0.9854	1.0167
45	1.036	0.9654	1.0499	1.0106	1.0403
46	1.0598	0.9716	1.0656	1.0136	1.0458
47	1.0333	0.9449	1.0397	0.9883	1.0207
48	1.0274	0.9416	1.0361	0.9853	1.0175
49	1.0362	0.9483	1.0452	0.9879	1.0206
50	1.0233	0.9566	1.0547	0.9911	1.0237
51	1.0523	1.0147	1.1108	1.0387	1.0699
52	0.9804	0.8739	0.9386	0.9544	0.9764
53	0.9709	0.8389	0.9163	0.9308	0.9565
54	0.9963	0.7946	0.8962	0.9069	0.9398
55	1.0308	0.7617	0.8852	0.8922	0.9315
56	0.9684	0.8821	0.9858	0.9428	0.9778
57	0.9648	0.8773	0.9812	0.937	0.9721

4.5 Conclusion

In this chapter, an optimal voltage algorithm to control the voltages of power systems is proposed based on the voltage sensitivity matrix derived from the FDLFJ. This algorithm finds the best set of inputs by using the eigenvalue decomposition technique. This set of inputs is used to modify the generator voltages to control the voltage of the violated load bus(es). In case of any conflicts between the two generators, the previous set of inputs is modified to clear the existing conflict. In addition, the modified IEEE case studies with higher R/X ratios are also investigated to examine the effect of the proposed algorithm on controlling the voltages of the violated buses in the high resistive systems. The results achieved from eight (original/modified) IEEE cases indicate that the voltage of the violated buses can be effectively controlled with the proposed algorithm.

5 Fully distributed secondary voltage control in power systems

5.1 Introduction

There is a constant trend in the recent literature to move from the centralized secondary voltage controller to the distributed one because of the high dependency on a massive amount of exchanging communication messages and the problem of a single point of failure. Although each DG only communicates with its neighboring DGs to control the voltage in the distributed methods in the literature, the messages still circulate among the whole DGs. Therefore, a real distributed controller that limits the communication messages among a few players in the system (here DGs) is needed. This section focuses on developing a real distributed secondary voltage control for a microgrid system to show its advantage over the global distributed one.

5.2 Introduction to cyber-physical systems

Recent deployments of communication devices in power systems led to a more advanced system called a smart grid. In this modernized system, devices can talk to each other to alleviate the issues that may occur in the system. In Figure 5-1, two layers in power systems are shown. The first one is a cyber layer and the second one is a physical layer. The cyber layer is used to model the communication layer, and the physical layer is used to model the power system.

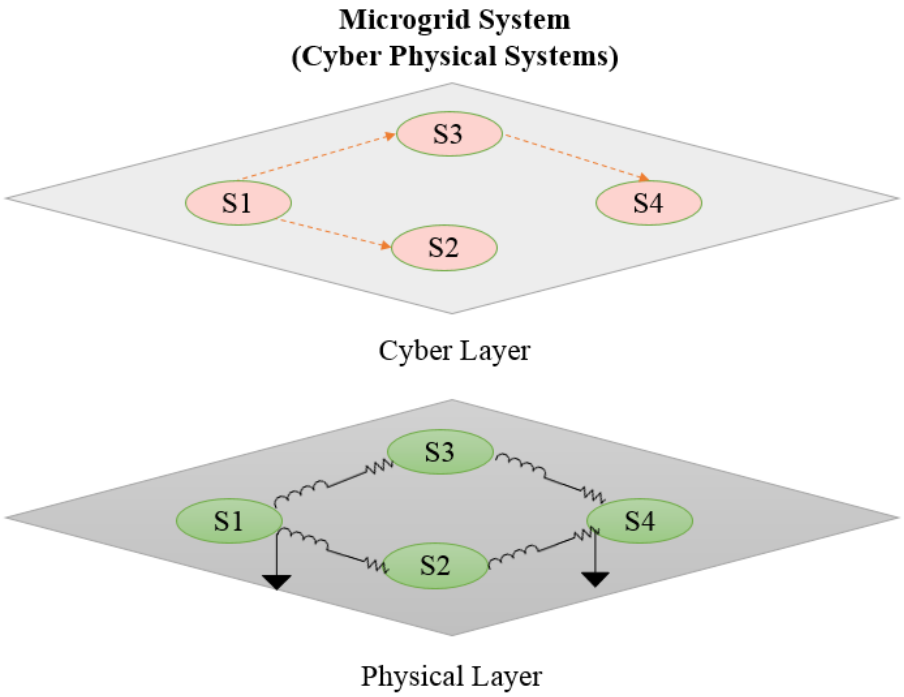

Figure 5-1: Cyber-physical systems consist of two layers: 1- Cyber layer 2- Physical layer [36]

Communication layer (cyber layer) in a distributed algorithm is designed to be a sparse network. Distributed algorithms have become a hotly debated area in other fields such as computer science, while it is a relatively new area in the power system. Although this area has been paid a lot of attention in the literature, no study has proposed a connection between these two layers. In other words, the effect of the physical layer (the power system) is not considered in designing the algorithm for the cyber layer (communication among DGs). In this chapter, I have utilized the developed method discussed in Chapter four to choose the optimal communication layer (cyber layer) for the physical layer (power system) in order to control the voltage in a distributed way.

For example, in a multi-agent system shown in Figure 5-2, which consists of several DGs and loads, an optimal communication layer can facilitate the voltage or frequency control in the system. In such system, the players(here DGs) communicate the necessary information among each other to solve a problem.

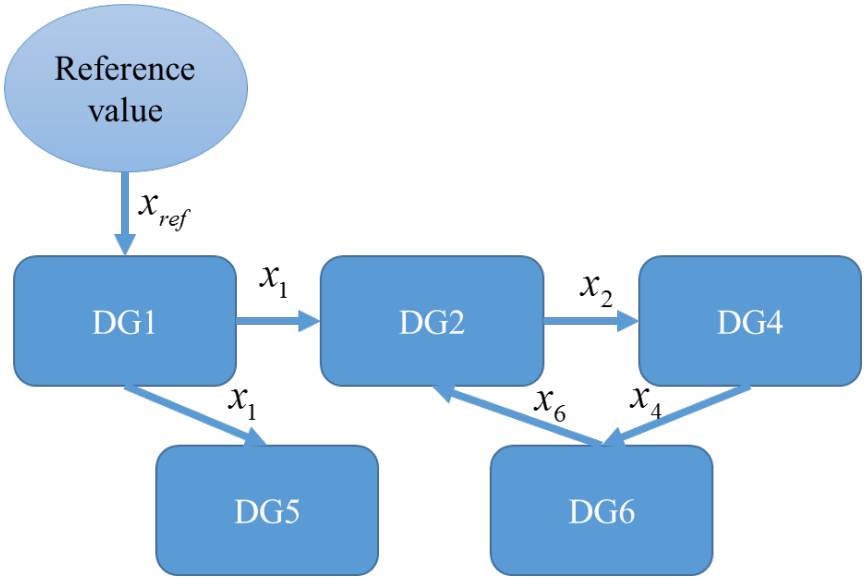

Figure 5-2 Multi-agent System with multiple DGs

Moreover, these DGs can automatically control the active power without any communication needs by implementing the droop controller at the primary control level. If the load increases, the frequency momentarily drops proportionally to the droop gains without any communication needs. Once the system is stabilized, the frequency in the system reaches a constant number which is no longer the nominal value. In this part, DGs can use the communication layer to communicate to each other in order to bring the frequency back to the nominal value in the secondary controller by increasing the ω_n. This process is shown in Figure 5-3.

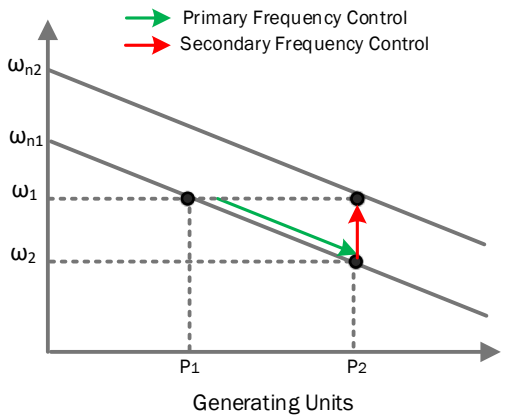

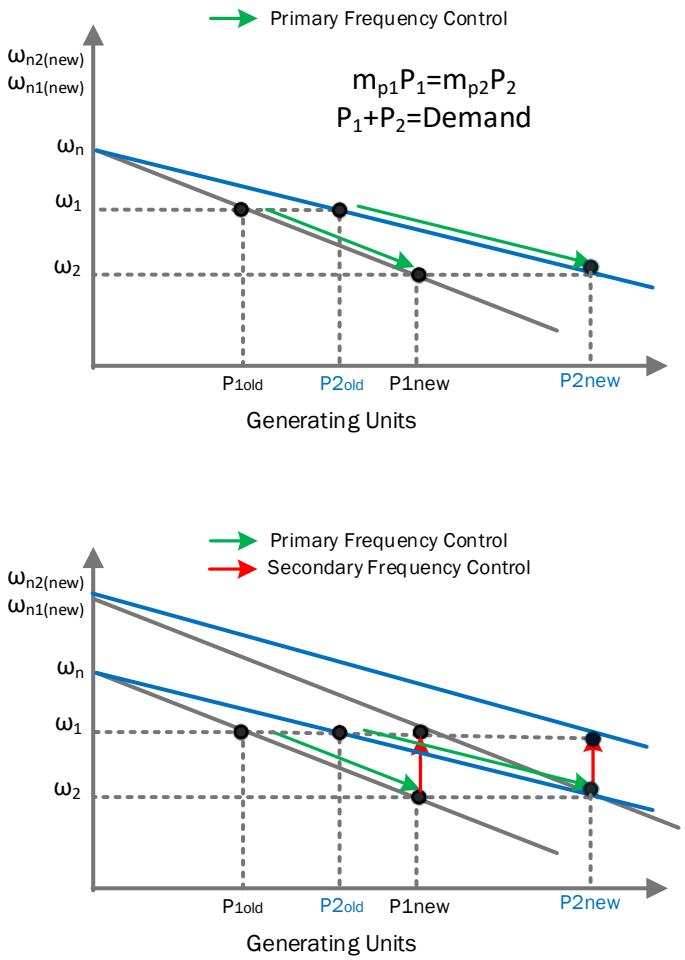

Figure 5-3 Primary and Secondary Controller

On the contrary, the voltage control is a local phenomenon, meaning that it cannot be controlled from a far distance. This means that the voltage control needs to be designed in a distributed way. In the next section, an overview of consensus methods is stated, followed by developing a fully distributed consensus algorithm for a microgrid system.

5.3 Overview of Consensus Methods

This section discusses a consensus method that is popular in coordinating the multi-agent systems in detail. Here, the consensus means an agreement that can reach among different agents of the system in a distributed way. There are two types of the consensus algorithm. The first one is a distributed tracker algorithm in which a leader agent shares a certain value with other agents through the communication layer. In the other one, the consensus value is not pre-

defined by a leader agent rather it is calculated from the information among the players in the system (such as an average value for the voltage). Average consensus algorithm can be applied to control areas such as sensor calibration (least squares), vehicle coordination (Kalman filter). [37]. These algorithms have been studied in the fields of computer science and robotics for a while, but they have recently been introduced to the field of power system. In the following, a preliminary review of the consensus algorithm is discussed.

5.3.1 Stochastic Matrix:

A stochastic matrix is a matrix in which the sum of each row equals one and all of its entries have positive values as it is shown in Equation 5-1:

$$Q(t)]_{ij} = q_{ij}(t) \geq 0, \sum_{j=1}^{N} q_{ij} = 1 \qquad (5\text{-}1)$$

Properties of stochastic matrix:

1- All of its eigenvalues are included in the unit circle. i.e. $|\lambda_i| \leq 1$.

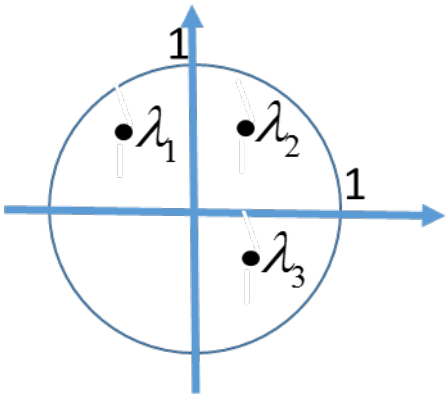

Figure 5-4 Eigenvalues of a Stochastic Matrix

2- It has a corresponding eigenvector 1 for its eigenvalue 1. i.e. $Q\mathbf{1}=1.\mathbf{1}$

The doubly Stochastic matrix is a stochastic matrix whose sum of each column also equals one. It is important to mention that convergence of consensus algorithms is related to the

eigenvalues of the Q matrix. For example, for the stochastic matrix, the second largest eigenvalue shows the rate of the convergence. This will be discussed in more details later but for now some basic definitions related to the graph theory will be discussed.

A graph is associated with a matrix Q by assigning nodes and edges to its entries. A corresponding graph to a matrix Q is shown with $G_Q = (N, E_Q)$, where N are the nodes related to the number of columns and rows of the matrix ($N = \{1,2, \dots, N\}$), and the edges are the connections between the nodes with the values equal to the entries of the matrix $E_Q = \{(j,i)|q_{ij} > 0\}$, i. e. $(j,i) \in E$).

Figure 5-5 Node i receives information from node j

$E_Q = (N, E)$ is the symbol used to show the graph related to a matrix Q.

Self-loop graphs (G_{sl}) are graphs in which each node has access to its own information. In such graphs, the corresponding matrix Q has nonzero diagonal entries.

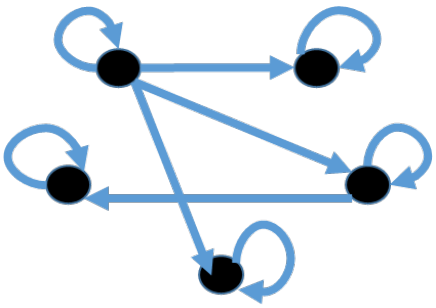

Figure 5-6: A self-loop Graph (G_{sl})

In-degree of a node is the number of edges that is connected to that node (in an undirected graph), or the number of incoming edges to that node (in a directed graph).

$$v_{in}(i) = \{j|(j,i) \in E, i \neq j\ j\},\ d_{in}(i) = |v_{in}(i)|$$

On the other hand, out-degree is the number of outgoing edges from that node (in directed graphs).

$$v_{out}(i) = \{j|(i,j) \in E, i \neq j\}, \; d_{out}(i) = |v_{out}(i)|$$

For instance, the in-degree of node 3 in Figure 5-7 is two, which comes from node 2 and 3.

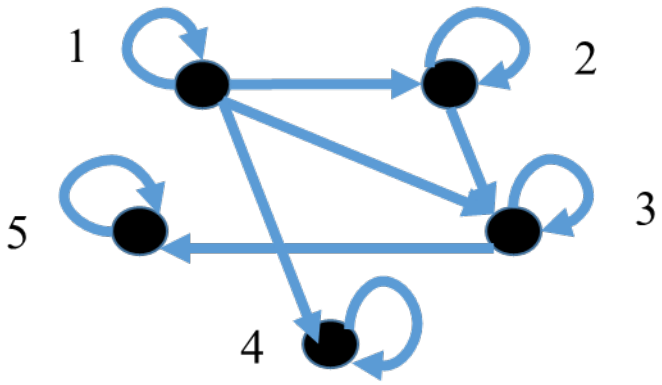

Figure 5-7: A graph for showing indegree and outdegree examples

Rooted graph:

A graph is rooted if there exists a node k such that for any other j, there is a unique path from k to j.

5.3.2 Linear Consensus Algorithms:

In this part, discrete linear systems is discussed, as is the case in communication systems. Let's consider Equation (5-3) as the updating equation for linear systems in which Q is a stochastic matrix:

$$x(t+1) = Q(t)x(t) \qquad (5\text{-}2)$$

It is proven that if the graph is rooted and contains the self-loops, then Q solves the consensus problem. For example, to control the voltage of some buses in the power system, a

communication layer via stochastic matrix can be established to regulate the voltage in the system through applying the distributed tracker algorithm.

Liner Conesus analysis:

There are two types of liner consensus algorithms defined in the literature. The first one is the static consensus "where updates at each node are performed simultaneously, thus being well-represented by constant matrices" [38]. There two common methods to design the constant Q matrix:

1- Metropolis-Hasting weights:

This method is an updated version of the uniform method. Unlike the uniform method, the weights are not constant through the network but they are related to the degree of each node, n_i . This method has shown improvement in terms of speed of convergence and also it is adaptable in terms of configuration changes in the system.

$$a_{ij} = \begin{cases} \dfrac{1}{[Max(n_i + n_j) + 1]} & j \in N_i \\ 1 - \displaystyle\sum_{j \in N_i} \dfrac{1}{[Max(n_i + n_j) + 1]} & j = i \\ 0 & otherwise \end{cases} \tag{5.11}$$

2- Mean Metropolis weight:

This method is another version of the previous method which has been inspired by the Lyapunov stability analysis. The updating formula for this method can be found in the following formula (5.12), where the Ɛ is a very small number:

$$a_{ij} = \begin{cases} \dfrac{2}{(n_i + n_j + \varepsilon)} & j \in N_i \\ 1 - \displaystyle\sum_{j \in N_i} \dfrac{2}{(n_i + n_j + \varepsilon)} & j = i \\ 0 & otherwise \end{cases} \qquad (5.12)$$

The rate of convergence in this category is relatively fast, however, establishing the communication system is not an easy task since it requires a coordination among all nodes of the system.

The second category of consensus algorithm which is called dynamic consensus method which needs little to none coordination among nodes to reach the consensus. The three main approaches are given below:

1- Asymmetric gossip: in this approach one node sends its value to another node in the network. The receiving node updates its value based on that. Although this approach, needs less communication coordination, it may converge to a value but does not guarantee to average consensus.

$$Q^{ij} = I - w\, e_j (e_j - e_i)^T$$

Where Q(t) ={ Q^{ij} | (i,j) ∈ , i ≠ j }, w ∈ (0,1) and e_i is a vector of all zeros except for the i-th entry which is set to one" [61].

2- Symmetric gossip: in this approach two nodes at a time talk to each other to update their values. Since Q^{ij} is doubly stochastic matrix here, it guarantees the average consensus. However, it requires some efforts to coordinate between those two nodes to update their values at the same time.

$$Q^{ij} = I - w\, (e_j - e_i)(e_j - e_i)^T$$

3- Broadcast: in this approach, one node at a time broadcasts its value to all other nodes to update their values. This method requires the following equation in which the states update their values:

$$Q_i = I - w \sum_{j \epsilon V_{out}(i)} e_j (e_j - e_i)^T$$

The convergence speed of these three dynamic consensus algorithm is given in figure below.

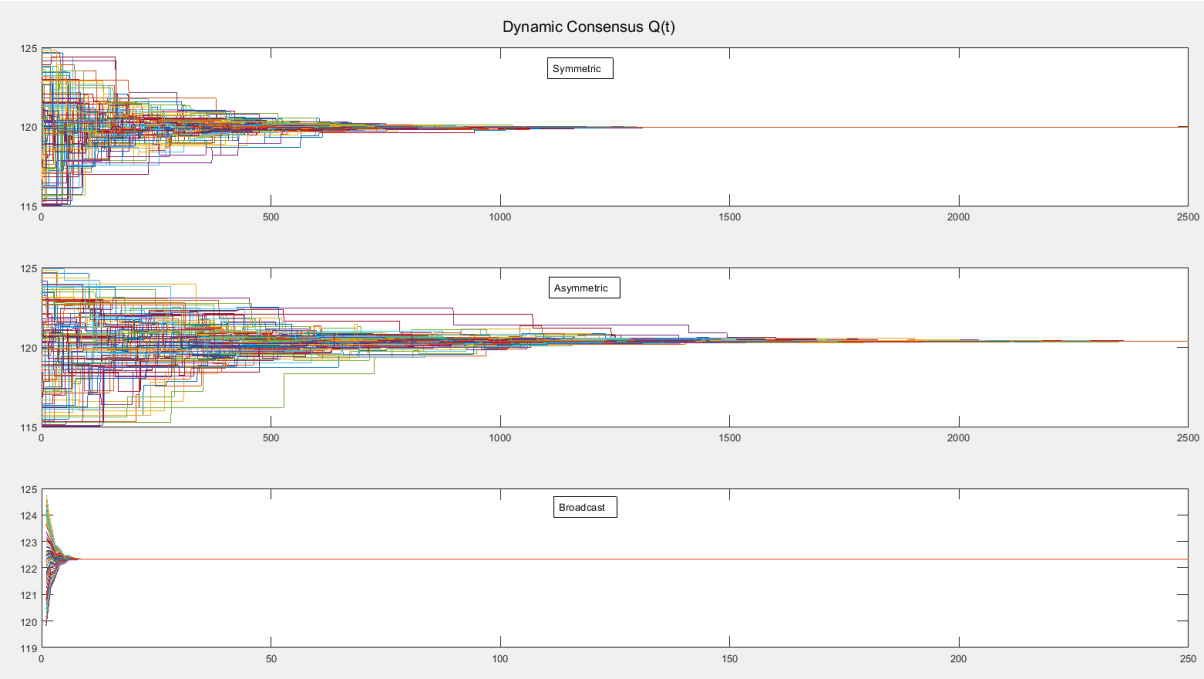

Figure 5-8 Dynamic Consensus Convergence Speed

In the following scenario, an ideal average consensus algorithm is implemented at t=1 second. As it is shown in the figure, the average voltages of the DGs are improved.

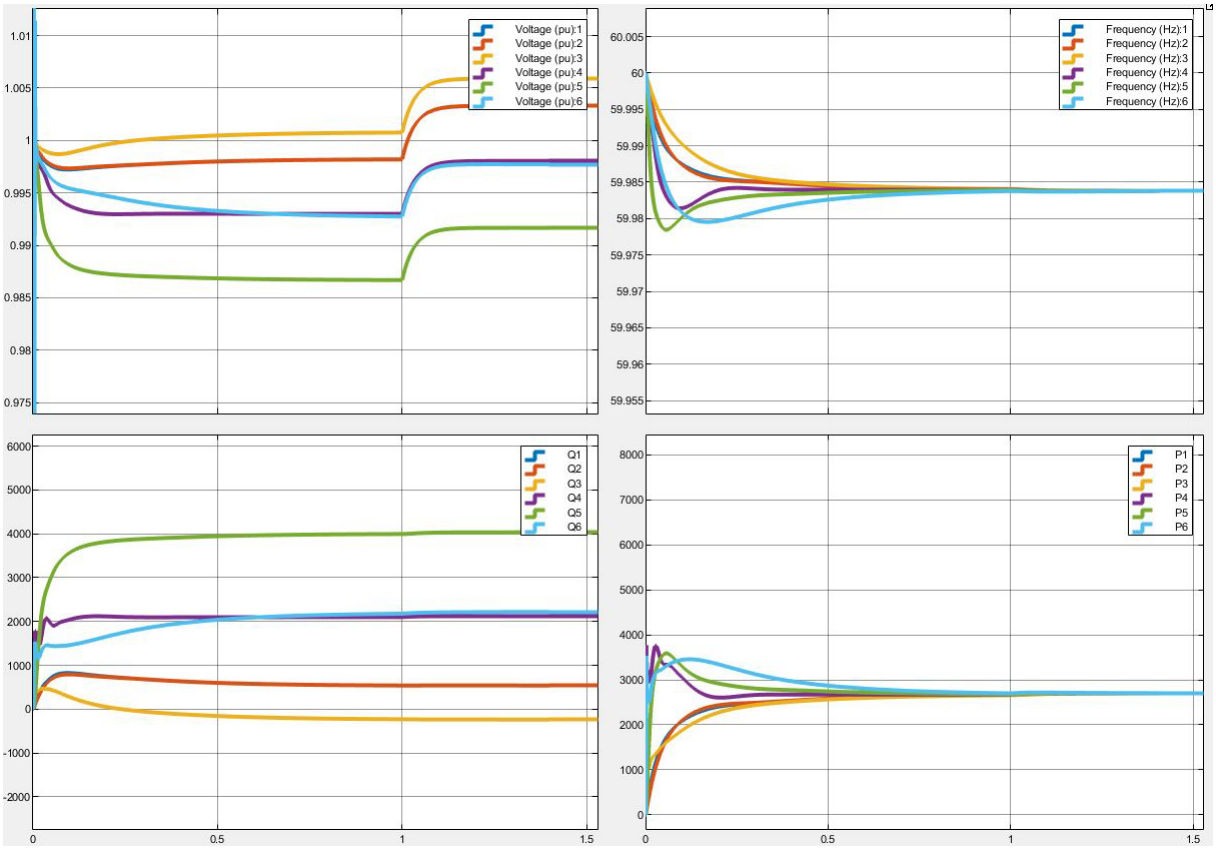

Figure 5-9 Average Consensus Result (Ideal Case)

5.3.3 Proposing fully distributed secondary voltage control with considering the physical layer

Although a primary voltage control may stabilize the system without needing of any sort of communications, it might not be able to fully alleviate the voltage deviation in the power system. To bring the voltages back to their nominal values, a centralized secondary voltage controller has been utilized widely in the power system. Due to the possibility of single point of failure in centralized algorithm, distributed algorithm has been recently discussed in the literature. In the proposed distributed algorithm in the literature, each DG communicates only with its own immediate neighbors, however, the communication messages are still circulated among all DGs to control the voltage of the system. Moreover, it is also possible that the desired reference value cannot be reached in this algorithm due to the local nature of voltage controllers; therefore, in this dissertation, a fully distributed algorithm is proposed in which the

communication messages are only transmitted among DGs in each zone rather than the whole power system. For example, to apply the fully distributed algorithm in the system shown in Figure 5-8, first, the system is first divided in two voltage zones using the voltage sensitivity matrix mentioned in the previous chapter. Second, to control the voltage of each zone, only the DGs in that zone transmit messages in a distributed way rather than communicating the messages with all DG in the system. For instance, to control the voltage of load number 4, it is efficient that DGs number 4, 5, and 6 transmit messages in zone one rather than using the DGs in zone two. The following section discusses this example in more detail.

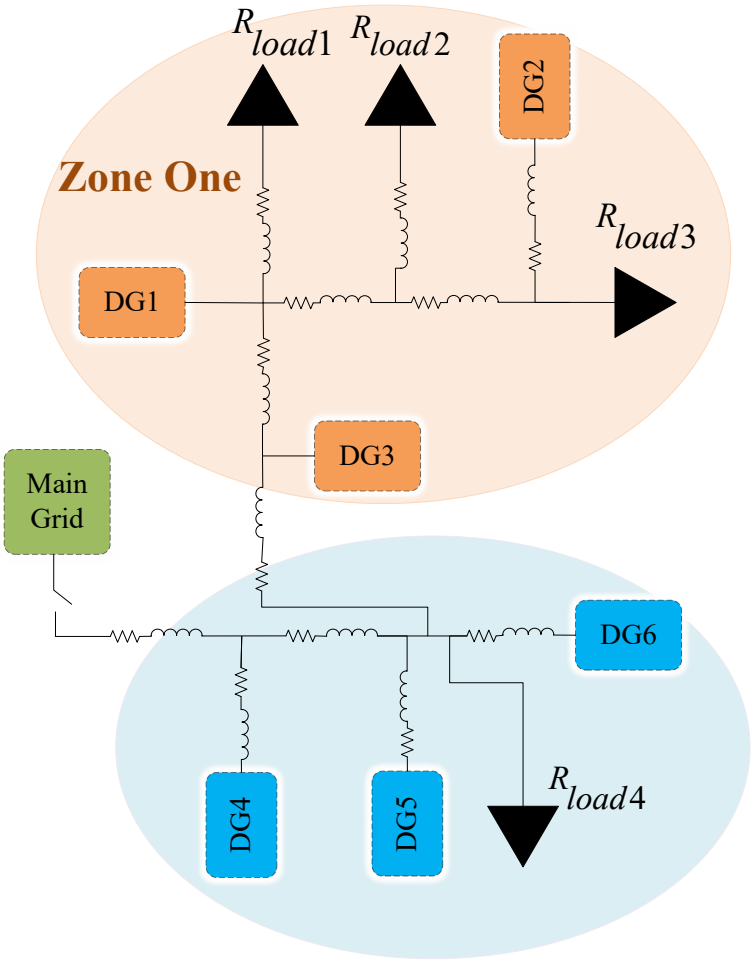

Figure 5-10: Zonal Analysis for Voltage Control

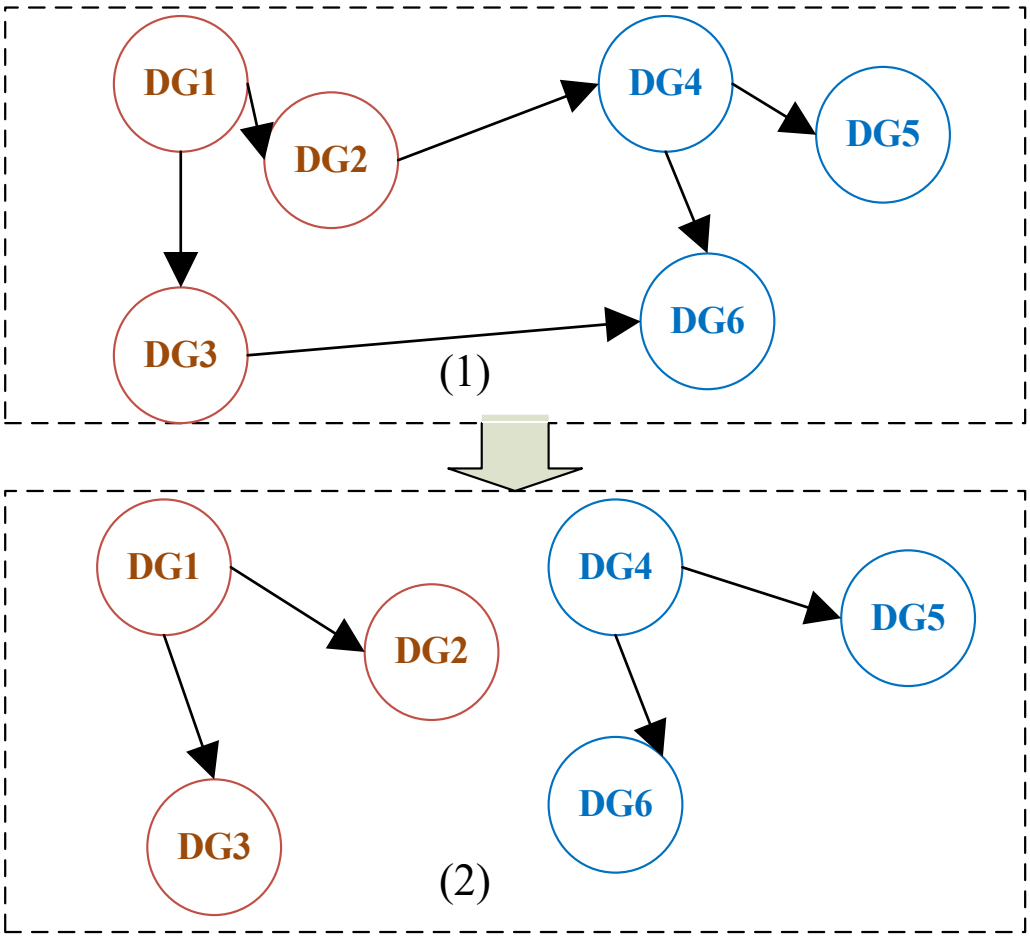

Figure 5-11: Two different DGs' Wireless Connection (1) Global consensus connection; (2) Zonal consensus connection

5.4 Simulation Results

A power system with six DGs and four loads is presented in this dissertation study. Line impedance is chosen Z=0.23 + j0.132 Ohm. Load values are chosen to be 20 + j11.31 Ohm. DGs have been modeled in Matlab software by implementing the equations given in chapter II. Multiple scenarios to show the effectiveness of the proposed method is discussed in the following sections.

5.4.1 Scenario One (voltage: two zones, frequency: two zones)

The zonal division between two zones has been done as it is shown in Figure 5-8 and the communication between DGs are shown in Figure 5-9 part 2. A fully distributed secondary controller is activated at t=1 second to show how it can improve the voltage deviation due to the primary controller. The result in Figure 5-10 shows that the voltages of each group successfully converge to its reference value in less than 0.4 seconds.

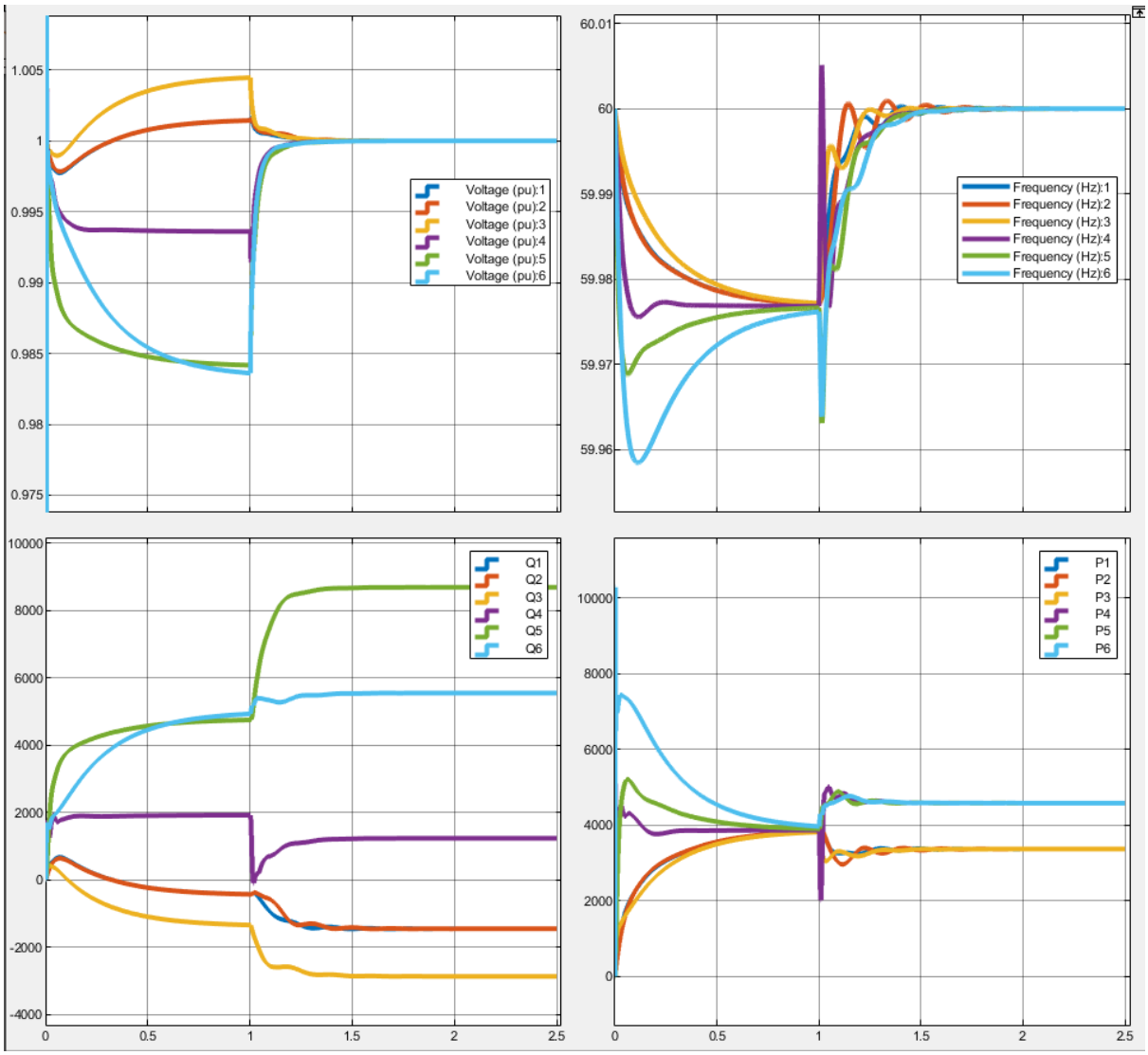

Figure 5-12 Scenario one (two zones): V, F, P, and Q

5.4.2 Scenario Two (voltage : one zone; frequency: one zone)

In this scenario, voltage zoning is not applied to the system, therefore, communication of DGs are done as it is shown in Figure 5-9, part 1. DG1 is the leader here, unlike the previous part that there was one leader for each zone (DG1 for zone 1 and DG4 for zone 2). Figure 5-11 shows that although the voltages still reach the reference value, it took more than quadruple in comparison to the case in scenario one. This shows, the importance of fully distributed algorithm in controlling the voltage of the system.

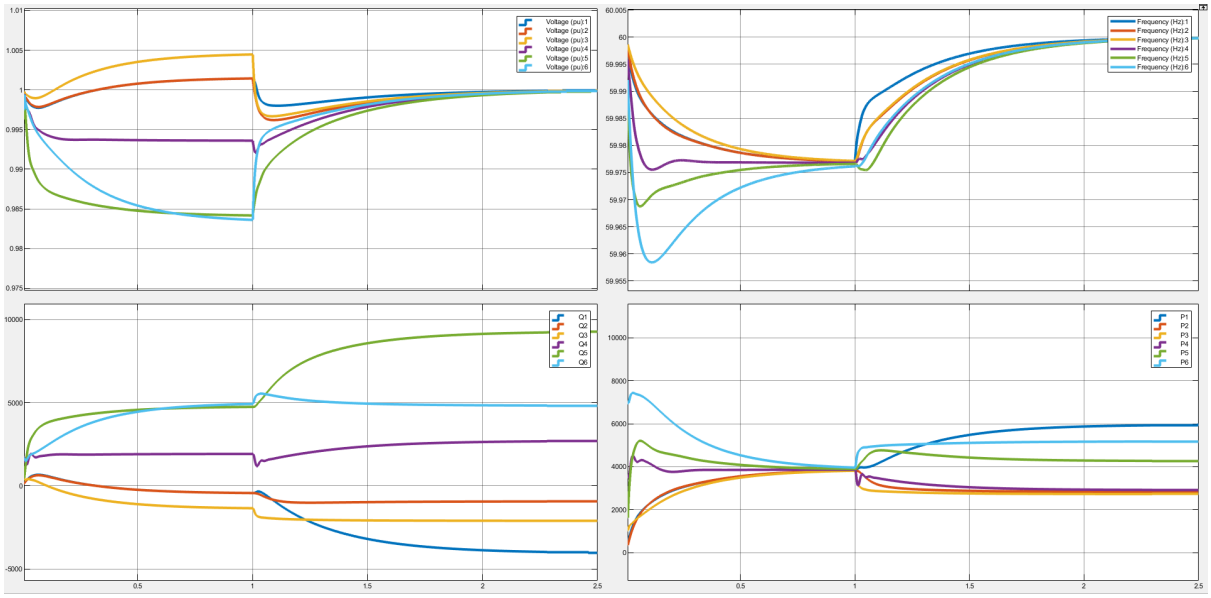

Figure 5-13 Scenario two (one Zone): Voltages of DG1-6

5.4.3 Scenario Three (voltage: two zones; frequency: one zone; with a step load change of 1kW)

In this scenario, the distributed secondary voltage is controlled in two zones but distributed frequency control is controlled in one zone. The secondary voltage control is applied at one second. It takes only one second to converge the voltage to their nominal values in contrary to the previous case (one voltage zone) where it took two seconds to control the voltage. In addition, in this scenario, a step load of 1kW is added to load four in the system at two seconds. Since there is no zoning defined for the frequency control in this scenario, the increase in the

load four is compensated the most by the closest DG to it, which is DG6 and then DG5. Although offsetting the demand by the closest DG is beneficial in terms of having less distribution line loss, it may overload the closest DG very fast. Therefore, clustering the DGs in two zones to control the system's frequency is used in the following scenario to solve this issue.

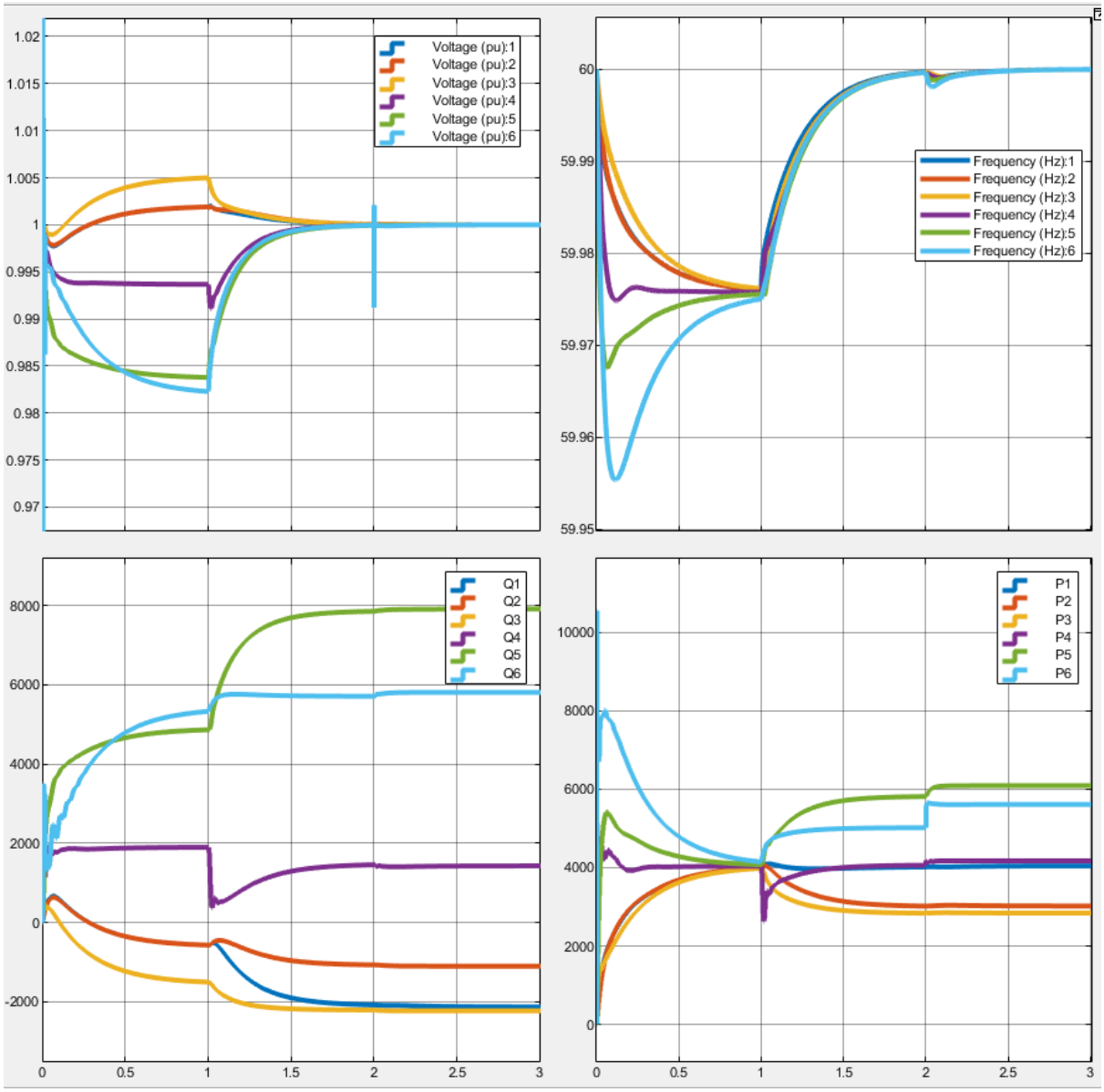

Figure 5-14 Scenario 4 (voltage controlled in two zones. Frequency controlled in one zone)

5.4.4 Scenario Four (voltage: two zones; frequency: two zones; with a step load change of 1kW)

In this scenario, the secondary voltage and frequency control are divided into two regions, and then the effect of 1kW change in load four is observed on the system at two seconds. The results in Figure 5-13 indicate that the neighboring DGs to load four (i.e., P4, P5, and P6) compensate the required power together rather than the previous case that the closest source (P6) contributed the most. This is an essential factor because in the microgrid system with small-scale renewable energies, it is more reliable to compensate for the increase in the demand with the neighboring DGs rather than one DG to avoid the possibility of overloading a single DG. It is also important to note that the frequency convergence time is improved in this case versus scenario three by about 0.1 seconds. This indicates one more time the advantage of clustering the DGs to control the frequency of the system.

.

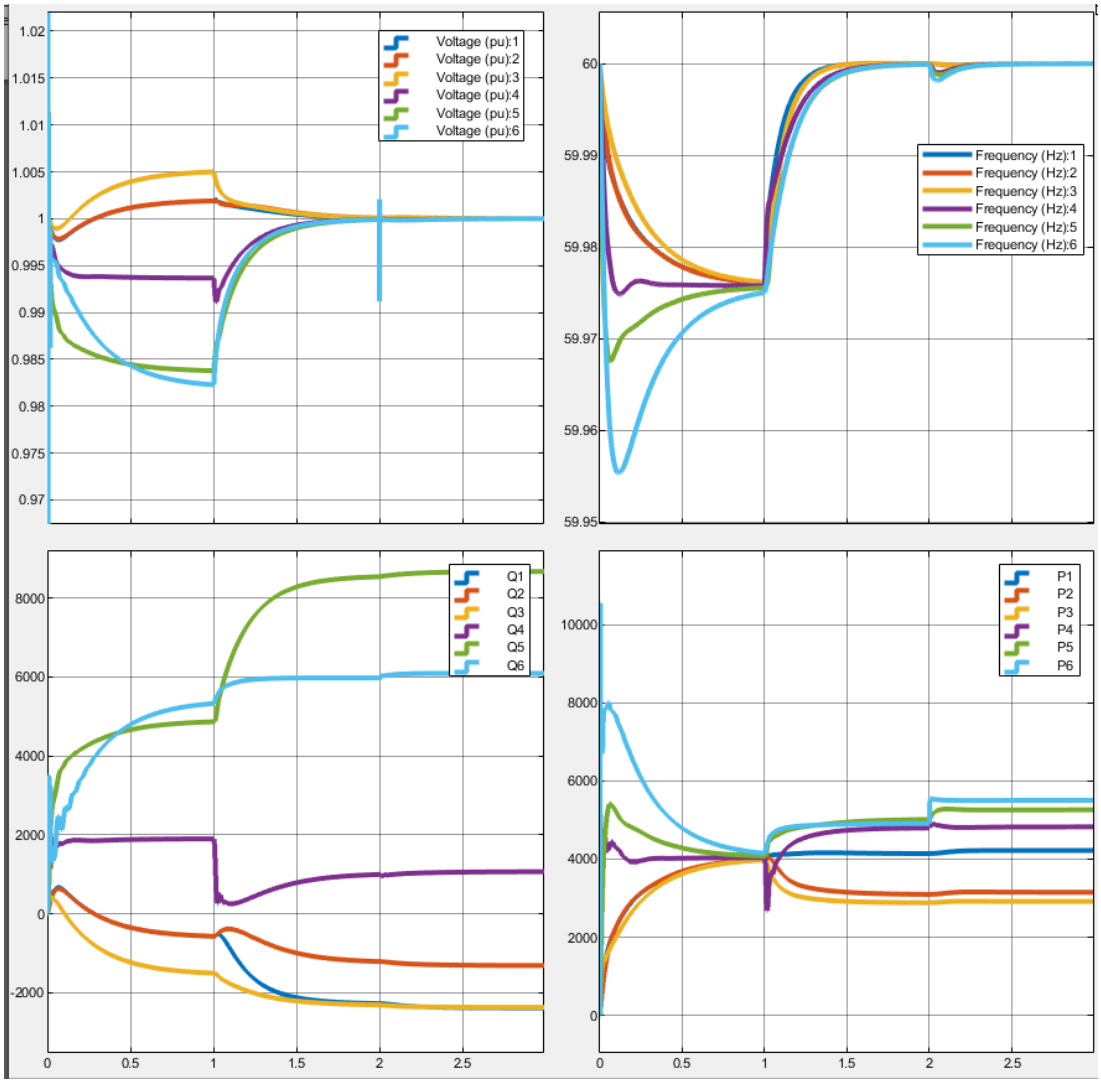

Figure 5-15 Scenario four (voltage and frequency controlled in two zones)

5.4.5 Considering the effect of communication delays in the system

This section implements an actual communication protocol to analyze the impact of communication delays and packet loss on the secondary control level. An appropriate communication protocol for this application should be able to send a short message such as the voltage or the frequency to other devices repeatedly. Furthermore, in case of having multiple devices to communicate simultaneously, this protocol should be able to handle the situation by first detecting the collision and then giving priority to the highest priority device (leader node in this application). One suitable communication protocol here is the Control Area Network (CAN). “CAN is a serial communications bus developed initially for the automotive industry

to replace the complex wiring harness with a two-wire bus" [39]. This protocol is also is capable of handling the message collision when there are more than one device trying to communicate with other devices. In this protocol, devices can be ranked based on their priorities which can then be used to avoid message collision. It is also is a fault-tolerant protocol in an electrically noisy environment. Furthermore, CAN protocol is a carrier-sense, multiple-access protocol with collision detection and arbitration on message priority (CSMA/CD + AMP). In addition, this protocol sends relatively small blocks without any supervision need of a central bus. "These features have led to CAN's popularity in a variety of industries building automation, medical, and manufacturing" [39]. For this reason, this protocol is used in this study.

In Figure 5-14, a schematic of implementing the CAN protocol for the previously discussed microgrid system with six DGs is shown. Each DG (shown with a CAN ID in Figure 5-14) communicates its voltage/frequency value with the CAN bus in a serial communication. The CAN bus broadcasts the data to other DGs. If two devices broadcast the data at the same time, the CAN bus has a collision detection technique to make sure that no data is lost.

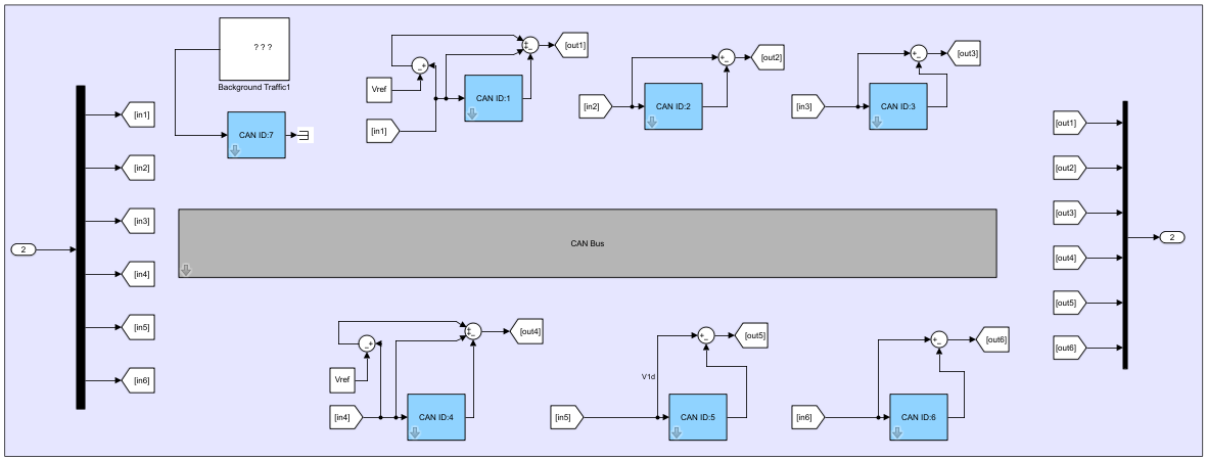

Figure 5-16 Simulating a real communication protocol (CAN protocol) between the six DGs in the system

To account for the background traffic, a CAN ID number seven is used as it is illustrated in Figure 5-15.

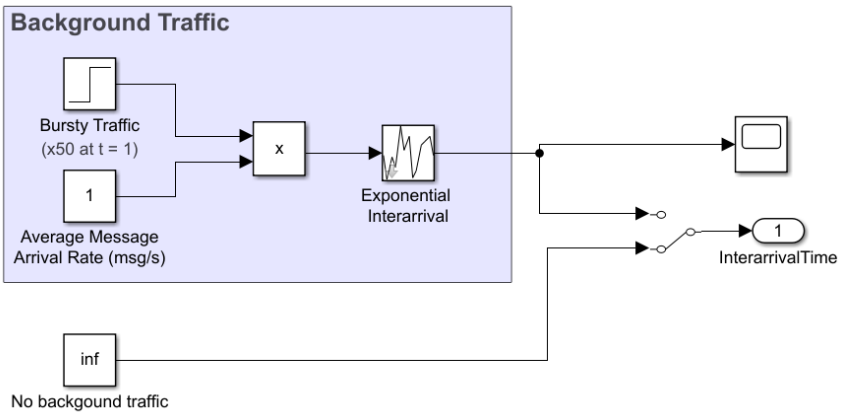

Figure 5-17 Simulating background traffic in CAN ID seven [82]

In Figure 5-16, the detailed Simulink modeling for each DG is shown. Each DG has a communication system that consists of two parts: transmitter and receiver. The transmitter makes a communication package that includes the data as well the as the sending ID and the receiving ID. CAN bus protocol is capable of ranking the data based on the prespecified priority in the system. If multiple transmitters send the data at the same time, the CAN bus keeps the highest priority data and drop the other ones. In this case, the receiver of each CAN ID listens

to the broadcasted message from the CAN bus to verify that the message is delivered by CAN bus, otherwise, CAN ID retransmit the lost message to the CAN bus.

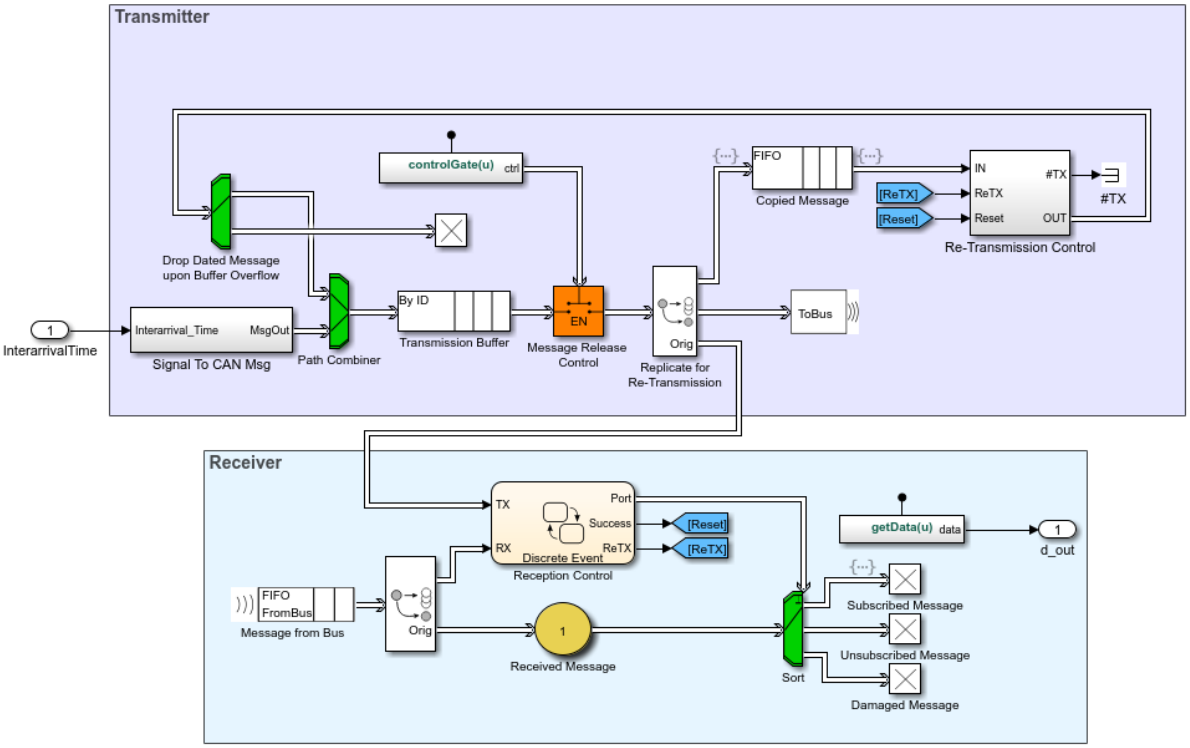

Figure 5-18 Matlab simulation of a real communication protocol that is used in each DG [44].

In Figure 5-17, the CAN bus model is shown. The messages received by the CAN bus is then broadcasted to the receivers. If two messages arrive at the same time, the one with a higher priority passes through the bus and the other one will be dropped. CAN bus makes it easy for different parts of the system to talk to each other in a robust and noise free environment.

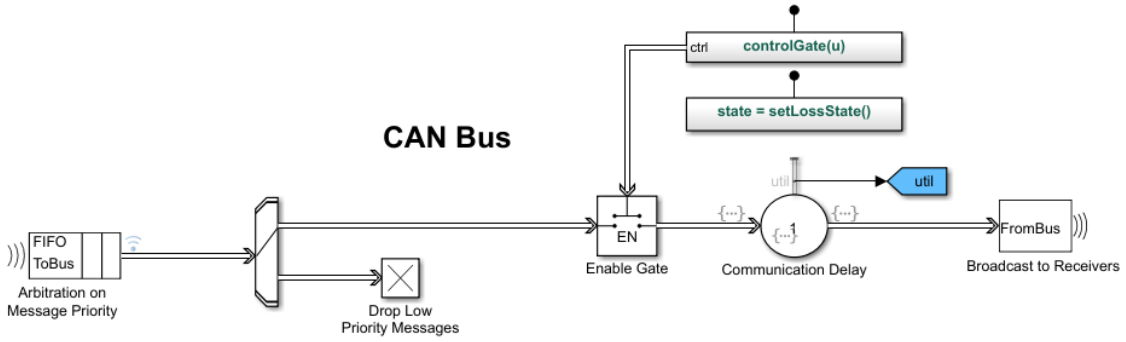

Figure 5-19 Matlab simulation of CAN bus [82]

The CAN protocol simulated in Matlab that is explained above is adopted as a communication protocol used in the microgrid system illustrated before in Figure 5-8 to regulate the voltage and frequency of the system. Different scenarios are simulated to show the effectiveness of the packet loss and delays in the system.

In case one shown in Figure 5-14, CAN communication protocol with no background traffic noise and the probability of packet loss to be .001 is assumed. This communication protocol is activated at time 0.6 seconds among DGs to regulate the voltage and the frequency in the secondary controller level. The result indicates that the system is capable of bringing the voltages and frequencies of the system around their nominal values; however, a small fluctuation in the values is observed.

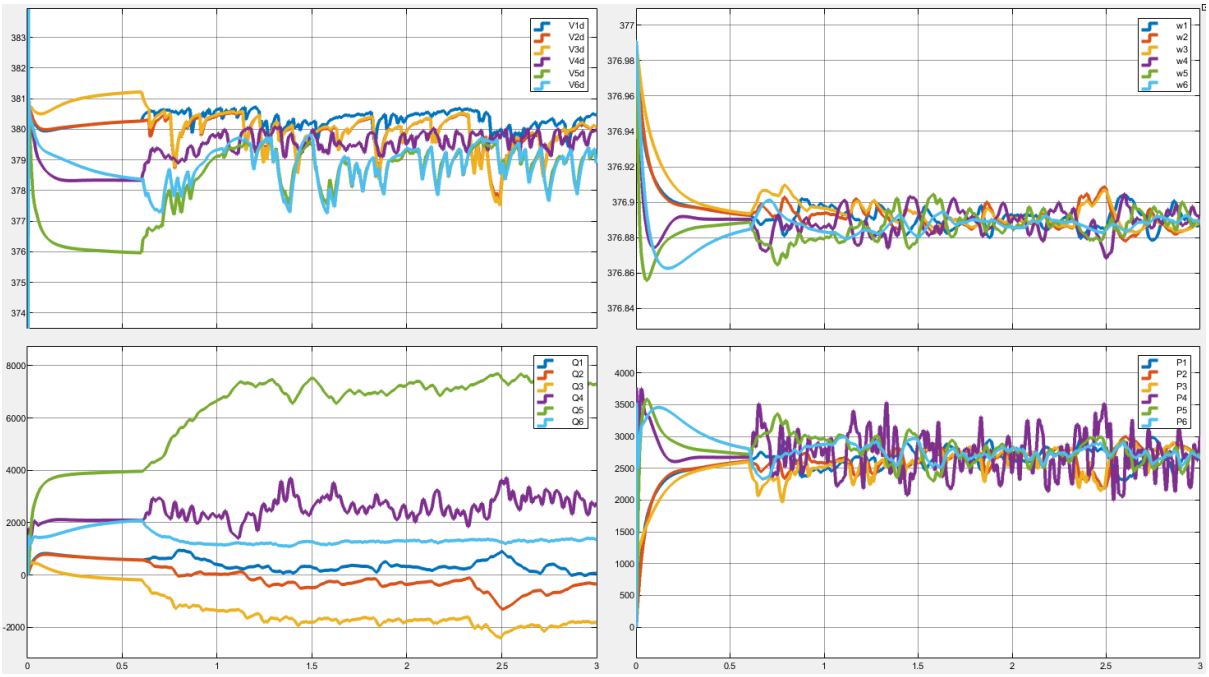

Figure 5-20 Case one: the effect of implementing a CAN communication protocol on the distributed controller (packet loss probability 0.001, no noise traffic)

In case two, a background traffic noise is added to the bus channel with a bursty traffic of 1000. The communicating messages are also limited to 4 message/second. These limitation are added to the system to check the effect of them on controlling the voltage and frequency of the system. Figure 5-15 demonstrates an almost similar results in terms of controlling the voltage and frequency as the previous case that no background traffic was modeled. This shows the robustness of this protocol to the noises which is an important factor in power systems. This robustness comes from the fact that this protocol is a CSMA-CD protocol which senses the channel to send a data when channel is not busy and is capable of retransmitting the data in case of a data loss.

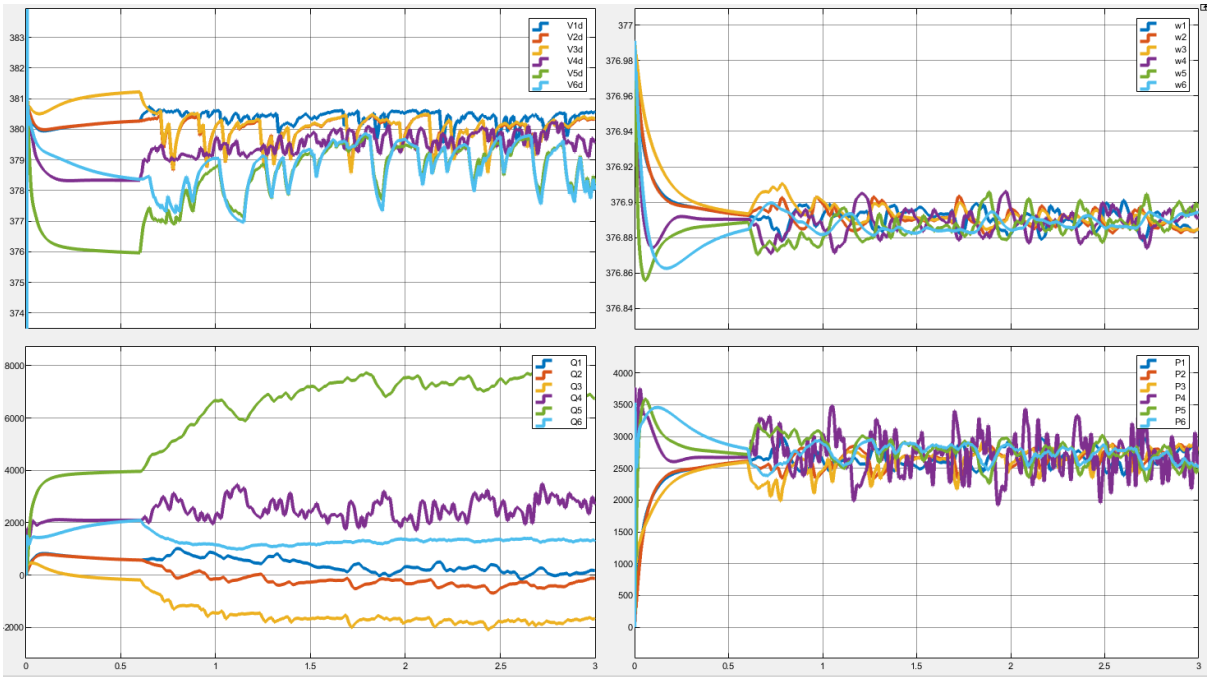

Figure 5-21 Case two: the effect of implementing a CAN communication protocol on the distributed controller (loss probability 0.001, Bursty Traffic of 1000, 4 message / second)

In case two, the rate of changes in the frequency and the voltage of the system is extremely high. To resolve this issue, a data limiter is simulated to update the status of each controller after some interval time in case three. The results regarding controlling the voltage and frequency are improved in this case as it is illustrated in Figure 5-16.

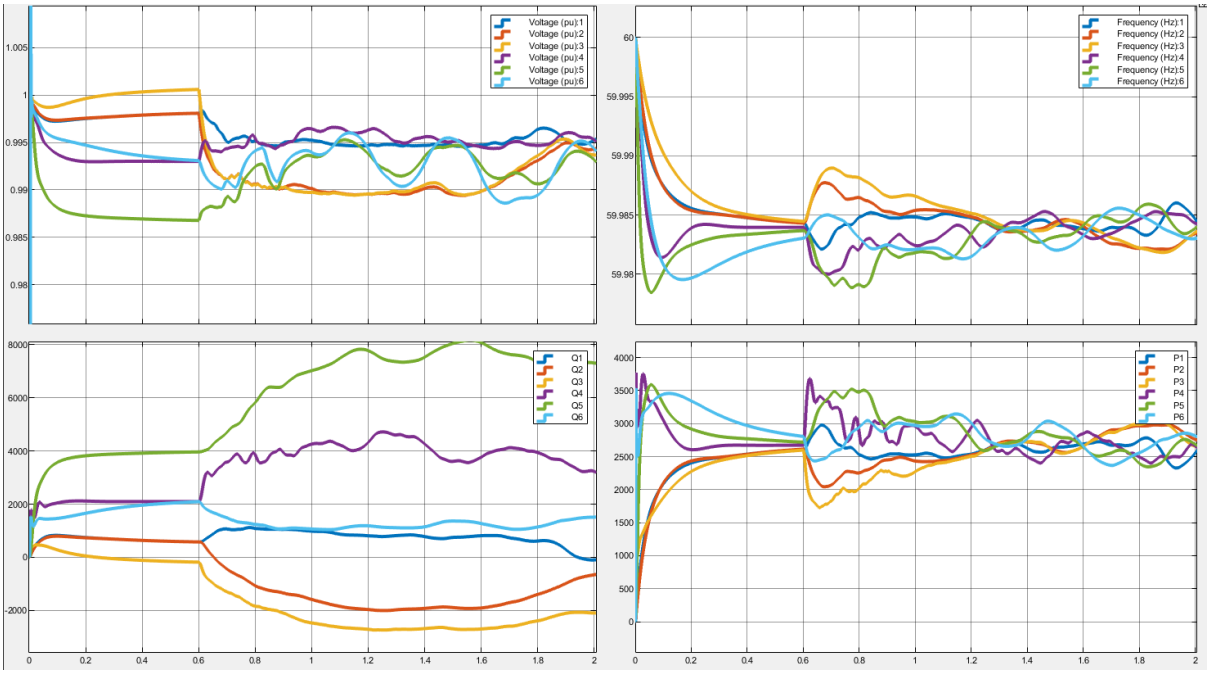

Figure 5-22 Case three: The effect of implementing a CAN communication protocol on the distributed controller (loss probability 0.001, bursty traffic of 1000, 4 message / second)

Implementing a CAN time communication protocol that has CSMA-CD in the microgrid system, reveals an important lesson in the area of distributed controller systems. The results from the last three simulations confirm that if the communicated messages among the DGs are not updated at the same time, then no consensus will be reached in the system. This shows the importance of modeling a CAN communication protocol in Matlab rather than using a simplified communication system. It also offers the room for a new communication protocol to be developed in the distributed system to update the states of each DG simultaneously.

5.5 Modified IEEE 13 Bus Feeder Result

In distribution systems the ratio of R/X in power lines are lower than transmission systems. To evaluate the effectiveness of the proposed distributed controller in the distribution systems, a modified IEEE 13 bus feeder is developed in this section. This IEEE 13 bus feeder is modified to represent a balanced system by averaging the load of each phase. Moreover, four DGs are added to the system to make it like a microgrid system. The schematic of this modified IEEE 13 bus feeder is given in Figure 5-17.

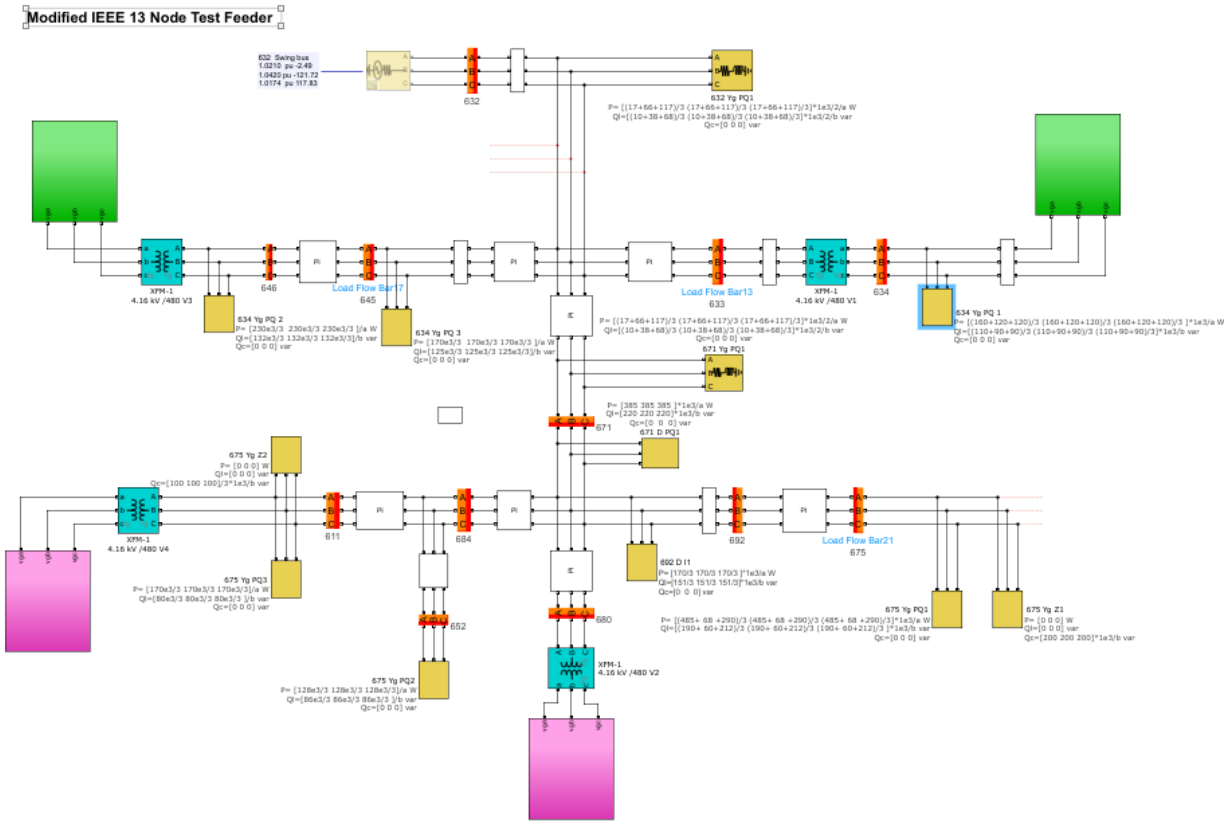

Figure 5-23 Modified IEEE 13 Bus System

Two zones are selected in this system to evaluate the zoning effect on distributed voltage controller. Zone one includes the green DGs and zone two includes the purple DGs as it is shown in Figure 5-17. The distributed secondary controller is activated at time 0.4 seconds. As it is shown in Figure 5-18, voltage and frequency of the system is successfully regulated to their nominal values.

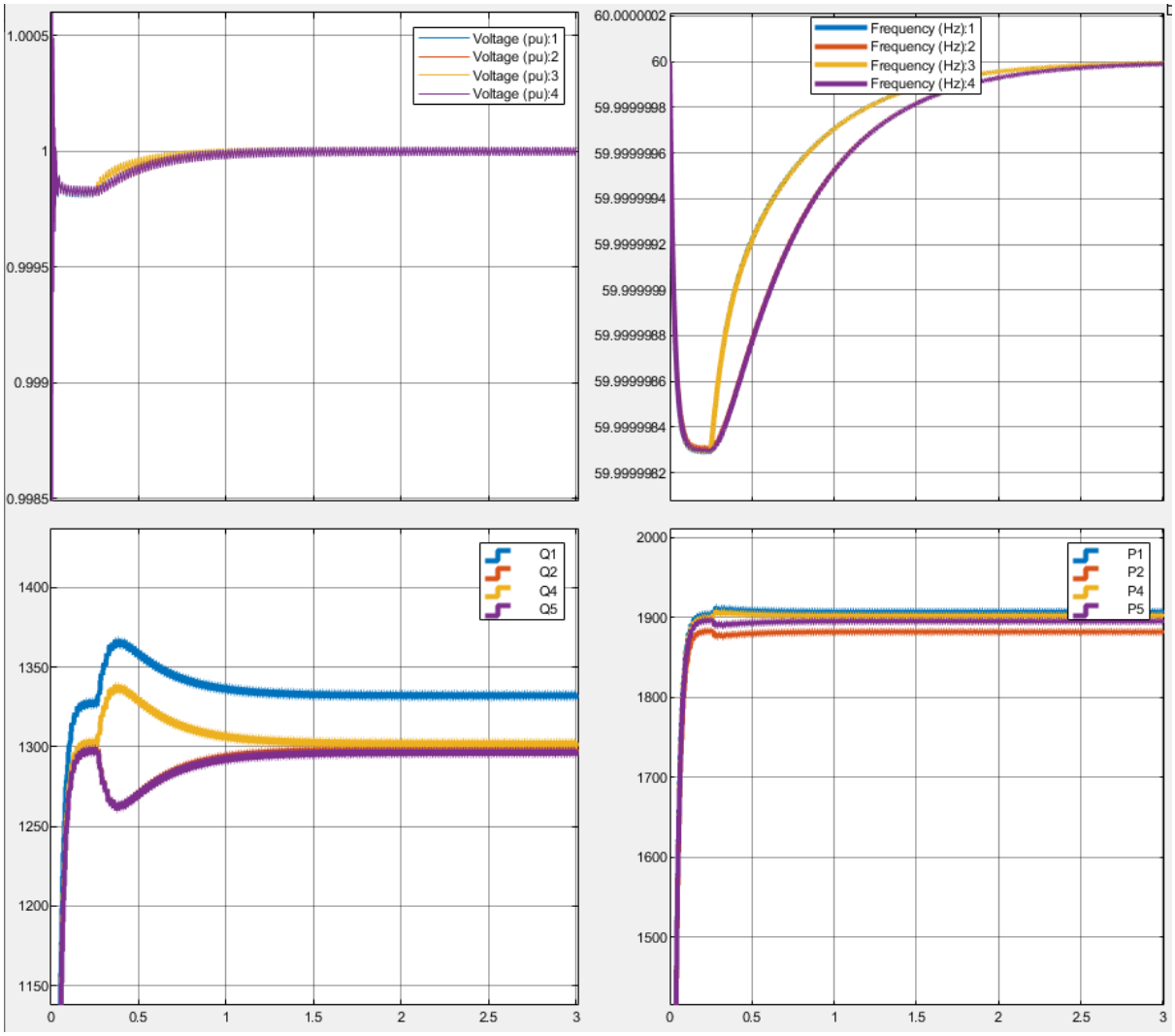

Figure 5-24 Results from running a distributed controller on modified IEEE 13 bus

5.6 Distributed Economic Dispatch Control:

Along with the voltage and frequency control algorithms discussed before, there are other applications of distributed algorithms in the power system. In this case, an economic dispatch problem is implemented on the following system with two DGs using a distributed algorithm. Although these algorithms have already been proposed in the power system, to the best of the author's knowledge, they have not been implemented on a detailed microgrid system. In this

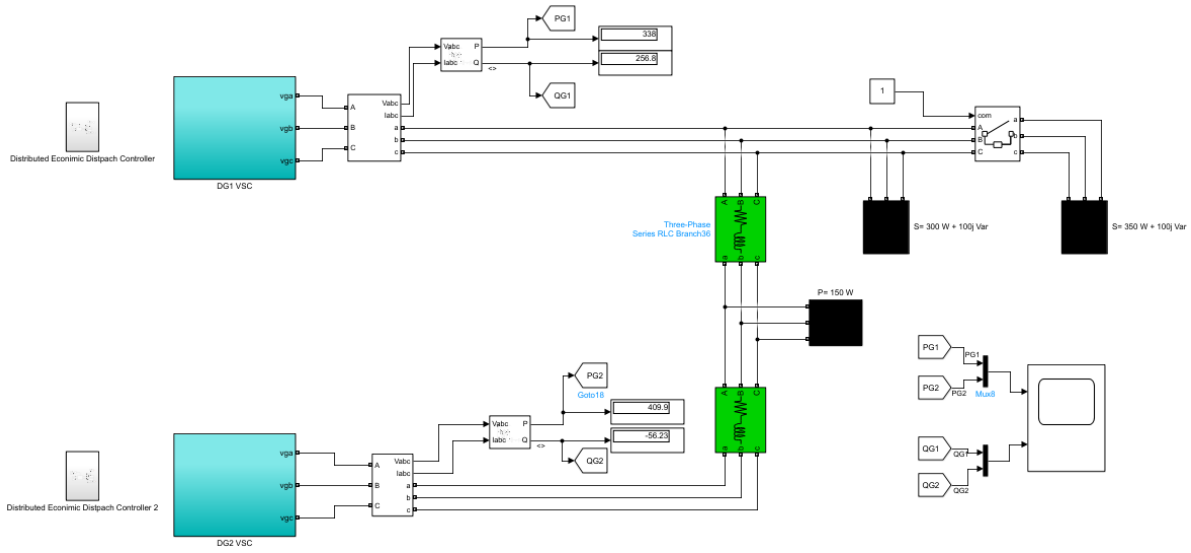

Figure 5-25 Implementing the distributed economic dispatch problem on a system with two DGs:

case, communications are local and the new setpoint for each DG is calculated locally based on limited communication.

In the following case shown in Figure 5-20, DGs share the load equally around t=0.4 seconds where only the primary controller is activated. Although this controller is beneficial to compensate for any sudden changes in the system, it may not dispatch the power optimally among the DGs. Therefore, a distributed economic dispatch controller is activated at t=0.4 seconds to adjust the output power of P1=225 W and P2 =225 W to P1= 450 W and P2=200 W. At t=0.8 seconds, the distributed algorithm is deactivated again and as it is shown in Figure 5-20, both DGs share the load equally again at P=125 W. At t= 1.4 seconds, a load with the given power of S= 300 W + j100 VAR is added to the system which brings PG1 and PG2 to

375 W. At t= 1.8 seconds, the economic dispatch controller is activated which makes PG1= 420 W and PG2=330 W. The lambda in this case is set to 14.11.

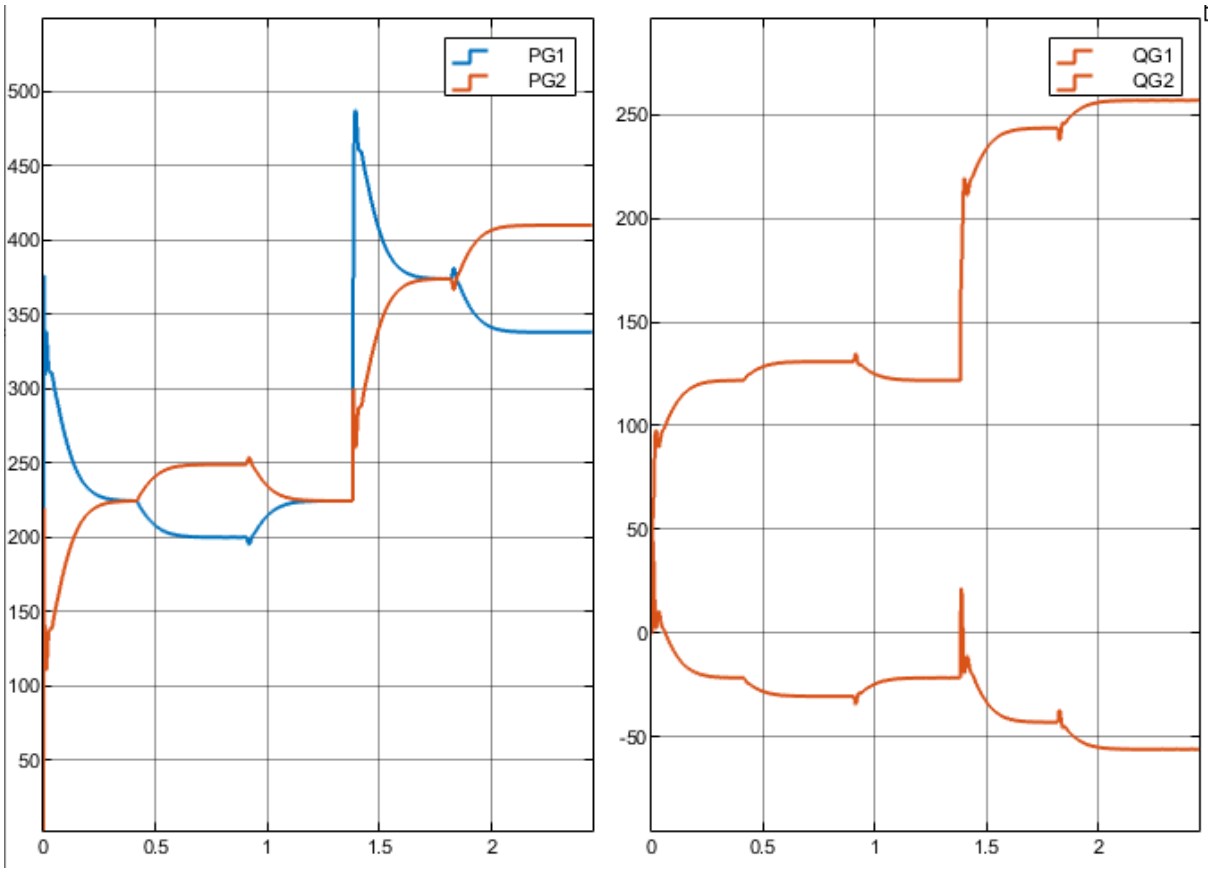

Figure 5-26 Output active and reactive power for distributed economic dispatch problem

This example shows the advantage of implementing the economic dispatch controller. It is especially beneficial for a microgrid system where the renewable energy sources connect and disconnect to the system frequently. If a MG system is capable of automatically dispatching the power among the DGs that are ready to provide the power at a moment (in a plug and play mode), then it can save so much money from it. For instance, in the above example, let's assume that DG1 is a solar/wind farm and DG2 is a diesel engine that feed a big farm. Since solar/wind output power alternates in a day, the diesel engine should be there to make sure that the power is provided to the system. However, when the energy of solar/wind is available, the system shares the power among the sources using the distributed dispatch controller to bring down the cost of power production.

5.7 Active and Reactive Power Limits in Secondary Controllers:

Renewable energies can produce both active and reactive power depending on the system's needs. Still, they have been incentivized only to deliver the maximum active power, such as what is known as maximum power point tracking (MPPT) in solar inverters. In the recent years by higher penetration of solar energies, the active power generated in the system is more than the demand during noon, where sunlight is available the most. This has caused huge issues and extra costs for the power utility companies. For example, multiple times in 2017, where the generating power was more than the load in California, they paid Arizona utility companies to take the excess energy coming primarily from solar energy [40]. This issue can somewhat be resolved by increasing the capacity of the storage units which is expensive. However, ideas such as incentivizing the solar energy owners to limit their power at certain times or produce reactive power as well as active power, unlike the current MPPT approach, are good alternatives that can be implemented into the future of solar energy inverters. Moreover, it can partially solve the issue of excessive power than the demand during certain daytime hours. It can also solve the voltage drop in some rural areas far from the source by providing reactive power for the system. In this section, a controller that can adjust the active and reactive power of each DG is implemented due to the essential impact of this feature as discussed above.

As it is presented in Figure 5-21, there are two integrals in each controller to monitor the maximum and minimum values [41]. The first one compares the actual active power with the Pmin and sends the difference into a PI controller. This PI controller has a maximum upper limit of 0.2 and a minimum lower limit of 0. Whenever the actual P is less than Pmin, a small positive value goes to the droop controller to increase the frequency of the DG, consequently providing more power.

On the other hand, if the actual P is more than Pmax, another PI integrator comes into play. In this case, a small negative value comes out of this PI controller to reduce the frequency of the DG and consequently reduce its active power. A similar approach is used to limit the reactive power within its boundaries, as shown in Figure 5-25.

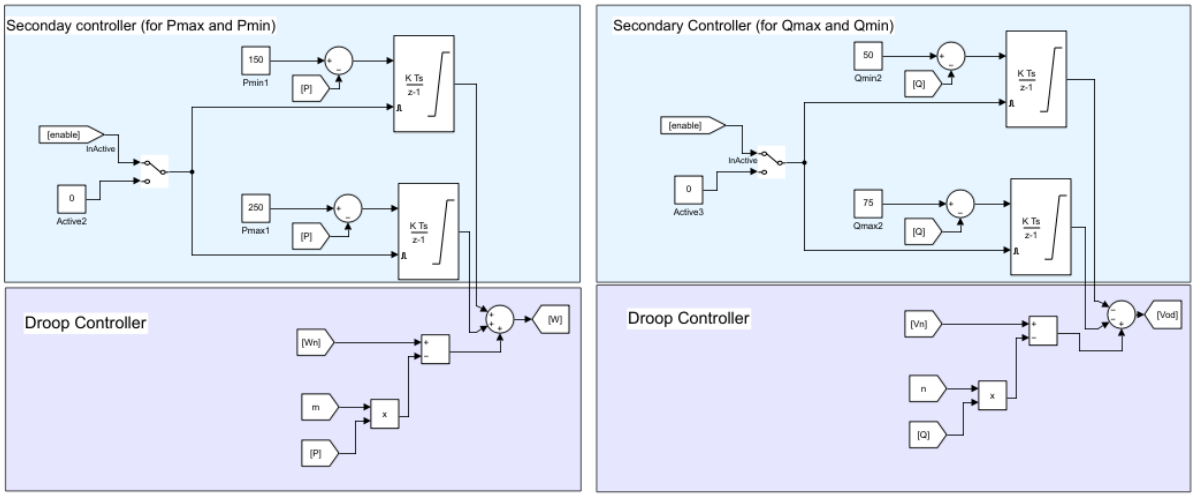

Figure 5-27 Output active and reactive power for distributed economic dispatch problem

Implementing Active and Reactive Power Limits for the Controller A case study is run to show the effectiveness of this algorithm as it shown in Figure 5-22.

- Before t=0.4 seconds, the droop controller is only active. In this case, PG1=PG2=360 W (due to the droop controller) and QG1= 175, QG2= 25.
- At t=0.4 seconds, the maximum and minimum reactive power of DG1 is set to new values of 75 Var and 50 Var, respectively. It is shown that the controller successfully brought the reactive power of DG1 from 175 var to 75 var in less than 0.1 seconds.
- At t=0.9 seconds, the new values for the maximum and minimum active power of DG1 are set to 250 W and 150 W, respectively. In this case, the controller successfully brings down the PG1 from 375 W to 250 W.

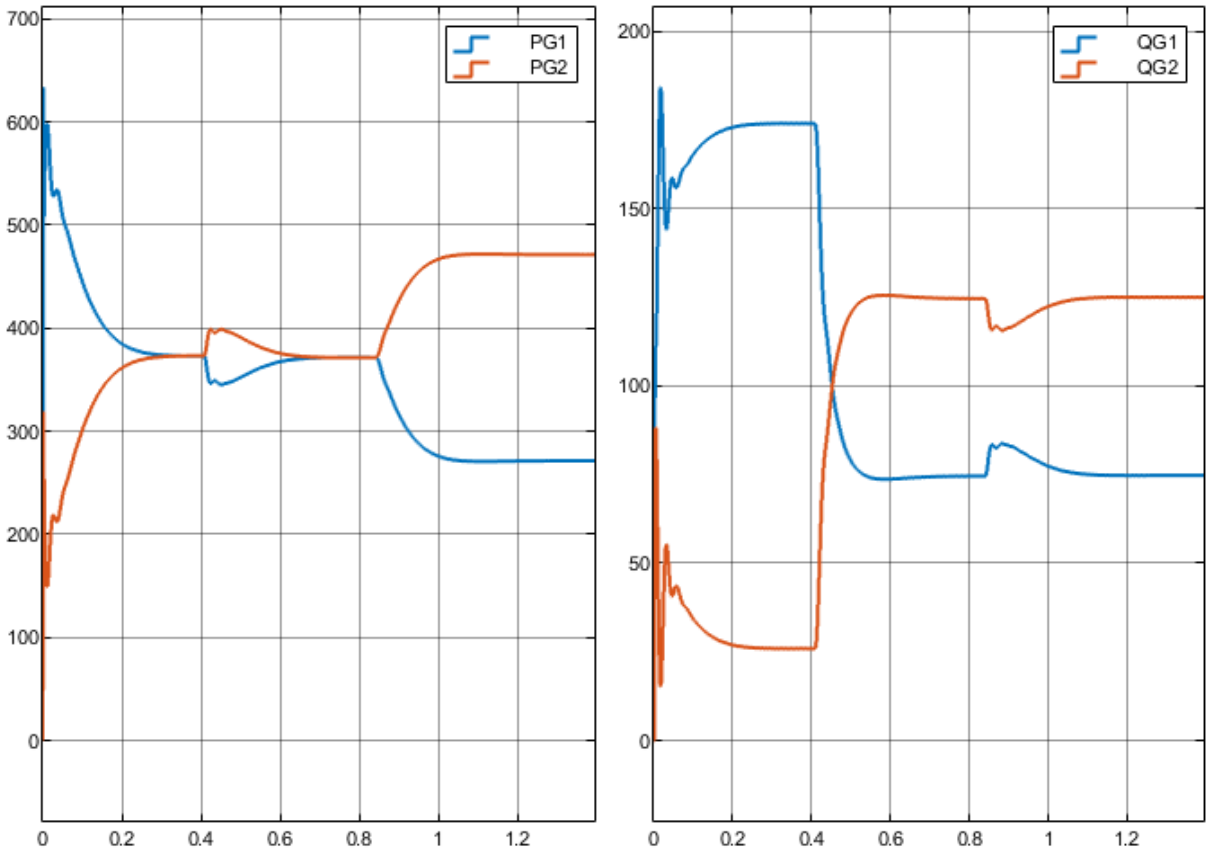

Figure 5-28 A case study to show the effectiveness of the active and reactive power limit controller

5.8 Designing Setpoint for CSI Inverters:

In grid connected mode where the voltage and frequency come from the infinite bus, DGs should operate in PQ mode (i.e. current source mode). These DGs have a current controller block as well as a PLL block to sync the source with the grid. The reference input currents to the current controller block, are the setpoints that are calculated from the desired PQ points. These points can be found from the following two Equations: Idref= P^*/Vodi and Iqref=-Q^*/Vodi. Their implementation in Matlab is shown in the figure 5-23:

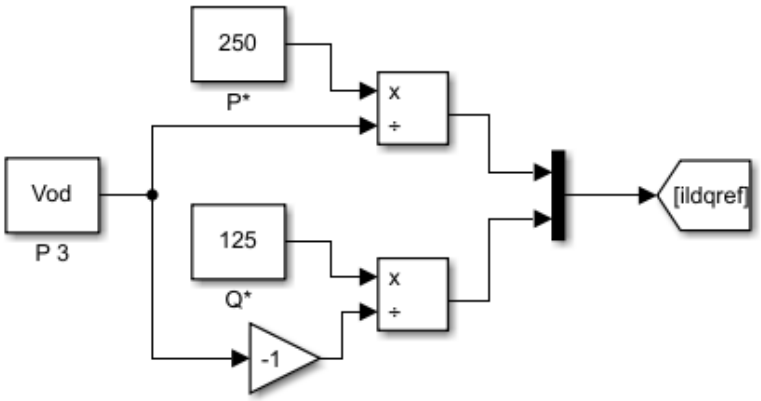

Figure 5-29 Implementation of PQ setpoints for PQ controller

Here is an example to show the effectiveness of these points in setting PQ for CSIs. On the same previous system, DG1 is assumed to be in the VSI mode and DG2 is in the CSI mode. The setpoints for DG2 is PG2=250 W and QG2=125 var. The following simulation results illustrated in Figure 5-24 confirms that the controller for the CSI is working perfectly.

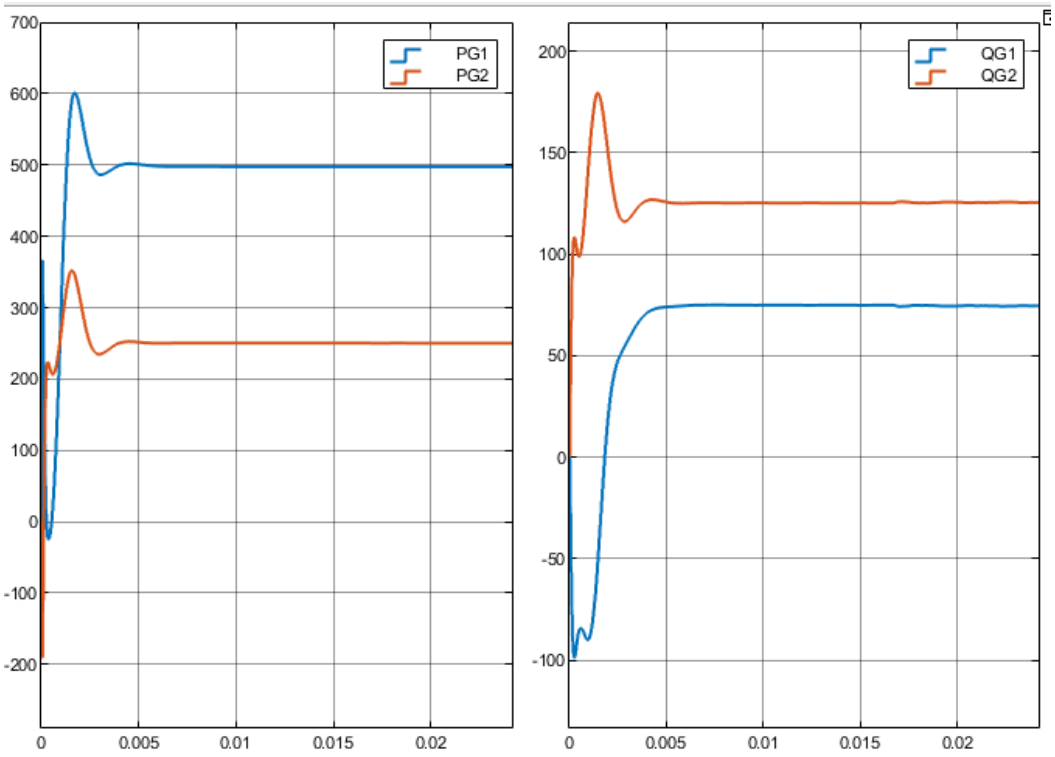

Figure 5-30 A case study to show the effectiveness of the PQ controller setpoints

5.9 Conclusion:

Unlike the frequency, voltage is a local phenomenon which requires the system to be optimally clustered for the purpose of voltage control. In this chapter, the impact of zoning analysis on the voltage control, in terms of the faster convergence rate and reducing the number of messages communicated among the DGs, is discussed. Then CAN communication protocol that works based on the CSMA-CD is simulated. This protocol is robust and is capable of detecting the lost messages. The result shows that while the system is still capable of converging to a certain range around the desired value, it is not capable of converging to the exact desired value. This is due to the fact that the consensus algorithm does not converge unless all of the updated values are applied at the same which is not part of this protocol. This shows the future effort in implementing and designing a robust algorithm that has the benefits of this protocol but is also capable of updating the status of each node simultaneously.

6 Microgrid Simulation and Hardware-in-the-Loop Testing

This chapter focuses on a detailed documentation on hardware-in-the loop (HIL) testing with the OPAL-RT OP4510 real-time simulator and the SEL 351S digital protection relay. In the first step, the setup and connection of the HIL environment is discussed. Then, the developed microgrid in chapter five is tested in the real time simulator.

6.1 Hardware-in-the-Loop Testing

When the performance and behavior of physical components, such as breakers or protections relays, needs to be observed, hardware-in-the-loop testing can be applied to provide a safe, accurate and cost-efficient environment for researchers [42]. It is especially well suited for microgrid research, since various simulation platforms to simulate power grids exist.

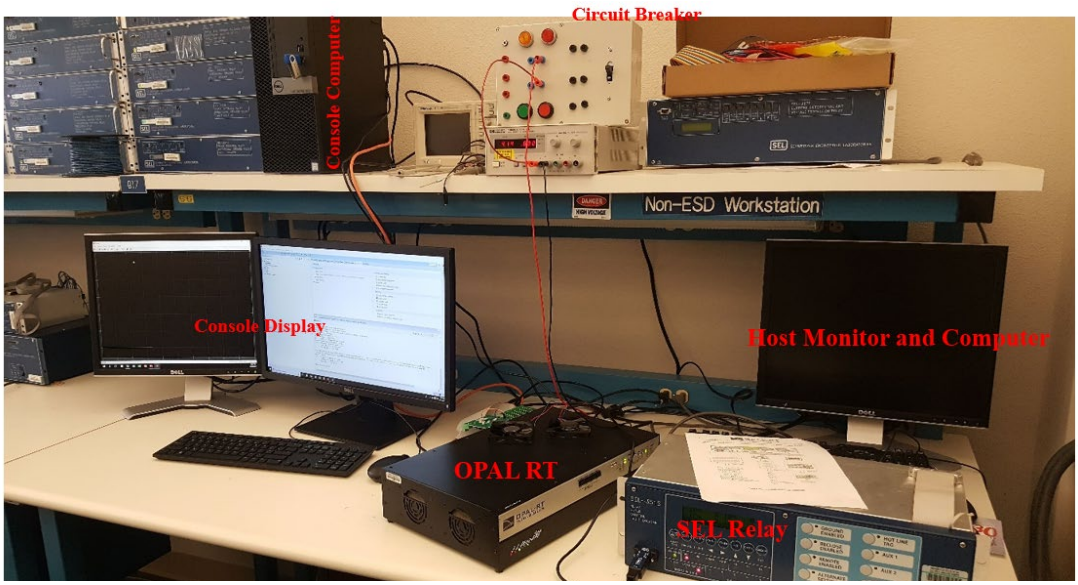

Figure 6-1 Real Time Simulator Setup

6.1.1 Hardware: OPAL-RT OP4510 and SEL 351S

For the real time simulator, the OPAL-RT OP4510 V2, a compact, entry level real-time power grid digital simulator is used. With its large number of I/O channels and its simulation software RT-LAB, which is fully integrated with MATLAB/Simulink, it provides flexibility and scalability. Simulink offers a complex model-based design for interaction with real-world environments. Therefore, it is well suited for the microgrid protection study. For the digital protection relay, the SEL 351s is used. The SEL 351s is more than a relay, it offers various features such as metering, controlling and location the fault [42].

6.1.2 Connection

Another useful feature of the SEL-351S is its low-level test interface, which allows testing the relay by applying low magnitude ac voltage signals to the interface, instead of applying ac current signals to the relay inputs [43]. The interface accepts signals with a maximum amplitude of 9V peak-to-peak, the OP4510 is capable of outputting signals up to 16V peak-to-peak [2]. Figure 6-2 shows the connection of the OP4510 with the SEL 351S. The analog outputs of the OP4510 are connected to the low-level test interface via ribbon cable. The relay contact of the SEL351S, which is closed when the relay trips, is connected to a digital input of the OP4510. This allows monitoring whether the relay has tripped.

The low-level test interface can be accessed by removing the front panel. The connector information is shown in Figure 6-3.

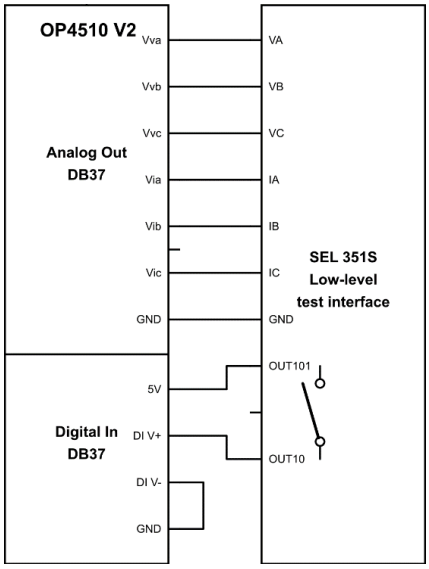

Figure 6-2 Connection of OP4510 with SEL 351S

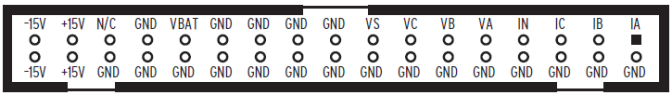

Figure 6-3. [62] Low-level test interface (J1 or J10) connector

6.1.3 Scale Factors

The low-level signals are scaled and fed to the calibrated input model, Figure 6-4 shows the resultant scale factor for the input module from the SEL 351S user manual. As seen in Figure 6-3, the scale factor depends on the input channel nominal rating. For the relay used in this study, the input channel nominal rating values are 1A and 300V. The scale factors in the corresponding row apply.

Input Channels (Relay Rear Panel)	Input Channel Nominal Rating	Input Value	Corresponding J1 Output Value	Scale Factor (Input/Output) (A/V or V/V)
IA, IB, IC, IN	1 A	1 A	100 mV	10.00
IA, IB, IC, IN	5A	5 A	100 mV	50.00
IN	0.2 A	0.2 A	114.1 mV	1.753
IN	0.05 A	0.05 A	50 mV	1.00
VA, VB, VC, VS	150 V	67 V_{LN}	1313.7 mV	51.00
VA, VB, VC, VS	300 V	134 V_{LN}	1313.7 mV	102.00
Power (+, -)	48/125 Vdc or 125/250 Vdc	125 Vdc	1.25 Vdc	100.00

Figure 6-4 [62] Scale factors for input module

6.1.4 System Modeling

The OPAL-RT simulator uses the RT-LAB software, which can simulate power grids under different simulation platforms. Using eMEGAsim, simulations can be created in MATLAB/Simulink. In the following sections, a simple test model is created to verify the configuration as well as the connection of the OPAL-RT and the SEL 351S.

6.2 Simple Test Model

Once RT-Lab has been installed and a new project with the template model for the OP4510 created according to the RT-Lab Quick start Guide, the model can be edited in Simulink [2]. The first step is to change the solver type to fixed-step and to use 50 microseconds for the fixed-step-size under Simulation -> Model Configuration Parameters -> Open Solver details. This corresponds to the sample time of the OP4510. Next, create two subsystems in the root layer of the Simulink model: SM_[name] and SC_[name]. SM_[name] stands for subsystem master, it is the only subsystem that will be run on the simulator, all the real-time simulation will occur in this subsystem. SC_[name] stands for subsystem console, it will be an asynchronous subsystem that will run on the host computer and act as a user interface. It is important that no calculations are executed in the console subsystem, or an error will occur while trying to build or load the model. Additionally, the powergui block from the Simscape Electrical needs to be added in the root layer in order to perform simulations on the host PC. The simulation type of the powergui block is set to discrete with a sample time of 50 microseconds. Figure 6-5 shows the root layer of the implemented test model with the described blocks.

In RT-Lab models, for all subsystems receiving signals from other subsystems, all inports must go through the RT-Lab communication block OpComm. In the OpComm block, the sample time must be set. In the master subsystem SM_[name], the OpCtrl block must be included and

the primary bitstream filename added. The filename can be found in the root layer of the model, its extension is .bin.

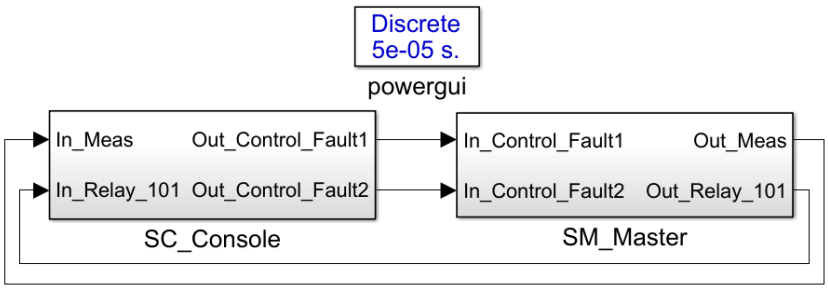

Figure 6-5 Root layer of test model

The master subsystem of the test model is shown in Figure 6-6.

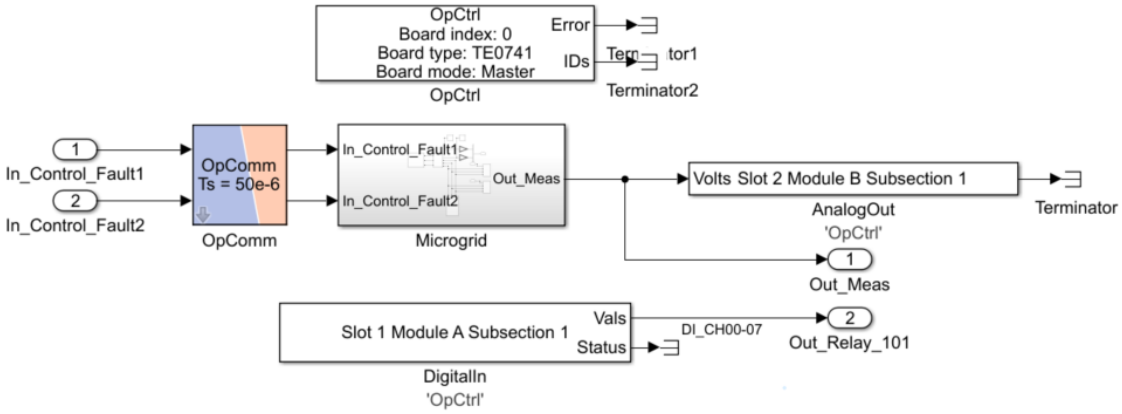

Figure 6-6 Master subsystem of test model

The master subsystem shown in Figure 6-6 contains the OpCtrl and the OpComm blocks that have already been discussed. The Microgrid block contains the test subsystem that is run on the real-time simulator. The block has two inputs which are connected to the OpComm block and one output connected to the AnalogOut block as well as to an outport. The master subsystem also contains a DigitalIn block whose Vals output is directly connected to an outport.

Each DigitalIn/Out or AnalogIn/Out block represents 8 channels of one physical DB37 connector, located on the rear-side of the OP4510, which is represented in Figure 6-7.

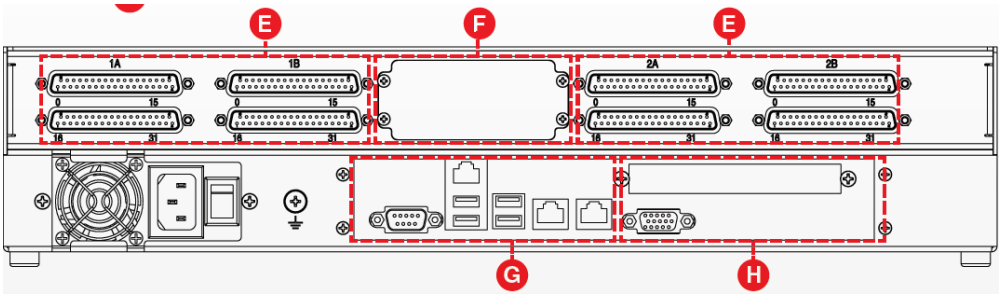

Figure 6-7 [2] OP4510 rear-side with DB37 connectors

The DataOut/DataIn port number parameter must be set accordingly for each output/input block in order to select the desired physical channels the block should be linked to. In the .conf file in the model root layer each port number is assigned to its respective slot, section and subsection. A part of the file is shown in Figure 6-8.

TE0741_3-EX-0001-3_1_8_105-CC180228_OP4510_IOs-01-01.conf

	PortName	Description	Slot	Section	SubSection	Count	Si
2	DataIn1	AO	2	B	1	8	16
3	DataIn2	AO	2	B	2	8	16
4	DataIn3	DO	1	B	1	8	1
5	DataIn3	PWMO	1	B	1	8	64
6	DataIn3	TSDO	1	B	1	-1	32
7	DataIn4	DO	1	B	2	8	1
8	DataIn4	PWMO	1	B	2	8	64
9	DataIn4	TSDO	1	B	2	-1	32
10	DataIn5	DO	1	B	3	8	1
11	DataIn5	PWMO	1	B	3	8	64
12	DataIn5	TSDO	1	B	3	-1	32
13	DataIn6	DO	1	B	4	8	1
14	DataIn6	PWMO	1	B	4	8	64
15	DataIn6	TSDO	1	B	4	-1	32
16	DataOut1	AI	2	A	1	8	16
17	DataOut2	AI	2	A	2	8	16
18	DataOut3	DI	1	A	1	8	1

Figure 6-8 Config-file of OP4510

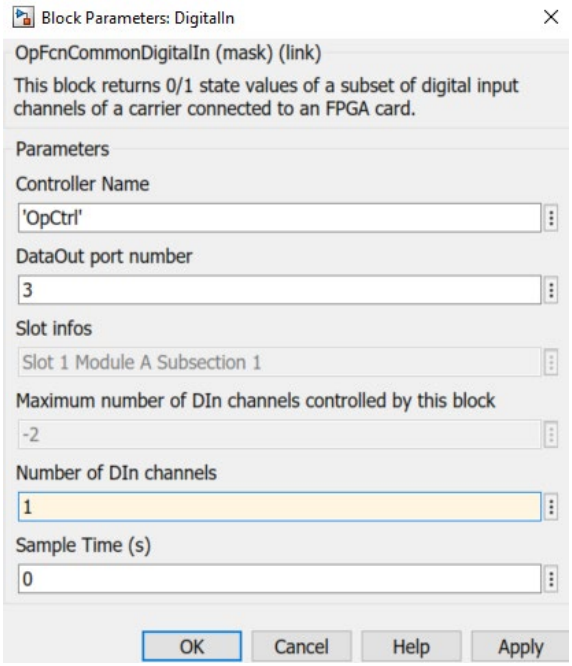

Figure 6-9 DigitalIn block parameters

For the DigitalIn block in the model, subsection 1 of slot 1 in section A is intented to use. This corresponds to PortName DataOut3. Therefore, the DataOut port number parameter of the DigitalIn block is set to 3, as shown in Figure 6-9. The number of Din channels is set to 1 as only 1 digital input is used for this application.

The test subsystem is shown in Figure 6-10. It contains a three-phase source connected to a three-phase load via a transformer and a three phase V-I measurement block which measures voltage and current at the node. Scopes are used to monitor voltage and current measurements. The measured voltages and currents are scaled with the inverse of the respective scale factor of the relay input module, shown in Figure 6-4. This is done in order to have the actual grid voltage and current values of the microgrid at the input module of the relay. These scaled values are finally multiplexed and fed to an outport. Additionally, two three-phase fault blocks are connected to the node. The faults are configured as symmetrical phase-ground faults with fault

resistance $R_{On} = 0.5\Omega$ and controlled via external signals, controlled in the SC_console subsystem, illustrated in Figure 11.

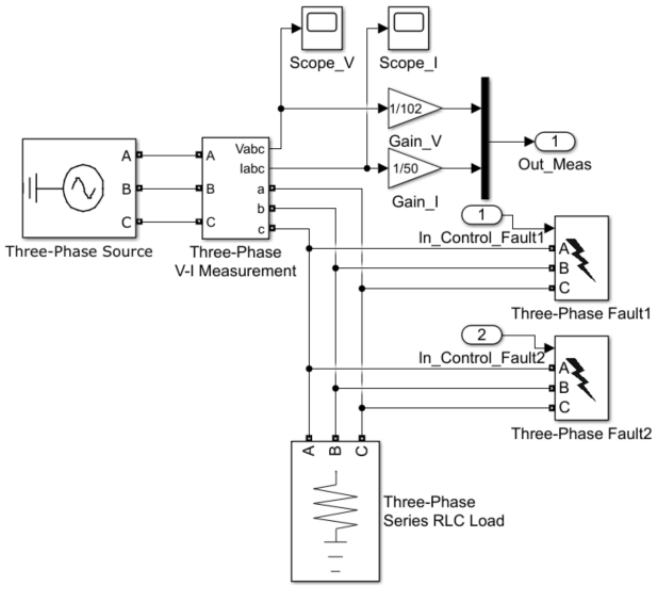

Figure 6-10 A simple test system

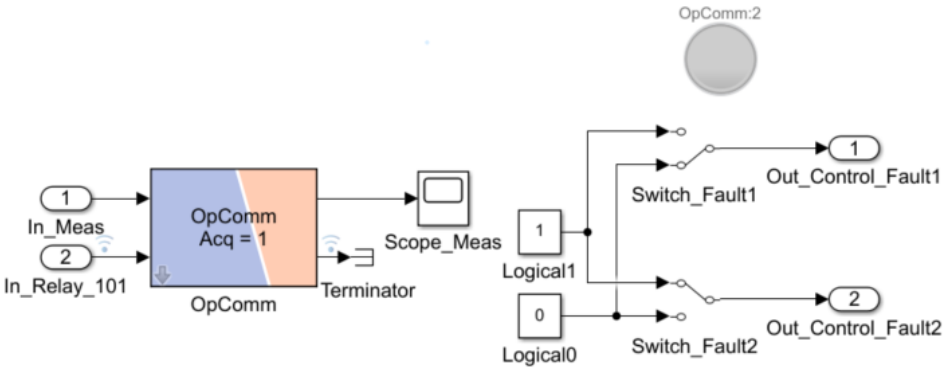

Figure 6-11 SC_Console subsystem

A few additional elements are used in the console subsystem depicted in Figure 6-11: a scope to monitor the voltage and current values which are fed to the relay, an input to monitor the OUT101 contact of the relay, which indicates if the relay has tripped. The test model can therefore be used in the following way to verify the hardware-in-the-loop setup: first, a Simulink simulation is performed on the host PC to determine the fault currents. It is important

to verify that the currents and voltages are within the specified range of the SEL 351S before applying voltage signals to the low-level test interface. The maximum values can be found in the Specifications chapter in the user manual [43]. The relevant specifications for the ac voltage and current inputs are displayed in Figure 6-12. Another limitation to take into consideration is the maximum peak-to-peak voltage value applied to the low-level test interface, which is specified as 9 Volt [43]. To determine the maximum acceptable voltage and current in the microgrid, the 9 Volts are multiplied with the respective scale factor, as shown in (1) for the voltage and in (2) for the current.

$$V_{\max\ \_grid} = k_{scale\_V} * V_{\max\ \_lowLevel} = 918V \quad (3) \quad I_{\max\ \_grid} = k_{scale\_I} * V_{\max\ \_lowLevel} = 450A \quad (4)$$

It must be assured that the grid values do not exceed these values at any point in order to avoid damaging the low-level test interface. To determine the voltage and current values, the steady-state simulation of the powergui block can be run. Alternatively, the scope in the console subsystem can be observed, as it displays the voltage signals which are fed to the low-level test interface.

AC Voltage Inputs

300 V_{L-N}, three-phase four-wire (wye) connection or 300 V_{L-L}, three-phase three-wire (open-delta) connection (when available, by global setting PTCONN=DELTA)

Continuous:	300 V (connect any voltage from 0 to 300 Vac) 600 Vac for 10 seconds
Burden:	0.03 VA at 67 V; 0.06 VA at 120 V; 0.8 VA at 300 V

AC Current Inputs

IA, IB, IC, and Neutral Channel IN

5 A Nominal:	15 A continuous, 500 A for 1 s, linear to 100 A symmetrical, 1250 A for 1 cycle
Burden:	0.27 VA at 5 A, 2.51 VA at 15 A

Figure 6-12 [62] Specifications for ac voltage and ac current inputs

6.3 SEL 351S Configuration

The SEL351S is configured with the Accelerator Quickset software. The settings of the SEL 351S are laid out in a tree structure format. There are 6 different setting groups. By default, only group 1 is active; all the other groups are inactive. The other groups can be activated using the global settings. Global settings are overall settings that impact all the other groups [61]. Each group contains Set and Logic subgroups. In the Set subgroup, elements such as overcurrent, voltage, synchronism check, frequency and power can be configured. In the following section, the setting of the phase instantaneous overcurrent element is described.

6.3.1 Phase Instantaneous Overcurrent

The instantaneous/definite-time overcurrent elements are found in Group 1 -> Set 1 -> Phase Instantaneous Overcurrent Elements. Six different levels are available, levels 1-4 are shown in Fig. 12. The pickup settings for each level (50P1P-50P6P) are compared to the magnitudes of the individual phase currents I_A, I_B and I_C. The logic outputs in Figure 6-13 are relay word bits and operate as follows:

50A1 = 1 (logical 1), if $I_A >$ pickup setting 50P1P

= 0 (logical 0), if $I_A \leq$ pickup setting 50P1P

In this example, two overcurrent elements are set: one at a level of 5A with delay of 10 cycles and the second one at a level of 10A without delay [43].

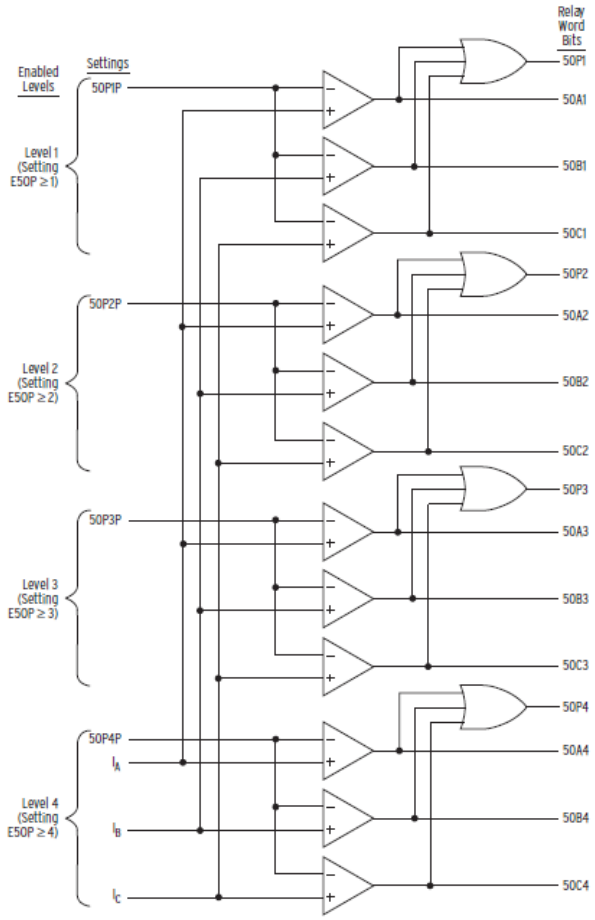

Figure 6-13 [62] Levels 1-4 of phase instantaneous overcurrent elements

The current levels are set in amps secondary, referring to the current after the current transformer of the measuring unit. The conversion factor from amps primary to amps secondary needs to be looked up in Group 1 -> Set 1 -> General Settings. The factor for this particular relay is 1, amps secondary are therefore equal to amps primary in this case. The elements can now be set. If one of the overcurrent elements gets activated, the relay should trip. For this purpose, the trip logic is configured in the following section.

6.3.2 Trip Logic

The relay trip logic provides flexible tripping with the control Equation settings. Detailed information can be found in section 5 of the SEL 351S user manual [43]. The block diagram of the trip logic is displayed in Figure 6-14. As recognizable in the block diagram, all trip conditions are combined into the OR-1 gate. The output of this gate asserts relay word bit TRIP

to logical 1, regardless of other trip logic conditions. The TRIP relay word is asserted to logical 1, until the minimum trip duration timer stops timing, output of OR-1 deasserts to logical 0 and front-panel target reset pushbutton is pressed/ tar r command is executed via the serial port [43]. The control equations can be set in Group 1 -> Logic 1 -> Trip/Comm.-Assisted Trip Logic, as seen in Figure 6-16.

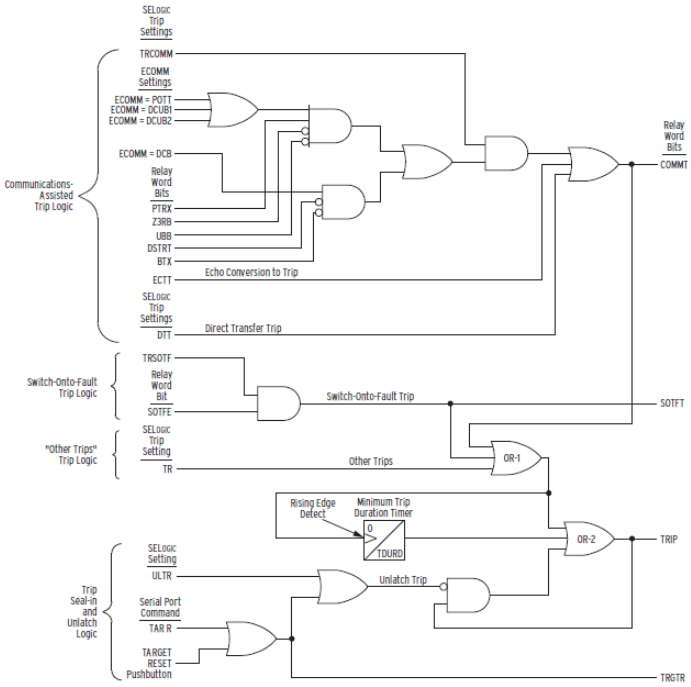

Figure 6-14 [62] Trip logic

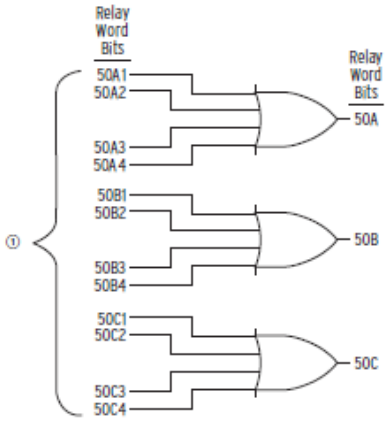

Figure 6-15 [62] Combined single-phase instantaneous overcurrent elements

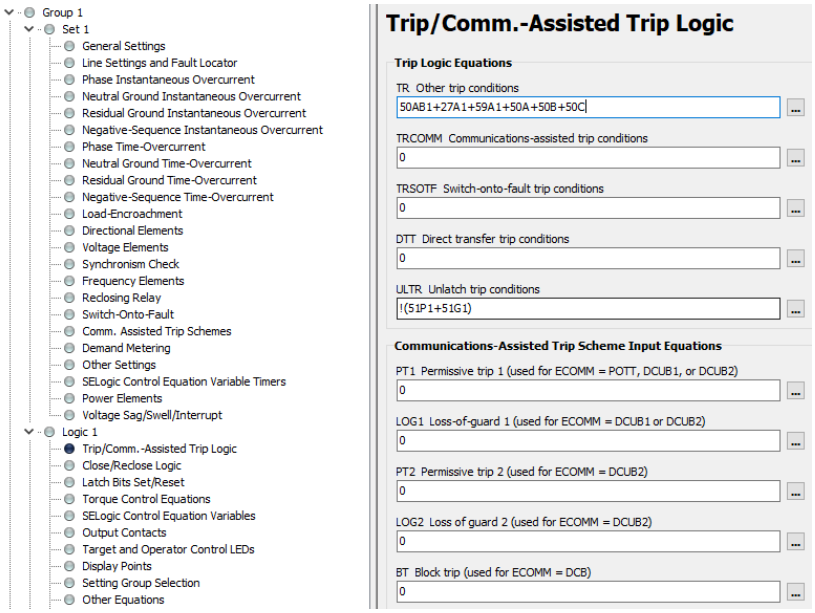

Figure 6-16 Trip/Comm.-Assisted Trip Logic

In this example, the relay should trip in case of any instantaneous overcurrent. The combined single-phase instantaneous overcurrent element relay word bits 50A, 50B and 50C can be used for this application, as they indicate the presence or absence of overcurrent in a particular phase, as shown in Figure 6-15.

6.3.3 Output Contacts

The output contacts of the digital protection relay can be configured in Group 1 -> Logic 1 -> Output Contacts. In factory setting, output contact 101 is routed to the TRIP relay word. The contact closes, when the relay trips, else the contact is open.

6.4 Microgrid Simulation Result in Matlab

In this section, the system that has been developed in chapter five is modified by adding a new DG (shown in grey). This system, as discussed before, is a modified IEEE feeder system where the loads are balanced. A three-phase fault happens at the terminals of the added DG at 10/60 seconds. The breaker isolate the fault 11/60 seconds.

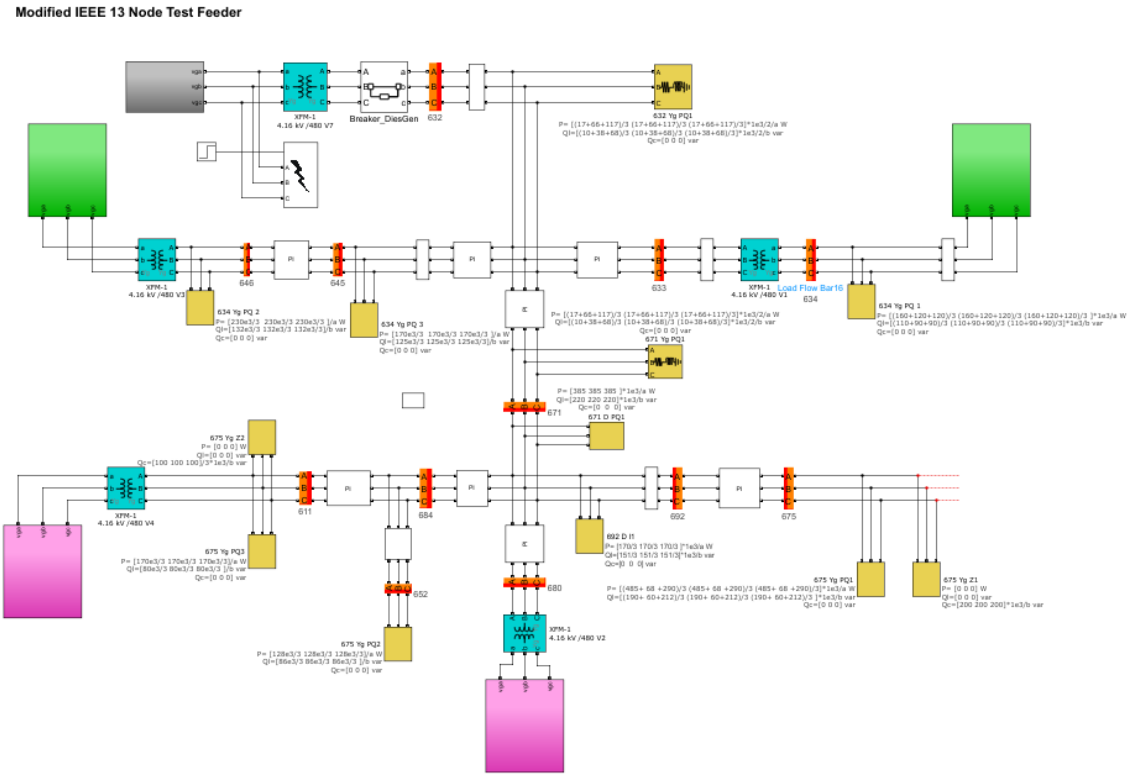

Figure 6-17 Microgrid System

The two DGs that are shown in green and the other two magenta DGs regulate the voltage and frequency of the system successfully. As the Figure 6-18 shows, the three phase fault at the terminals of the grey DG affect the voltage of the system (in the worst case scenario the voltage drops to .92 pu) but after clearing the fault by the breaker the other DGs handle the power mismatch due to the loss of that DG.

In the first scenario, the fault is applied 10/60 seconds and is cleared at 11/60 seconds. The distributed voltage and frequency controller is activated at 1 second, and it is shown in Figure 6-18, the system operating point goes back to its nominal values in four seconds.

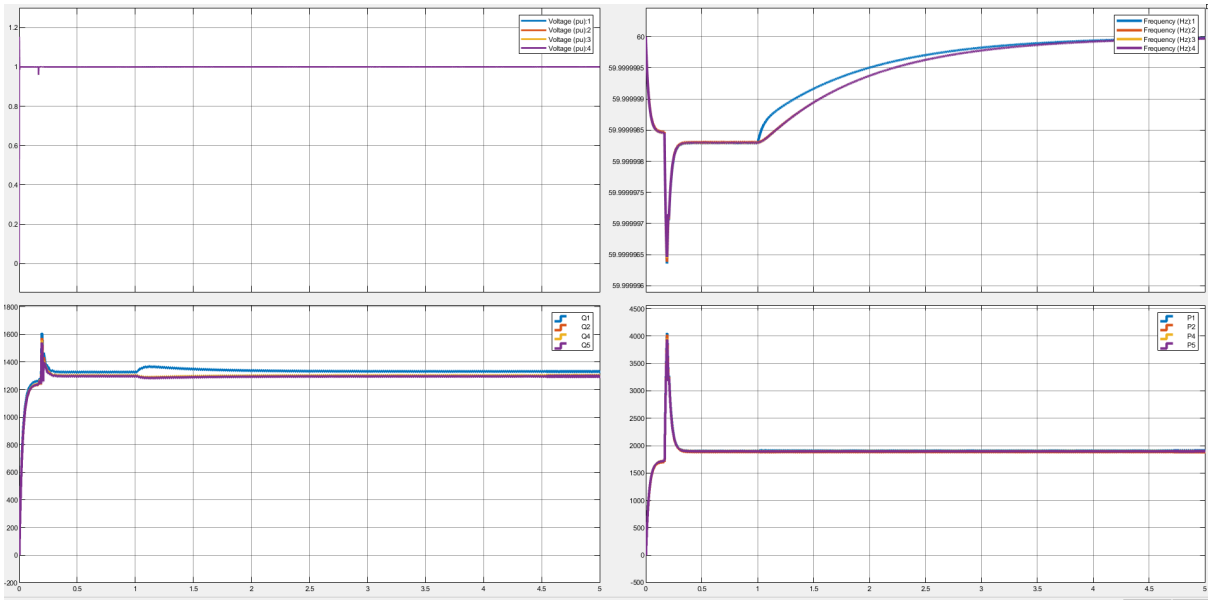

Figure 6-18 System's results after disconnecting the grey DG from the rest of the microgrid due to the fault at its terminal at t=10/60 seconds. The distributed voltage and frequency are activated at t=1 second.

In the second scenario, the three-phase fault is applied and cleared at the same time as case one, but the secondary voltage and frequency control are activated at t=0.25 seconds which is 0.75 seconds earlier than case one. The result shown in Figure 6-19 that the system goes back to its normal situation in three seconds, two seconds faster than the previous case, which shows the advantage of the distributed secondary controller in the system.

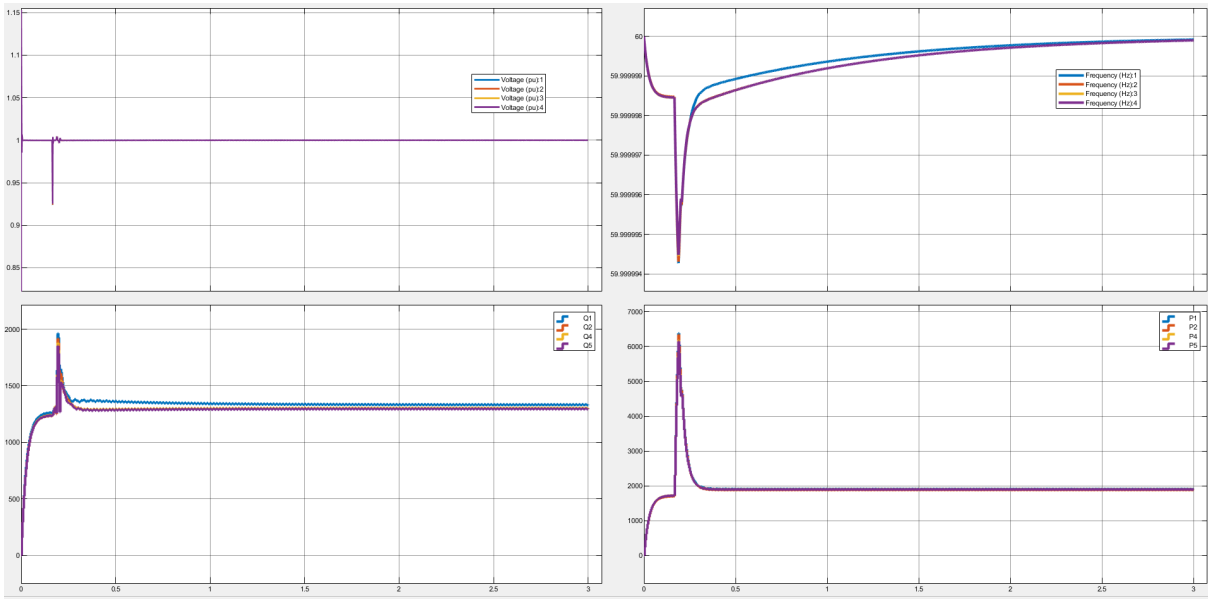

Figure 6-19 System's results after disconnecting the grey DG from the rest of the microgrid due to the fault at its terminal at 10/60 seconds. The distributed voltage and frequency are activated at t=0.25 second

6.5 Comparing the real-time simulator result (OPAL-RT) with the software simulation (Matlab)

To verify the accuracy of the simulation file in Matlab, this model is implemented in the real time simulator OP4510. This OP4510 is connected to an actual SEL relay as well as a breaker as it shown in Figure 6-5. The microgrid model is prepared into two parts: SC_console and SC_master as discussed before. The relay low-voltage interface is used to be connected to the OP4510. The simulation runs in RT-Lab and the three-phase fault is applied at the same time as before (on 11/60 seconds). The relay is set to monitor the current and send the command to open the line in case of overcurrent detection. The result of voltage control in real-time simulator (connected to the SEL relay) as well as the Matlab simulation is shown in Figure 6-20. The result verifies that the Matlab simulation closely follows the real-time simulator.

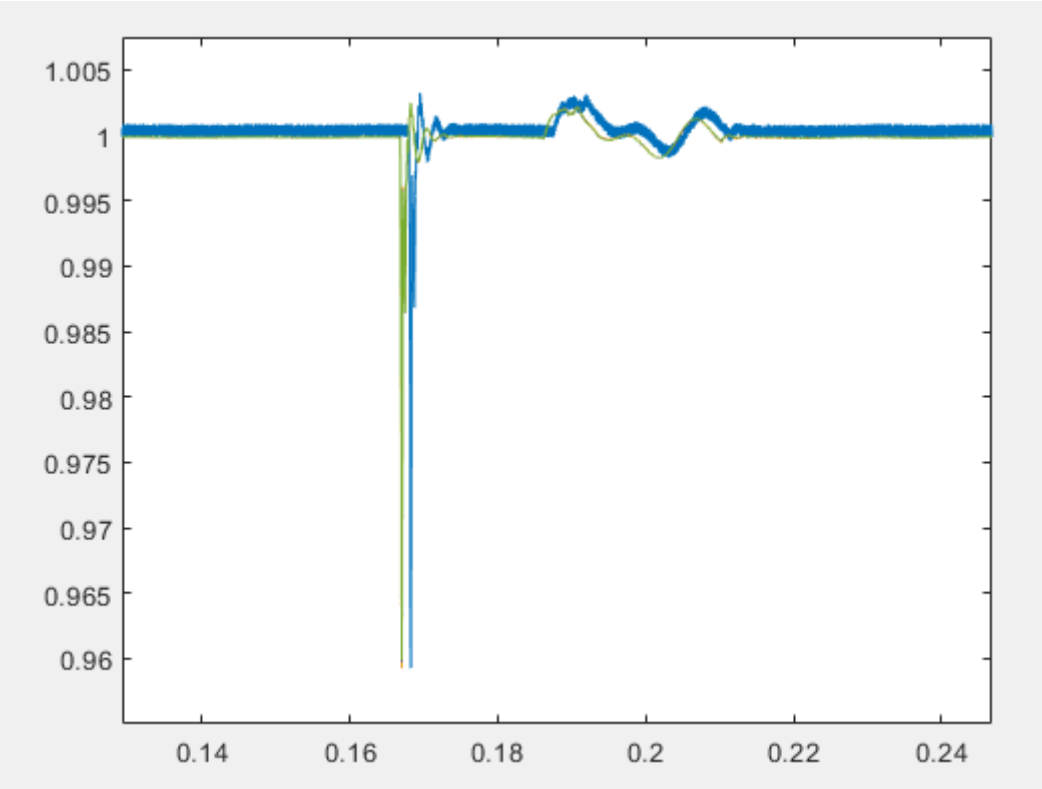

Figure 6-20 Comparison regarding voltage control of DG1 in OPALRT (blue color) vs. Matlab (green color)

6.6 Conclusion

In this chapter, the hardware-in-the-loop environment has successfully been set up. A simple test model has been utilized to verify the correct configuration and connection of the OPAL-RT and the SEL 351S. Furthermore, a case study is implemented to connect the real-time simulator with the hardware (SEL relay). The result of controlling the voltage of the system in case of losing one DG in the real-time simulator versus the software simulation (Matlab) is studied. The result verifies that the Matlab simulation coordinates with the real-time simulator. Future projects can use the developed model in this study to integrate actual distributed controllers or DGs into the real-time simulator (power amplifier is needed).

7 Bibliographys

[1] A Dehghan Banadaki, T Taufik, A Feliachi, “Big Data Analytics in a Day-Ahead Electricity Price Forecasting Using TensorFlow in Restructured Power Systems,” in *2018 International Conference on Computational Science and Computational Intelligence (CSCI)*, 2018.

[2] E. Foruzan, S. Asgarpoor, and J. M. Bradley, “Hybrid system modeling and supervisory control of a microgrid,” in *North American Power Symposiumm (NAPS)*, 2016.

[3] V. Verma, S.K. Solanki, J. Solanki, “Modeling and Criterion for Voltage Stablity of Grid Connected Droop Controlled Inverter,” in *North American Power Symposium*, 2017.

[4] H. Pourbabak, J. Luo, T. Chen, and W. Su, “A Novel Consensus-based Distributed Algorithm for Economic Dispatch Based on Local Estimation of Power Mismatch,” in *IEEE Transactions on Smart Grid*, 2017.

[5] Pogaku, Nagaraju, Milan Prodanovic, and Timothy C. Green, “Modeling, analysis and testing of autonomous operation of an inverter-based microgrid.,” in *IEEE Transactions on power electronics* , 2007.

[6] Katiraei, F., M. R. Iravani, and P. W. Lehn., “Small-signal dynamic model of a micro-grid including conventional and electronically interfaced distributed resources.,” in *IET generation, transmission & distribution* , 2007.

[7] Guerrero, J. M., De Vicuna, L. G., Matas, J., Castilla, M., & Miret, J., "A wireless controller to enhance dynamic performance of parallel inverters in distributed generation systems.," in *IEEE Transactions on power electronics*, 2004.

[8] E.A.A. Coelho, P.C. Cortizo, P.F.D. Garcia, "Small-signal stability for parallel-connected inverters in stand-alone AC supply systems," in *IEEE Transactions on Insutry*, 2002.

[9] E.A.A. Coelho, Dan Wu, J.M. Guerrero, J.C. Vasquez, T. Dragičević, Č.S.P. Popovski, "Small-signal analysis of the microgrid secondary control considering a communication time delay," in *IEEE Transactions on Industrial Electronics*, 2016.

[10] F. Mohammadi, "Modeling, Simulation and Decentralized Control of Microgrids," in *West Virginia University*, 2017.

[11] T. Amraee, A. Soroudi, and A.M. Ranjbar, "Probabilistic determination of pilot points for zonal voltage control," in *IET generation, transmission and distribution*, 2012.

[12] Turaj Amraee AM Ranjbar and Ren, "Immune-based selection of pilot nodes for secondary voltage control," in *European Transactions on Electrical Power* .

[13] A. Conejo and M. J. Aguilar, "Secondary voltage control: nonlinear selection of pilot buses design of an optimal control law and simulation results," in *Generation Transmission and Distribution IEE Proceedings*, 1998.

[14] J. S. Thorp, M. Ilic-Spong, and M. Varghese, “Optimal secondary voltage-VAR control using pilot point information structure,” in *The 23rd IEEE Conference on Decision and Control*, 1984.

[15] A. Conejo J.I. De La Fuente and S. Goransson, “Comparison of alternative algorithms to select pilot buses for secondary voltage control in electric power networks,” in *Electrotechnical Conference 1994*.

[16] La Gatta, Paula O., João A. Passos Filho, and José LR Pereira., “Comparison among methodologies for identification of pilot buses and its impact on the steady state secondary voltage control,” in *IEEE International Conference on Industry Applications* , 2014.

[17] Alimisis, Varvara, and Philip C. Taylor., “Zoning evaluation for improved coordinated automatic voltage control.,” in *IEEE Transactions on Power Systems*, 2015.

[18] Prada, Ricardo B., Jelitza L. Ceballos Infantes, and João A. Passos Filho, “Identifying voltage control areas based on the interdependence of control equipment,” in *Journal of Control, Automation and Electrical Systems*, 2013.

[19] R. Schlueter, I.-P. Hu, M. Chang, J. Lo, and A. Costi, , “MEthods for determining proximity to voltage collapse,” in *IEEE Transactions on power systems*, 1991.

[20] C. Aumuller and T. Saha, “Determination of power system coherent bus groups by novel sensitivity-based method for voltage stability assessment,” in *IEEE Transanctions on Power Systems*, 2003.

[21] A.D. Banadaki, T. Iqbal, A. Feliachi, *Voltage Control Using Singular Value Decomposition of Fast Decoupled Load Flow Jacobian,* Chicago: IEEE PES (Poster), 2017.

[22] A. Bidram, A. Davoudi, F. K. Lewis, and S.S. Ge, "Distributed adaptive voltage control of inverter-based microgrids," in *IEEE Transactions on Energy Conversion*, 2014.

[23] Mohammadi, F. D., Keshtkar, H., Banadaki, A. D., & Feliachi, A., "A novel cooperative distributed secondary controller for VSI and PQ inverters of AC microgrids," *Heliyon,* 2019.

[24] V. Verma, S.k. Solanki, J. Solanki, "State Space Modeling of Three Phase Transformers for Small-Signal Analysis of A Microgrid," in *North American Power Symposium (NAPS)*, 2017.

[25] B. Barbier, "An analysis of phenomens of Voltage Collapse on a Transmission System," in *Revue General d'Electricite*, 1980.

[26] Hsu, P., Muljadi, E., Wu, Z., & Gao, W. , "Voltage regulation using a permanent magnet synchronous condenser with a series compensator," in *Energy Conversion Congress and Exposition (ECCE)*, 2015.

[27] Zecchino, A., Marinelli, M., Hu, J., Coppo, M., & Turri, R., "Voltage control for unbalanced low voltage grids using a decoupled-phase on-load tap-changer transformer and photovoltaic inverters.," in *Power Engineering Conference (UPEC), IEEE*, 2015.

[28] C. Long, and L.F. Ochoa., "Voltage control of PV-rich LV networks: OLTC-fitted transformer and capacitor banks.," in *EEE Transactions on Power Systems 31.5*, 2016.

[29] Das, G. Sasank, and B. Mohan., "Optimal Allocation of FACTS Device with Multiple Objectives Using Genetic Algorithm.," in *International Journal of Modern Engineering Research (IJMER) Vol 4*, 2014.

[30] Singh, Mithilesh, and Shubhrata Gupta. , "UPFC facts devices in power system to improve the voltage profile and enhancement of power transfer loadability.," in *IEEE International Conference on Power Electronics*, 2016.

[31] M. E. Moursi, G. Joos, and C. Abbey, "A secondary voltage control strategy for transmission level interconnection of wind generation.," in *2008*, IEEE Transactions on Power Electronics 23.3.

[32] Paul, J. P., and J. Y. Leost, "Improvements of the secondary voltage control in France.," in *The IFAC Symposium.* , 2014.

[33] A. Ameli, M. Farrokhifard, A. Shahsavari, A. Ahmadifar, H. Shayanfar, "Multi-Objective DG Planning Considering Operational and Economic Viewpoints," in *Environment and Electrical Engineering (EEEIC)*, 2013.

[34] E. Reihani, S. Sepasi, L. R. Roose, M.. Matsuura, "Energy management at the distribution grid using a Battery Energy Storage System (BESS)," *International Journal of Electrical Power & Energy Systems,* vol. 77, 2016.

[35] R. D. Zimmerman, C. E. Murillo-Sánchez, and R. J. Thomas, MATPOWER: Steady-State Operations, Planning, and Analysis Tools for Power Systems Research and Education, IEEE Transactions on Smart Grid , 2013.

[36] A Dehghan Banadaki, A Feliachi, V Kulathumani, "Fully Distributed Secondary Voltage Control in Inverter-Based Microgrids," in *2018 IEEE/PES Transmission and Distribution Conference and Exposition (T&D*, 2018.

[37] F. G. a. L. Schenato, "A Survey on Distributed Estimation and Control Applications Using Linear Consensus Algorithms," in *Networked control systems*, . Springer, London,, 2010.

[38] Schenato, Federica Garin and Luca, "A Survey on Distributed Estimation and Control," in *Networked Control Systems*, Springer-Verlag, 2010.

[39] S. Corrigan, "Introduction to the Controller Area Network(CAN)," Texas Instrument, 2016.

[40] I. Penn, "Los Angles Times," 2017. [Online]. Available: https://www.latimes.com/projects/la-fi-electricity-solar/.

[41] Eto, Joseph H., Robert Lasseter, David Klapp, Amrit Khalsa, Ben Schenkman, Mahesh Illindala, and Surya Baktiono, "The CERTS Microgrid Concept, as Demonstrated at the CERTS/AEP Microgrid Test Bed," 2018.

[42] A. S. Makhzani, M. Zarghami, B. Falahati and M. Vaziri, “"Hardware-in-the-loop testing of protection relays in distribution feeders with high penetration of DGs,",” in *2017 North American Power Symposium (NAPS)*, Morgantown, WV, 2017.

[43] “Schweitzer Engineering Labaratories, “SEL 351S,” SEL351S user manual,,” July 2016.

[44] “https://matlab.mathworks.com/,” Mathworks. [Online].

[45] A Dehghan Banadaki, F Doost Mohammadi, A Feliachi, “State space modeling of inverter based microgrids considering distributed secondary voltage control,” in *2017 North American Power Symposium (NAPS)*, 2017.

[46] A Dehghan Banadaki, A Feliachi, “Voltage control using eigen value decomposition of fast decoupled load flow jacobian,” in *2017 North American Power Symposium (NAPS)*, 2017.